Glycine Transporter-1 Antagonist Provides Neuroprotection Following Stroke *in Vivo*

JULIA DOMINIQUE CAPPELLI

This thesis is submitted as a partial fulfillment of the requirements of the Master of Science Degree in Neuroscience

DEPARTEMENT OF CELLULAR AND MOLECULAR MEDICINE
NEUROSCIENCE PROGRAM
UNIVERSITY OF OTTAWA
AUGUST 2021

AUTHORIZATION

Figure. 1. Adapted from Khoshnam et al., 2017. Reproduced with permission from Springer.

Figure. 2. Adapted from Ge et al., 2020. Reproduced with permission from Cell Press.

Figure. 5. Adapted from Jonhson and Ascher 1987. Reproduced with permission from Nature.

Figure. 6. Adapted from Marques et al. 2020. Reproduced with permission from Elsevier.

ABSTRACT

Ischemic strokes are a major cause of death and disability, yet efficacious pharmacotherapies remain limited. Although neuronal cell death during stroke is primarily induced *via* excessive Ca^{2+} influx through NMDARs following overactivation by uncontrolled glutamate release, antagonism of these receptors has been shown to be ineffective due to intolerable side effects. This thesis highlights a novel therapeutic strategy for stroke wherein NMDAR-mediated excitotoxicity is temporarily and dynamically mitigated *via* the initiation of a process termed "glycine induced NMDAR internalization" (GINI). While GINI occurs *in vitro* following application of high doses of glycine, achieving these levels of glycine *in vivo* has long been thought impossible as glycine transporters (GlyT1) maintain synaptic glycine levels well below saturating concentrations. Here, we show that GINI can be triggered *in vivo* when mice are administered a glycine transporter-1 antagonist (GlyT1-A) prior to stroke and that this strategy provides neuroprotection. Mice pre-treated with a GlyT1-A, which elevates glycine levels, exhibited significantly smaller stroke volumes, reduced cell death, and significantly minimized behavioural deficits following stroke induction by either photothrombosis (PT) or endothelin-1 (ET-1). Moreover, we observed preservation of vasculature function and morphology in the peri-infarct area. These data strongly suggest that elevating brain glycine levels with GlyT1-As should be considered as a novel pharmacotherapy for ischemic stroke.

TABLE OF CONTENTS

AUTHORIZATION ii
ABSTRACT iii
LIST OF TABLES viii
LIST OF FIGURES ix
LIST OF ABBREVIATIONS xi
ACKNOWLEDGEMENTS xii
1. INTRODUCTION 1
1.1 Ischemic stroke 1
1.1.1 General overview 1
1.1.2 The ischemic cascade 2
1.1.3 Current treatment strategies 4
1.1.3 Treatment research 5
1.1.3.1 The past 5
1.1.3.2 The present 7
1.1.3.3 The future 7
1.2 N-Methyl-D-Aspartate Receptors (NMDARs) 8
1.2.1 NMDAR: A general overview 8
1.2.2 NMDARs: Binding sites and functions 10
1.2.3 Role of NMDARs in stroke 11
1.2.3.1 Excitotoxicity 11
1.2.3.2 Subunit hypothesis 11
1.2.3.3 Localization hypothesis 12
1.2.4 Endocytosis of NMDAR 13
1.2.5 Glycine induced NMDAR internalization 15
1.3 Glycine 18
1.3.1 Glycine as an inhibitory neurotransmitter 18
1.3.2 Glycine as an excitatory neurotransmitter 19
1.3.3 Glycine transporters: synaptic glycine regulation 20
1.4 Glycine Transporter-1 Antagonists (GlyT1-As) 23
1.4.1 History of use 23
1.3.3 As a novel treatment strategy for ischemic stroke 24

2. HYPOTHESIS 25
3. OBJECTIVES 25
4. MATERIAL AND METHODS 26
4.1 Animals 26
4.1.1 Animals 26
4.2 Pharmacology 26
4.2.1 NFPS preparation 26
4.3 Surgical procedures 27
4.3.1 Photothrombotic stroke 27
4.3.2 Cortical endothelin-1 stroke 27
4.3.3 Intracranial cortical injection of Adeno Associated Virus (AAV) 28
4.3.4 Medial pre-frontal cortex endothelin-1 stroke 28
4.3.5 2 Vessel occlusion model of global ischemia 29
4.3.6 Laser doppler flowmetry and photothrombosis 30
4.4 Histology and microscopy 30
4.4.1 Brain tissue preparation 30
4.4.2 Quantification of stroke volume - Magnetic resonance imaging 31
4.4.3 Quantification of stroke volume - Triphenyltetrazolium chloride 31
4.4.5 Quantification of stroke volume - Cresyl violet 32
4.4.6 Stroke volume measurements and analysis 32
4.4.7 Quantification of neuronal loss - FluoroJade C 33
4.4.8 Quantification of neuronal loss - FluoroJade C analysis 33
4.4.9 Immunohistochemistry 33
4.5 A714L mutation generation, viral packaging, and quantification 34
4.5.1 Generation of WT and A714L constructs 34
4.5.2 Sub-Cloning into pcDNA3.1 35
4.5.3 *In vivo* viral constructs 35
4.5.4 Viral spread quantification 36
4.6 NMDAR internalization quantification 36
4.6.1 HEK293 cells maintenance, transfection, and whole-cell electrophysiology 36
4.6.2 NMDAR internalization imaging in HEK cells 37
4.7 Light Sheet Fluorescence Microscopy 38
4.7.1 Imaging and segmentation 38
4.7.2 Automated stroke volume measurement 39

4.7.3 Post-stroke vascular morphology quantification ... 39
4.8 Tissue clearing for Light Sheet Fluorescence Microscopy ... 40
4.8.1 CUBIC$_{2019}$ tissue clearing ... 40
4.8.2 CUBIC$_{2015}$ tissue Clearing ... 41
4.8.3 Scale A2 tissue clearing ... 41
4.8.4 Scale S4 tissue clearing ... 42
4.8.5 SeeDB tissue clearing ... 42
4.8.6 PEGASOS tissue clearing ... 42
4.8.7 iDISCO$^+$ tissue clearing ... 43
4.9 Behavioural tests and statistical analysis ... 43
4.9.1 Habituation to behavioural testing ... 43
4.9.2 Adhesive removal test ... 43
4.9.3 Horizontal ladder test ... 44
4.9.4 Cylinder test ... 45
4.9.5 Morris water maze (MWM) ... 46
4.9.6 Forced swim test ... 47
4.9.7 Open field test ... 48
4.9.8 Novel object test ... 48
4.10 Electrophysiology ... 49
4.10.1 Hippocampal brain slice preparation ... 49
4.10.2 Whole-cell electrophysiology on hippocampal slices ... 50
4.10.3 Sniffer-patch technique ... 51
4.10.3 Oxygen-glucose deprivation paradigm ... 51
5. RESULTS ... 52
5.1 High concentrations of glycine induce NMDAR internalization, *in vitro* ... 52
5.2 Glycine is released during oxygen-glucose deprivation paradigm ... 52
5.3 Genetic elevation of brain glycine reduces infarct size following photothrombotic stroke ... 53
5.4 Pharmacological elevation of brain glycine reduces infarct size and improves motor behavioural deficits following photothrombotic stroke ... 53
5.6 Pre-stroke administration of NFPS decreases stroke volume and improves motor behavioural deficits following endothelin-1 stroke ... 55
5.7 Blocking NMDAR internalization abolishes the effect of NFPS ... 59
5.8 NFPS and animal models of cognitive impairment ... 64
5.9 Pre-stroke administration of NFPS is beneficial to post-stroke vascular health ... 68

6. DISCUSSION 72
7. CONCLUSION 78
8. TABLES 79
9. SUPPLEMENTAL FIGURES 81
10. VIDEOS 85
11. REFERENCES 86

LIST OF TABLES

Table 1 List of antibodies.

Table 2 Primers used for GluN1 variants subcloning into pcDNA3.1.

LIST OF FIGURES

Figure. 1. Adapted from Koshnam et al., 2017.

Figure. 2. Adapted from Ge et al., 2020.

Figure. 3. Depiction of N-Methyl-D-Aspartate Receptor.

Figure. 4. Adapted from Nong et al., 2004.

Figure. 5. Adapted from Jonhson and Ascher 1987.

Figure. 6. Adapted from Marques et al. 2020.

Figure 7. Elevation of extracellular glycine results in a smaller infarct volume and decreased motor behavioural deficits following photothrombotic and endothelin-1 stroke.

Figure 8. Infection of the stroke site with the non-internalizing GluN1-A714L mutation abolishes the protective effect of elevating extracellular glycine on stroke volume and during a behavioural task.

Figure 9. Assaying ischemic models of cognitive deficits.

Figure 10. NFPS has a protective effect on vascular function and morphology.

Supplemental Figure 1. Elevated glycine concentrations result in NMDAR internalization and can occur during ischemia.

Supplemental Figure 2. *In vivo* control experiments.

Supplemental Figure 3. GluN1-A714L mutation control experiments.

Supplemental Figure 4. Light sheet and tissue clearing control experiments.

LIST OF VIDEOS

Supplemental Video 1 (Video S1): Live cell imaging of GINI occurring.

Time lapse image of live cells expressing WTGluN1-NMDARs following application of an internalizing dose of glycine. NMDARs co-labeled with both green and red are shown to be internalizing.

Supplemental Video 2 (Video S2): Live cell imaging of GINI not occurring.

Time lapse image of live cells expressing A714LGluN1-NMDARs following application of an internalizing dose of glycine. NMDARs co-labeled with both green and red are shown to not be internalizing.

Supplemental Video 3 (Video S3): 3D Vasculature of a cleared left-brain hemisphere with a PT-induced stroke.

Vasculature of cleared whole brain 48hrs following PT stroke, imaged with light sheet microscope.

Supplemental Video 4 (Video S4): A closer look at 3D vasculature.

A more in depth look at the cortical vasculature of a cleared whole brain vasculature, imaged with light sheet microscope.

Supplemental Video 5 (Video S5): Automated detection of stroke volume in cleared tissue.

Depiction of our deep neural network segmenting the stroke volume.

LIST OF ABBREVIATIONS

AAV: Adeno associated virus;
ACSF: Artificial cerebrospinal fluid;
AMPAR: α-amino-3-hydroxy-5-methylsoxazole-4-propionic acid
CHO: Chinese Hamster Ovary;
CPA: Cyclopiazonic acid;
CV: Cresyl violet;
DBP: Dynamin blocking peptide;
ddH_2O: Double distilled water;
EPSCs: Excitatory postsynaptic currents;
ET-1: Endothelin-1;
FJC: FluoroJade C;
GBS: Glycine binding site;
GINI: Glycine-induced NMDAR internalization;
GluN2A$^{-/-}$: NMDAR GluN2A subunit knockout;
GlyR: Glycine receptor;
GlyT1: Glycine transporter type 1;
GlyT1$^{+/-}$: Heterozygous glycine transporter type 1;
GlyT1-A: Glycine transporter type 1 antagonist;
GO: Glycine oxidase;
iGluR: Ionotropic glutamate receptors
i.p.: Intraperitoneal;
LDF: Laser Doppler flowmetry;
LSFM: Light sheet fluorescence microscopy;
tMCAO Transient middle cerebral artery occlusion;
MRI: Magnetic resonance imaging;
NFPS: *N*-[3-(4′-fluorophenyl)-3-(4′-phenylphenoxy)propyl]sarcosine;
NMDAR: *N*-methyl-D-aspartate receptor;
NMDG: *N*-methyl-D-glucamine;
OGD: Oxygen-glucose deprivation paradigm;
PBS: Phosphate buffered saline;
PBSGT: 0.25% (w/v) gelatin and 0.2% Triton X-100 (v/v) in PBS;
PFA: Paraformaldehyde;
P_{open}: Open probability;
PT: Photothrombosis;
RT: Room temperature;
SR$^{-/-}$: Serine racemase knockout;
TTC: 2,3,5-triphenyltetrazolium chloride;
2VO: 2 vessel occlusion
WT: Wild type

ACKNOWLEDGEMENTS

I would like to express my gratitude to my supervisor, Dr. Richard Bergeron, for giving me the opportunity to complete my master's degree in his laboratory. Working in this lab has been an extraordinary experience which allowed me to not only develop a strong understanding of the field of neuroscience, but also allowed my passion for science to grow. Dr. Bergeron has been an inspiring mentor whose *crazy ideas* have truly pushed me to become a better scientist.

I would also like to extend my gratitude to all members of Dr Bergeron's laboratory, including Dr. Pamela Khacho, Dr. Melissa Snyder, Dr. Adrian Wong, Dr. Prakash Chudalayandi, Dr. Jessika Royea, Alex Sokolovski, Sophie Raymond, Boyang Wang, Julian Pitney, Thinh Nguyen, Kayla Fleming, Kieran McCann, and Mia Danis and for providing me with a collaborative and stimulating work environment, rich with insightful and intelligent discussions. A very special thank you to Roger for providing the lab with endless hours of spooky entertainment!

The electrophysiological experiments presented in this work were completed exclusively by Dr. Pamela Khacho, Boyang Wang, Sophie Raymond. I added intellectual input to experimental rationale and design but did not perform these experiments. The construction of the light sheet microscope and the implementation of the AI deep learning segmentation tool used to automatically calculate stroke volume from cleared tissue samples was completed in collaboration with Boyang Wang, Julian Pitney and Junzheng Wu. A714L-GluN1 mutant constructs were generated and designed by Dr. Prakash Chudalayandi. Laser doppler flowmetry experiments were performed using Dr. Baptist Lacoste's equipment.

1. INTRODUCTION

1.1 Ischemic stroke

1.1.1 General overview

Stroke is a cerebrovascular disease characterized by an obstruction or disruption in blood flow to the brain leading to neuronal injury and/or death. This temporary deprivation of blood flow to the brain is the result of either a tear (hemorrhagic stroke) or a blockage (ischemic stroke) in a cerebral blood vessel, with the latter being more prevalent (Casals et al., 2011). This results in the death of a portion of neural tissue (ischemic core) and severe inflammation and damage in the surrounding area (ischemic penumbra). In fact, it is estimated that for each hour that a stroke is left untreated, 120 million neurons die; equivalent to roughly 3.6 years of natural neuronal loss (Saver, 2006). These events often result in quite severe, long-lasting symptoms and in some cases, death. During the acute phase of ischemia, many patients report fatigue, unilateral numbness, tingling or paralysis, slurred speech, and confusion. Post stroke symptoms vary depending on the region of the brain affected, however unilateral muscle weakness, severe headaches, trouble articulating and/or speaking coherently, and cognitive impairments are among the most common, and often result in long lasting disability (Goldstein & Hankey, 2006; Khoshnam, Winlow, Farzaneh, Farbood, & Moghaddam, 2017; Warlow, Sudlow, Dennis, Wardlaw, & Sandercock, 2003).

According to the Public Health Agency of Canada's 2017 annual stroke report, strokes are the 10th leading cause of adult disability and the third leading cause of death in Canada with over 57 000 new strokes reported annually (Collaborators, 2016 ;Statistics Canada, 2019). Due to the

more recent shift from mortality to disability in stroke, the costs to the Canadian public health system can reach up to $2.8B (Mittmann et al., 2012). Although there are many ways in which Canadians may reduce their risk of suffering a stroke, including leading a healthy lifestyle promoting good cardiovascular health, being aware of family medical cardiovascular history, and/or taking a daily dose of aspirin (Ansara, Nisly, Arif, Koehler, & Nordmeyer, 2010) or statins (Arnett et al., 2019a) to reduce the risk of vascular obstructions, there exists only limited ways to effectively treat and prevent stroke. When the complexity of the ischemic cascade is considered however, the lack of success in the development of novel pharmacotherapies becomes more understandable as the number of potential pharmacological targets is quite staggering.

1.1.2 The ischemic cascade

The ischemic cascade describes the many molecular pathways initiated in the brain during stroke (Fig. 1). Following the disruption in blood flow to neural tissue, there is a sharp decrease in levels of vital molecules such as oxygen and glucose being delivered to neurons. This deprivation initiates three main ischemic pathways which lead to cell death: switch to anaerobic metabolism, failure of Na^+/K^+ and ATPase pumps, and initiation of stress signaling. The conversion from aerobic metabolism to anaerobic metabolism in neurons results in a marked increase in lactic acid production which initiates metabolic acidosis and leads to cell death. The quick depletion of ATP stores causes irreversible disruptions in the membrane electrochemical gradients leading to mass depolarization of cells and Ca^{2+} influx. This in turn, triggers an uncontrolled release of glutamate and glycine into the synapse. These activate post synaptic α-amino-3-hydroxy-5-methylsoxazole-4-propionic acid (AMPA) and *N*-methyl-D-aspartate

receptor (NMDAR) resulting in further Ca^{2+} influx and ultimately to the initiation of cell-death pathways. These include mitochondrial dysfunction, damage to DNA and cell membranes which trigger cytochrome release and caspase activation leading to apoptosis. Finally stress signals activate several microglia, astrocytes, and endothelial cells which induce oxidative stress *via* marked increase in reactive oxygen species (ROS) production (Khoshnam et al., 2017). This thesis specifically focuses on pharmacologically intervening at the beginning of the NMDAR-mediated pathway in the ischemic cascade.

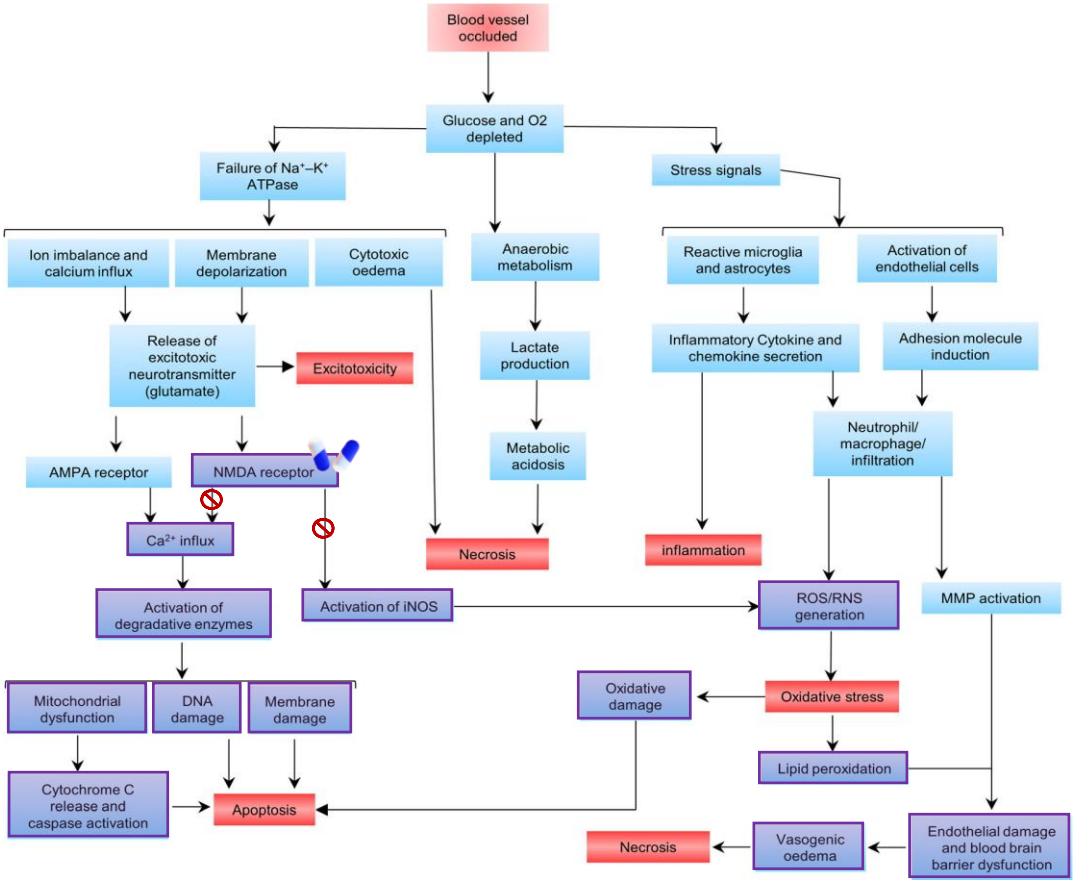

Fig. 1. *Adapted from Koshnam et al., 2017.* Depiction of the main pathways occurring in the ischemic cascade following disruption in blood flow to the brain due to stroke. Depiction of pathway discussed in this thesis is highlighted in purple.

1.1.3 Current treatment strategies

As previously mentioned, a universally administrable**,** efficacious pharmacotherapy for ischemic strokes does not currently exist. To this day, physicians are pharmacologically restricted to a single FDA/Health Canada approved thrombolytic, recombinant tissue plasminogen activator (rtPA) in acute cases, or low doses of aspirin in chronic, preventative cases (Arnett et al., 2019b). Although effective, these pharmacotherapies have significant disadvantages. rtPA has very stringent exclusion criteria as it carries a significant risk of intracerebral hemorrhaging (Hacke et al., 2008; National Institute of Neurological & Stroke rt, 1995). These criteria include a negative head CT and normal blood pressure values to rule out hemorrhagic stroke, onset of symptoms occurring less than 3-4.5 hrs ago, no recent history of anticoagulant or antiplatelet usage and an international normalized ratio (INR; measure of coagulation factors in the blood) below 1.7. This ultimately results in <4% of stroke patients being eligible to receive rtPA (Warlow et al., 2003). Should they be eligible, patients receive rtPA intravenously at a dose of 0.9mg/kg (not exceeding 90mg), whereby 10% of the dose is initially administered as bolus in 1min, and the remainder is infused over 60mins. Recently, Tenecteplase was shown to be non-inferior to alteplase (rtPA) in the treatment of stroke (Warach, Dula, & Milling, 2020). This genetically modified version of rtPA has increased affinity to fibrin, greater resistance to plasminogen activator inhibitor-1 and longer half-life. However, the risk factors associated with the usage of thrombolytics remain true.

Pharmacological prevention strategies also have their limitations. Chronic aspirin (81mg) regiments have been linked to significant irritation of the inner lining of the stomach leading to bleeding (Warlow et al., 2003) and short-term dual-antiplatelet therapy (DAPT) as a secondary stroke prevention measure may only be administered for the first 30 days post stroke (Arnett et al., 2019a). Alternative to pharmacotherapies, trained surgeons may perform endovascular

surgeries such as thrombectomies to physically remove or clear the obstruction from the affected cerebral vessel. Although this procedure has a much longer therapeutic window (6-12hrs), it is available at fewer hospital centers as it is technically difficult to perform and carries a risk of intracerebral hemorrhage in addition to surgical complications (Emberson et al., 2014). Furthermore, this procedure carries its own set of stringent exclusion criteria. Altogether, this highlights the immediate need for better preventative and acute treatment options for stroke.

1.1.3 Treatment research

1.1.3.1 The past

Prior to the discovery of rtPA, research into treatments was very limited and mainly aimed at managing post stroke symptoms. Since the discovery of rtPA in the late 1970's and implementation into the standard procedure of care for ischemic strokes in 1996 (Collen & Lijnen, 2009) following the ATLANTIS, ECASS, and NINDS clinical trials (Clark et al., 1999; Hacke et al., 1995; National Institute of Neurological & Stroke rt, 1995), there has been little progress in the development of novel pharmacotherapies (Ikonomidou, Stefovska, & Turski, 2000). This does not mean that there has not been research in this field, however. In fact, many compounds have been proposed and tested over the last 25 years, but they have not succeeded in clinical trials.

One important field of study to note is the work surrounding NMDAR-antagonists (NMDAR-A). Following the discovery that glutamate mediated excitotoxicity occurred during stoke, there was a surge in research investigating the possibility of blocking NMDARs to mitigate this excitotoxicity (Simon, Swan, Griffiths, & Meldrum, 1984). Multiple antagonists were designed to bind to the various binding sites located on the NMDAR (Fig. 2). These were extensively

assayed and showed promising degrees of neuroprotection in animal models. However, when these compounds were studied in clinical trials, patients largely showed no improvement with regards to overall post stroke outcome and often reported psychomimetic side effects. Taken together, this resulted in cessation of most studies investigating NMDAR based pharmacological compounds for stroke. This strategy likely failed due to the fact that these compounds completely blocked all NMDAR function despite this being crucial to normal, healthy neural transmission (Ikonomidou & Turski, 2002). Lipton (Lipton, 2004) describes a good analogy to help understand why this strategy ultimately failed by comparing NMDARs to volume knobs. In this scenario, the volume is analogous to the amount of ion influx through the receptor and NMDAR-As are compounds which completely turn off the volume. What is required to be effective however, is a compound which could reversibly turn down the volume, exclusively during ischemia and then turn it back up to normal levels following the ischemic event.

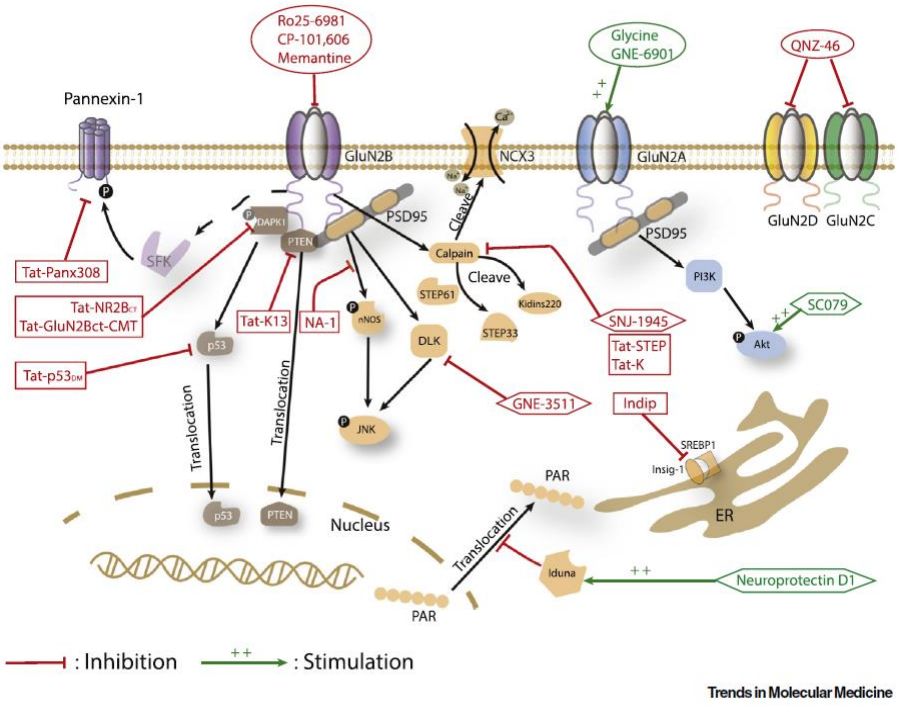

Fig. 2. *Adapted from Ge et al., 2020.* Depiction of the molecular targets of recent pharmacotherapies investigated for stroke treatment in both pre-clinical studies and clinical trials and the year they were published.

1.1.3.2 The present

These aforementioned trials revealed that the complete inhibition of NMDARs, by any means, is not a viable treatment option. However, NMDARs play a crucial role in the ischemic cascade and it seems premature to completely dismiss them as therapeutic targets as there exist many other ways to modulate their behaviour and downstream signaling pathways. One very recent and promising example demonstrating this is the ESCAPE-NA1 trial (Hill et al., 2020) which followed up on the ENACT trial (Hill et al., 2012) and impactful pre-clinical work (Cook, Teves, & Tymianski, 2012). These works demonstrated the possibility of utilizing a NMDAR-PSD-95-nNOS signaling pathway inhibitor to mitigate the downstream NMDAR-mediated excitotoxicity and showed that it was non-inferior to rtPA. This is an important development in acute stroke care. However, like many of the other novel pharmacotherapies tested in clinical trials, NA-1 was found to have important flaws. It was found that when administered after rtPA, NA-1 was subject to proteolytic cleavage which effectively nullified the previously observed beneficial effects (Mayor-Nunez et al., 2021; science translational medicine from Tymianski group).

1.1.3.3 The future

The work presented in this thesis also aims to pharmacologically disrupt the NMDAR-mediated excitotoxicity pathway. However, our strategy involves reducing the total number of NMDARs contributing to excitotoxicity rather than targeting one aspect of the signaling pathway as NA-1 did. Importantly, the use of glycine transporter 1 antagonists (GlyT1-A's) for stroke does not involve the direct antagonism of NMDARs and as our data will show, could be administered either chronically to the at-risk population or as an acute treatment administered shortly after the onset of symptoms. The following sections will describe how and why we tested the ability of

GlyT1-As to positively alter NMDAR behaviour specifically and temporarily during stroke and how this leads to a plethora of positive post stroke outcomes *in vivo*. Firstly, it is important to describe the receptors central to this thesis, NMDARs.

1.2 N-Methyl-D-Aspartate Receptors (NMDARs)

1.2.1 NMDAR: A general overview

NMDARs are one of the most extensively studied heterotetrameric ion channels belonging to the family of excitatory ionotropic glutamate receptors (iGluR). Excitatory synaptic strength throughout the CNS is regulated in large part by glutamate signaling and fluctuations in both the function and number of NMDARs at the synapse, along with other iGluRs, AMPAR and Kinate receptors (Hollmann, Boulter, Maron, & Heinemann, 1994). NMDARs are a unique subtype of iGluRs in that they are not activated through glutamate binding alone. For activation, NMDARs require a particular set of conditions: binding of co-agonist glycine (Johnson & Ascher, 1987; Kleckner & Dingledine, 1988) , or a glycine-like substance (D-serine) (Kleckner & Dingledine, 1988), to the glycine binding site (GBS) located on the GluN1 subunit, binding of glutamate to the GluN2 subunit, and depolarization of the cell to relieve a voltage-dependent Mg^{2+} block in the ion channel pore (Collingridge, Isaac, & Wang, 2004). The complex nature of these unique biophysical properties implicates the NMDAR in a number of both physiological and pathological functions.

NMDARs are encoded by a family of genes which give rise to a single GluN1 subunit (eight alternative splice variants), four variants of a GluN2 (GluN2*A*-*D*) subunit, and two variants of a GluN3 (GluN3*A*-*B*) subunit (Carroll & Zukin, 2002). These subunits are assembled in the endoplasmic reticulum (ER) and form a functional ion channel. Most commonly, two GluN1

subunits are paired with two GluN2 subunits, arranged around a central pore (Carroll & Zukin, 2002; Lau & Zukin, 2007; Paoletti & Neyton, 2007). The makeup and location of the NMDAR tetramers changes throughout development/aging across the nervous system in a highly regulated manner. While GluN1 subunits are uniformly expressed across the CNS, the GluN2 variants have specific regional distributions. Importantly, the composition of GluN2 subunits is in large part responsible for the overall NMDAR biophysical properties such as open probability, agonist affinity, and deactivation/decay kinetics (Hollmann & Heinemann, 1994). For example, NMDARs containing GluN2A subunits have the fastest decay, while GluN2D containing NMDARs have the slowest.

At the plasma membrane, NMDARs have an amino (N)-terminal extracellular domain, three transmembrane domains (M1, M3, M4), a re-entrant membrane loop (M2) which forms the pore region and connecting M1 and M3, and an intracellular carboxy (C)-terminal domain(Dingledine, Borges, Bowie, & Traynelis, 1999). The ligand binding domain (LBD) is a clamshell-like structure comprised of S1 and S2 domains which bind to the transmembrane domains M1 and M3/M4 respectively (Fig. 3).

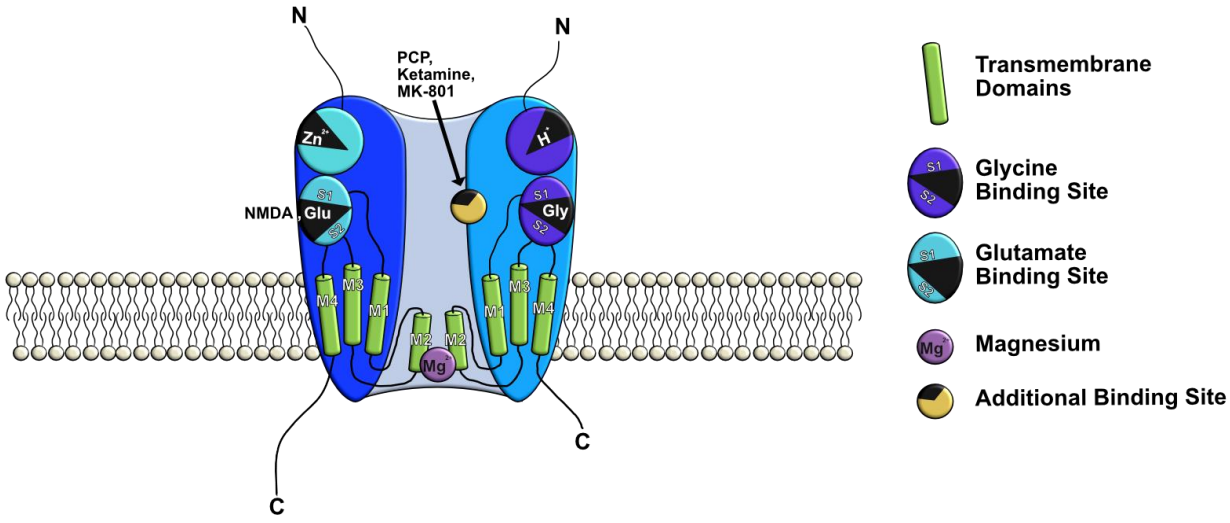

Figure. 3. Depiction of N-Methyl-D-Aspartate Receptor.

1.2.2 NMDARs: Binding sites and functions

NMDARs have multiple binding sites which are responsible for triggering various signaling cascades. Most notably are the GBS on the GluN1 subunit and the glutamate binding site on the GluN2 subunit. Once bound, NMDARs undergo conformational changes resulting in the opening of the pore and allowing non-specific influx of Ca^{2+} and Na^{2+} and efflux of K^{+} ions from the cell (Mayer, MacDermott, Westbrook, Smith, & Barker, 1987). Influx of Ca^{2+} into post synaptic cells initiates multiple intracellular cascades responsible for mediating both synaptic function and strength (L. Liu et al., 2004). This has been shown to be crucial in regulating long-term potentiation, long-term depression (LTP; LTD) and synaptic plasticity (Bannerman, Good, Butcher, Ramsay, & Morris, 1995). Dysregulation of NMDAR activity however, is known to be associated with pathological conditions such as schizophrenia, Alzheimer's disease (Lau & Zukin, 2007) and stroke. In fact, NMDARs play several roles in stroke pathology (Khoshnam et al., 2017).

1.2.3 Role of NMDARs in stroke

1.2.3.1 Excitotoxicity

NMDARs play an important role in excitotoxicity during stroke. Excitotoxicity describes the process by which NMDARs are overactivated by the release of large quantities of glutamate which triggers neuronal toxicity and/or death. Overactivation entails receptors remaining open for extended periods of time and results in a sustained ion influx, leading to abnormal signaling. This large release of glutamate is a result of three main events: release following depolarization, reversal of glutamate transporters (GluTs), and Ca^{2+} induced glutamate release. Together, this results in neuronal death occurring up to 4 days following stroke (Dirnagl, Iadecola, & Moskowitz, 1999; Ge, Chen, Axerio-Cilies, & Wang, 2020).

More specifically, ischemic conditions are characterized by sharp decreases in oxygen and glucose supply leading to the quick depletion of ATP in surrounding neurons. This causes immense disruptions to membrane ion gradients which triggers mass depolarization of cells resulting in excessive glutamate release. GluTs then begin to pump glutamate out into the synapse (rather than clear it) which in turn perpetuates excitotoxicity in neighbouring cells in a cascading fashion. NMDAR behaviour during stroke has been extensively studied and has been shown to initiate neuronal death or survival intracellular downstream pathways based on their localization as well as their subunit composition (Ge et al., 2020).

1.2.3.2 Subunit hypothesis

The NMDAR subtype hypothesis postulates that NMDARs comprised of GluN2A subunits contribute to neuronal survival and those comprised of GluN2B subunits are implicated in

neuronal death (Lai, Shyu, & Wang, 2011). This hypothesis has largely been accepted and even led to the development of subunit specific inhibitors. However, this hypothesis does not consider the contributions of the many other NMDAR subunit configurations (GluN3, GluN2C, GluN2D) which comprise 50% of NMDARs in the brain. Indeed, recent evidence suggests GluN3A subunits, most highly expressed in oligodendrocytes, contribute to cell death during ischemia (Micu et al., 2006). There has been mixed evidence reporting the involvement of GluN2C in both pro-death and pro-survival, and clearer evidence supporting the role of GluN2D in pro-death pathways (Doyle et al., 2018). This hypothesis also fails to acknowledge the temporospatial dynamic regulation of 2A/2B, and the triheteromeric GluN1-Glun2A/GluN2B NMDARs which are notoriously difficult to study (Stroebel, Casado, & Paoletti, 2018).

Nevertheless, an extensive body of literature suggests that specific antagonists of the GluN2B "pro death" subunit reduces neurotoxicity *in vitro* and *in vivo* but that antagonists of the GluN2A "pro-survival" subunit either have either no effect or exacerbate neurotoxicity (Y. Liu et al., 2007). This is thought to be due to specific motifs on the longer C-terminal domain (CTD) of the GluN2B subunit initiating a different set of downstream pathways. Despite this pre-clinical evidence, translating these findings into the human stroke population was again troublesome. Multiple compounds were screened in early phase clinical trials yet resulted in either negative or no beneficial effects in stroke patients (Y. Liu et al., 2007).

1.2.3.3 Localization hypothesis

The NMDAR localization hypothesis postulates that synaptic NMDARs are involved in pro-survival signaling while extrasynaptic NMDARs contribute to pro-death signaling. This hypothesis arose following the discovery that these two subsets of NMDARs are functionally

different in their ability to regulate synaptic plasticity: synaptic NMDARs mediating long-term potentiation LTP and extrasynaptic NMDARs mediating LTD. Interestingly, synaptic NMDARs have been found to be primarily comprised of GluN2A subunits while extrasynaptic NMDARs are mainly comprised of GluN2B subunits (Lai et al., 2011). This hypothesis gained much attention but continues to be questioned as more studies demonstrate that both synaptic and extrasynaptic are required to trigger pro-death downstream signaling pathways. In this case as well, despite pre-clinical evidence suggesting inhibiting extrasynaptic NMDARs may be beneficial for stroke outcomes, translating this information into the human stroke population was unsuccessful.

1.2.4 Endocytosis of NMDAR

The hypothesis our lab has been investigating is that fewer NMDARs present at the cell surface during an ischemic event may effectively minimize excitotoxicity and as such be beneficial to overall neuronal survival. To investigate this, we explored how to manipulate NMDAR endocytosis, or internalization, with temporospatial specificity.

NMDARs assembled in the ER are trafficked to the plasma membrane of postsynaptic glutamatergic synapses, together with AMPARs (O'Brien et al., 1998). Although NMDARs are largely considered to be stable components of the post synaptic membrane, they do undergo both constitutive and agonist-induced internalization *via* clathrin-mediated endocytosis (Nong et al., 2003; Nong, Huang, & Salter, 2004; Snyder et al., 2001; Vissel, Krupp, Heinemann, & Westbrook, 2001) albeit with a much slower turnover rate than AMPARs (Passafaro, Piech, & Sheng, 2001). Constitutive endocytosis occurs continuously and does not require activation of

the receptor by a ligand while agonist-induced endocytosis only occurs following ligand binding (Benmerah & Lamaze, 2007). Regardless of the reason it occurs, endocytosis of NMDARs is intrinsically involved in the regulation of several intracellular signaling cascades (Hoeller, Volarevic, & Dikic, 2005) as well as in the regulation of synaptic strength and maturity (Lau & Zukin, 2007).

NMDARs undergo endocytosis by first binding the μ1 or μ2 subunit of adaptor protein-2 (AP-2) (Schubert, Focking, Prehn, & Cotter, 2012) to a specific tyrosine-based internalization motif on the CTD of GluN2 subunits (YEKL 2B; YKKM 2A) (Roche et al., 2001). AP-2 is heterotetrameric protein comprised of the following tightly associated subunits: α-adaptin, β2 adaptin, μ1-2 adaptin, σ2 adaptin (Ochoa et al., 2000). These proteins resemble brick-like structures and are responsible for linking clathrin to the plasma membrane (Hirst & Robinson, 1998) and NMDARs with endocytotic motifs and lipid membranes (Rapoport et al., 1997). Next, clathrin binds to the β1 subunit of AP-2 as well as to other clathrin proteins to initiate the formation of a curvature in the membrane to create endocytotic pits. Clathrin is a three-legged triskeleta protein complex composed of three heavy (170kDa) and three light (33-35 kDa) chains (Owen, Vallis, Pearse, McMahon, & Evans, 2000). Following the formation of the clathrin-coated pit containing the receptor to be endocytosed, a GTPase dynamin protein severs the pit from the membrane to form a vesicle. More specifically, dynamin proteins are assembled into helical polymers and bind to the junction of the clathrin-coated pit and the plasma membrane. This complex undergoes a GTP hydrolysis-dependent conformational change which cleaves the junction and forms the endocytosed vesicle (Ferguson & De Camilli, 2012). Once endocytosed, NMDARs are either recycled to the ER or degraded by intracellular lysosomes (Fig. 4). Seeing

as NMDAR internalization is involved in the regulation of so many intracellular cascades, controlling NMDAR internalization may have important physiological and clinical implications, particularly if this internalization could be controlled during pathological states.

1.2.5 Glycine induced NMDAR internalization

Work from the Salter lab has demonstrated that it is indeed possible to trigger NMDAR internalization by priming the extracellular region with high levels of glycine (Nong et al., 2003; Nong et al., 2004). They showed for the first time that high levels of glycine induced internalization of NMDARs in a process they termed glycine induced NMDAR internalization (GINI) or glycine priming. This differs mechanistically from constitutive and agonist-induced internalization in that it is mediated by the A714 residue on the GluN1 subunit. This has important physiological and clinical implications, particularly in the context of this thesis.

Salter's group observed a significant decrease in evoked NMDAR-excitatory post synaptic currents (EPSCs) upon application of glycine to the cell (Nong et al., 2004). They suspected that this decrease was due to a decrease in surface NMDARs, as a result of internalization, as they did not detect any alterations in single channel conductance, mean open time or neuron integrity. This was first confirmed by ELISA readings demonstrating 30% of labelled NMDARs were internalized following glycine application. Their hypothesis was further confirmed as application of glycine in combination with an array of clathrin and/or dynamin inhibitors abolished the decrease in NMDAR-EPSC previously observed. They also revealed that GINI required binding and activation of glutamate and glycine to their respective binding sites to occur. Furthermore, Co-IP data indicated that pre-treating the extracellular solution with glycine significantly

increased co-precipitation of NMDARs with the AP-2 complex. This strongly suggested that glycine primed the receptors for internalization following activation by glycine and glutamate (Nong et al., 2003; Nong et al., 2004).

They went on to describe the specific amino acid responsible for glycine priming by investigating phenotypes of HEK293 cells transfected with GluN1.A714L/GluN2*A/B*. Here, they substituted alanine, at the 714th position, located within the ligand-binding domain of the GluN1 subunit, for a leucine (Han, Campanucci, Cooke, & Salter, 2013). As previously described, GluN1's LBD has a clamshell-like structure comprised of the S1 and S2 domains. Upon binding of glycine, S1 and S2 come together to form a closed clamshell shape which ultimately leads to conformational changes resulting in the recruitment of AP-2. When both glycine and glutamate are bound, the closing of their respective binding sites results in a cascade of conformational changes leading to the opening of the channel. In GluN1.A714L subunits, proper closure of the clamshell following glycine binding is disrupted and the subsequent conformational change required to bind AP-2 does not occur. This ultimately results in glycine priming to be abolished and the receptors not being able to undergo internalization.

Although this was a ground-breaking contribution to the field of NMDARs and glycine, the physiological relevance of their work was critiqued as it was largely assumed that such levels of glycine would never accumulate at the synapse since glycine transporter-1 (GlyT1s) maintain synaptic glycine levels so low. The work presented in this thesis shows that high levels of glycine may in fact be achieved *in vivo*. Indeed, when GlyT1-As are administered prior to stroke, the additional release of glycine during stroke results in levels of brain glycine elevated enough to trigger GINI *in vivo.* To further explain how these levels of glycine are achieved, it is important to understand the role of glycine in the CNS and how it is regulated by glycine transporters.

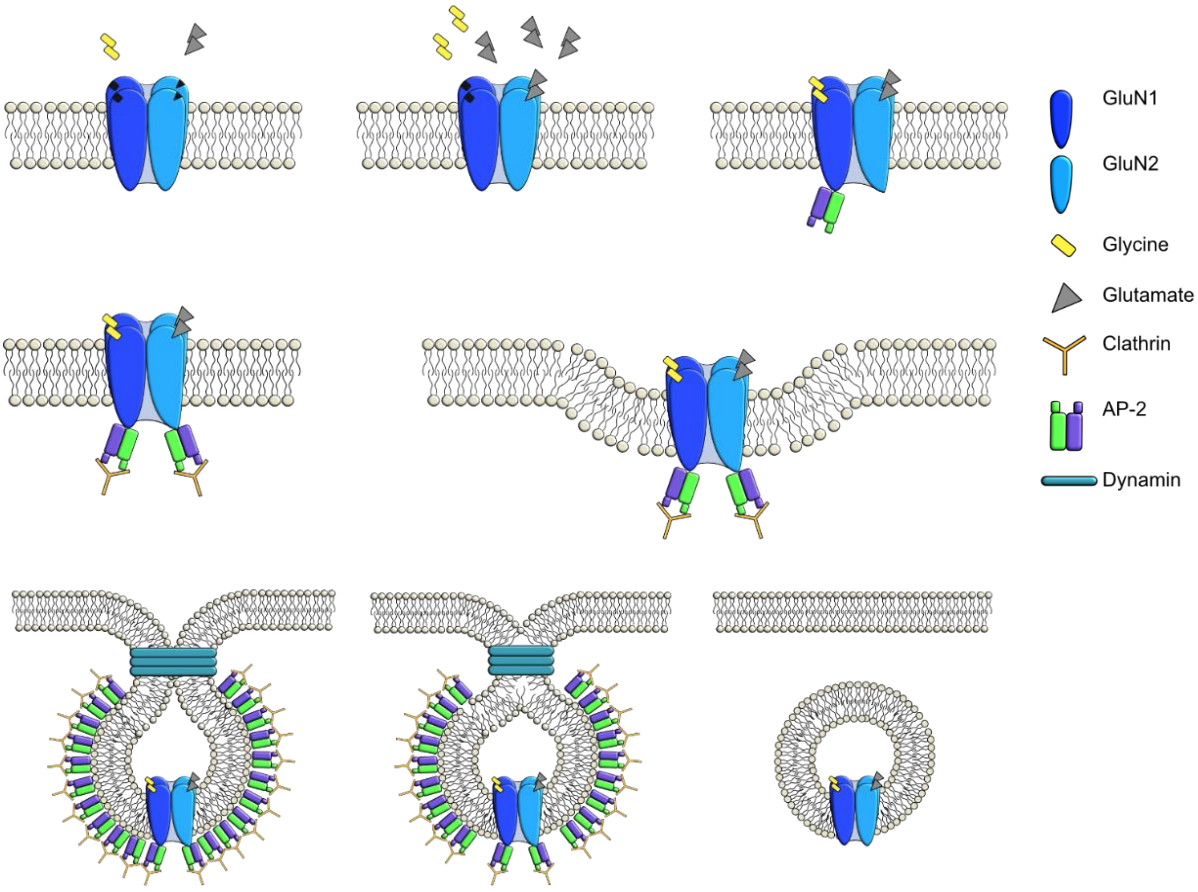

Fig. 4. *Adapted from Nong et al., 2004.* Depiction of clathrin-mediated, glycine-induced NMDAR internalization (GINI).

1.3 Glycine

1.3.1 Glycine as an inhibitory neurotransmitter

Glycine is the simplest of the amino acids yet plays many important roles in the CNS including protein synthesis and neurotransmission. However, glycine, along with GABA, are primarily known as inhibitory neurotransmitters in the CNS (Bowery & Smart, 2006). Through it's binding to the strychnine-sensitive glycine-A site on glycine receptors (GlyRs), glycine induces hyperpolarization of post-synaptic glutamatergic neurons by increasing Cl^- conductance. This results in an overall inhibitory effect to quickly cease excitatory neurotransmission (Hernandes & Troncone, 2009).

Glycine was first hypothesized to be a neurotransmitter following the observation that glycine levels were much higher in the spinal cord than in the rest of the CNS (Aprison & Werman, 1965). Glycine was then shown to be distributed in a manner which colocalizes with spinal interneuron terminals (Curtis, Hosli, & Johnston, 1967) and synthesized (Shank & Aprison, 1970) and released (Hopkin & Neal, 1970) from spinal cord neurons following stimulation. These key observations ultimately led to glycine being accepted as an inhibitory neurotransmitter in the late 1970s.

Functionally, glycine-mediated inhibitory transmission plays essential roles in voluntary motor control, sensory processing, reflex responses, auditory, cardiovascular, and respiratory functions when released in the medulla, brainstem, and spinal cord (Hernandes & Troncone, 2009). In the medulla, glycinergic Ia interneurons inhibitory neurotransmission by blocking stretching reflexes which results in the relaxation of antagonistic muscles and coordination of agonistic muscles. In

the spinal cord, glycine modulates Renshaw interneuron's ability to control the excitability of alpha motor neurons *via* recurrent inhibition by negative feedback (Wilson & Talbot, 1963). Due to the important nature of these roles, glycine release is tightly regulated but is ultimately a Ca^{2+}-dependent occurrence (Saransaari & Oja, 2009). Although mainly present in the brainstem and spinal cord, glycine acts as an inhibitory neurotransmitter throughout the entire brain.

1.3.2 Glycine as an excitatory neurotransmitter

Although glycine had long been thought to be solely implicated in inhibitory neurotransmission, it is now known to play an important role in excitatory neurotransmission, primarily *via* binding to the glycine-B site on NMDARs. Johnson & Ascher (Johnson & Ascher, 1987) were the first to show that glycine potentiated NMDAR response in murine cultured cortical neurons and Kleckner & Dingledine (Kleckner & Dingledine, 1988) confirmed its role as an obligatory co-agonist of the NMDAR the following year. Johnson & Ascher's work ultimately changed our understanding of both glycine and synaptic communication in the CNS. Their work evaluated the effect of an array of amino acids on NMDAR currents evoked by either NMDA (10μM) or glutamate (10μM) stimulation, using whole cell and single channel patch-clamp recordings. They discovered that at doses as low as 1μM, glycine enhanced potentiation of NMDARs (Fig. 5a, b) and that this response was not blocked by the GlyR antagonist strychnine (Fig. 5c). Furthermore, application of 1μM glycine resulted in a marked increase in NMDAR open probability (P_{open}) as recorded in an outside-out patch (e). Interestingly, glycine can also act as an excitatory neurotransmitter through its binding to GlyRs, although only in specific conditions (Hernandes & Troncone, 2009).

1.3.3 Glycine transporters: synaptic glycine regulation

Glycine levels are tightly regulated and maintained by two glycine transporters (GlyTs): glycine transporter type 1 (*GlyT1a-e*) and glycine transporter type 2 (GlyT2*a-c*). These transporters both belong to the SLC6 family of Na^+/Cl^- dependent neurotransmitter transporters and colocalize with NMDAR expression patterns in the brain (Smith, Borden, Hartig, Branchek, & Weinshank, 1992). GlyT1 and GlyT2s located at the plasma membrane to allow for influx of glycine, Cl^- and x2, $x3Na^+$ ions, respectively. They play an important role in inhibitory and excitatory neuronal transmission and have implications in several pathological conditions, namely hyperekplexia, neuropathic pain, schizophrenia, and stroke.

Although they share roughly 50% homology in DNA sequences, they are differentially expressed across the CNS (Guastella, Brecha, Weigmann, Lester, & Davidson, 1992) and have distinct roles (Smith et al., 1992). While GlyT1s are predominantly expressed in the hypothalamus, thalamus, diencephalon, retina, olfactory bulb (Zafra, Aragon, et al., 1995; Zafra, Gomeza, Olivares, Aragon, & Gimenez, 1995), cortex and hippocampus (Smith et al., 1992), GlyT2s are mainly expressed in the spinal cord, brainstem, and cerebellum (Borowsky, Mezey, & Hoffman, 1993). Both transporters were long thought to be solely expressed in glial cells but are now known to be expressed in neurons as well (Fig 6).

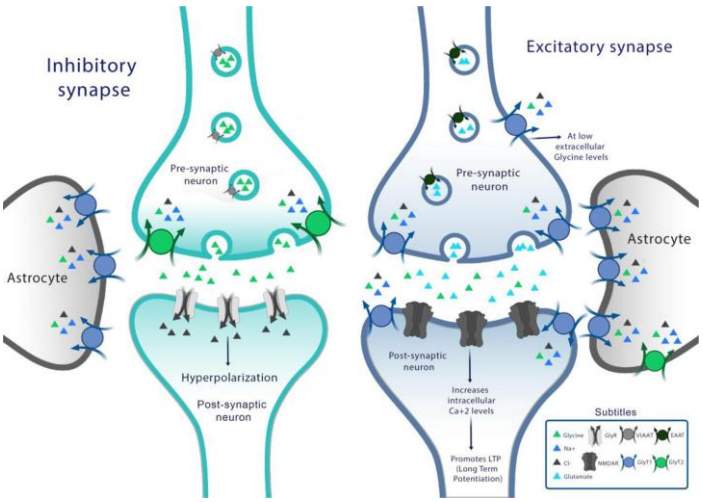

Fig. 6 *Adapted from Marques et al. 2020.* Depiction of GlyT1 and GlyT2 localization in astrocytes and neurons.

GlyT1s are typically involved in excitatory, glutamatergic transmission but play distinct roles based on their localization. GlyT1s located on glia clear glycine from the synaptic cleft in order to cease glycine-mediated inhibitory transmission. GlyT1s expressed in glutamatergic neurons regulate levels of glycine at synapses containing NMDARs, mediating excitatory transmission (Betz, Gomeza, Armsen, Scholze, & Eulenburg, 2006; Eulenburg & Gomeza, 2010). GlyT2s primarily mediate the re-filling of pre-synaptic vesicles. Interestingly, GlyT1s do not only take up excess glycine; in conditions where intracellular glycine or Na^+ (H. Huang, Barakat, Wang, & Bordey, 2004) concentrations are high, GlyT1s can reverse to release glycine into the synapse (Marques et al., 2020).

Under physiological conditions, extracellular glycine concentrations have been measured in the low nanomolar. The affinity of glycine to the GBS (on GluN1) is estimated to be 0.1-0.3μM (Danysz & Parsons, 1998) and the EC50 values range from 0.2 ± 1.7 mM, depending on the

GluN2 variant present in the NMDAR (Hollmann & Heinemann, 1994). Since glycine levels have been measured to be 5-10μM in the cerebrospinal fluid, it was long assumed that the GBS was perpetually saturated. However, when glycine transporter-1 (GlyT1) was cloned (Guastella et al., 1992; Smith et al., 1992) and GlyT1 specific antagonists were utilised, this hypothesis was quickly refuted because a robust potentiation of NMDAR-EPSCs in CA1 (Bergeron, Meyer, Coyle, & Greene, 1998) acute slice, whole-cell recordings was observed. It has since been understood that GlyTs maintain glutamatergic synaptic concentrations of glycine well below saturating levels of the GBS on the NMDAR (Coyle & Tsai, 2004).

Data from various transgenic mouse lines support observations of function of these transporters. In mice constitutively lacking either GlyT1 or GlyT2, extreme disruption to inhibitory and excitatory glycinergic signaling results in death at age P1-P3. In mice lacking GlyT1, neurotransmission is severely disrupted as glycine cannot be cleared from synapses (Coyle & Tsai, 2004). This causes a prolonged inhibition which results in death. In mice lacking GlyT2, neurotransmission is severely disrupted as pre-synaptic glycine vesicles cannot be refilled meaning these mice have no way of ceasing excitatory neurotransmission which is lethal (Gomeza et al., 2003). Specific knockout of astrocytic GlyT1 is also lethal as these mice also have no way to clear excess glycine resulting in sustained inhibition, particularly of respiratory centers in the brainstem. Interestingly, mice with a 50% reduction of GlyT1 expression ($GlyT1^{+/-}$) are healthy and normal but exhibit higher than normal brain glycine levels (Coyle & Tsai, 2004; Harvey & Yee, 2013). For this reason, we utilized these mice in many experiments. In the context of this thesis, we mainly focus on GlyT1's function in both physiological and pathological conditions as they are predominantly expressed in the cortex. Given GlyT1's

important roles in the CNS and in various pathological conditions, compounds aiming at inhibiting them have been extensively studied as potential pharmacotherapies.

1.4 Glycine Transporter-1 Antagonists (GlyT1-As)

1.4.1 History of use

GlyT1-As are a class of drugs which selectively inhibit GlyT1's and result in a marked increase in extracellular synaptic glycine levels in the brain. The use of GlyT1-As was first popularized in the late 1990s and early 2000s, in parallel to the emergence of the glutamate hypothesis of schizophrenia. This hypothesis postulated that several of the symptoms observed in schizophrenia were as a result of hypoactive NMDARs (Cioffi, 2018). Supporting this hypothesis was extensive pharmacology demonstrating that blocking NMDARs with compounds such as ketamine or PCP mimicked symptoms of schizophrenia. Since it was known that glycine could potentiate NMDARs (Bergeron et al., 1998; Johnson & Ascher, 1987), it was thought that elevating glycine levels *via* the administration of GlyT1-As, could increase NMDAR function and therefore attenuate symptoms of schizophrenia (Cioffi, 2018). This enhanced potentiation and the increase in open probability of NMDARs would only occur following depolarization to relieve the voltage dependent Mg^{2+} block giving this compound increased specificity and sensitivity. Therefore, prolonged and sustained activation of NMDARs results in seizures, psycho-mimetic symptoms and is ultimately cytotoxic (Harvey & Yee, 2013) never occurs.

The first GlyT1-A to be widely used in clinical trials was sarcosine, a weak but selective antagonist. Sarcosine had some effect in treating specific aspects of schizophrenia such as negative symptoms and cognitive deficits (Lane et al., 2008). These positive results encouraged many other research groups to develop and test a structurally diverse set of GlyT1-A's which

have varying degrees of specificity and competitivity for the glycine binding site of GlyT1 (Cioffi, 2018). One of the first sarcosine-based inhibitors to be reported was in fact the compound we have used in this thesis: (±)-N-[3-(4′-fluorophenyl)-3-(4′-phenylphenoxy)propyl]sarcosine (NFPS) (Bergeron et al., 1998)).

1.3.3 As a novel treatment strategy for ischemic stroke

Although it was originally hypothesised that elevating glycine levels *via* the administration of GlyT1-As increased NMDAR function (Cioffi, 2018), work outlined in this thesis has demonstrated that NMDARs actually undergo internalization. Given the literature suggesting that elevation of glycine levels can result in NMDAR internalization (Nong et al., 2003), the importance of the NMDAR in the ischemic cascade (Khoshnam et al., 2017), and the safety of GlyT1-As in humans (Harvey & Yee, 2013), we aimed to investigate utilising GlyT1As in the context of stroke. Indeed, no adverse reactions were reported following a number of studies involving GlyT1s administered at various doses and for various time periods (Harvey & Yee, 2013). It should be noted that motor and respiratory side effects are possible, yet unlikely to occur at therapeutic doses (Kopec et al., 2010). Pharmacotherapies targeting the NMDARs for stroke have thus far failed in clinical trials, therefore utilising GlyT1-As could effectively be a novel strategy. This is because rather than blocking NMDARs, GlyT1-As dampen NMDAR-mediated excitotoxicity exclusively during ischemia in a dynamic and reversible manner.

2. HYPOTHESIS

Elevating brain glycine levels, *via* administration of a GlyT1-A, induces GINI during ischemic events and provides neuroprotection.

3. OBJECTIVES

1. Assess the effect of NFPS on post-stroke motor behavioural outcomes
2. Assess whether NFPS acts *via* GINI
3. Assess the effect of NFPS on post-stroke cognitive outcomes
4. Assess the effect of NFPS on post-stroke vascular outcomes

4. MATERIAL AND METHODS

4.1 Animals

4.1.1 Animals

All procedures in this study were carried out on female and/or male 8–10-week-old mice in accordance with the guidelines of the Canadian Council on Animal Care and approved by the University of Ottawa Animal Care Committee. The following transgenic mouse lines were utilized: The heterozygous glycine transporter type 1 ($GlyT1^{+/-}$), and the serine racemase knockout ($SR^{-/-}$) along with their wild-type (WT) litter mates (on C57Bl/6;S129 backgrounds). $GlyT1^{+/-}$ (G. Tsai et al., 2004) and $SR^{-/-}$ (Basu et al., 2009) mice were generated by Dr. Coyle's laboratory at the Harvard Medical School. *In vivo* behavioural experiments were performed on C57Bl/6 wild type (WT) mice from Charles River ®. Animals were housed under standard conditions and had access to chow and water *ad libitum*.

4.2 Pharmacology

4.2.1 NFPS preparation

N-[3-([1,1-Biphenyl]-4-yloxy)-3-(4-fluorophenyl)propyl]-*N*-methylglycine (NFPS; Tocris) was injected intraperitoneally (*i.p.*) into C57Bl/6 mice either 24hrs prior to stroke, or 10mins/30mins/60mins/120mins post-stroke, at a dose of 5mg/kg. NFPS was made as a stock solution of 8mM in DMSO, and then diluted to 1.27mmol with sterile 0.9% sodium chloride. Vehicle control solution was prepared in the same way with the volume of stock NFPS substituted for DMSO and then diluted in 0.9% sodium chloride.

4.3 Surgical procedures

4.3.1 Photothrombotic stroke

Photothrombotic stroke (PT) was induced as described by (J. K. Lee et al., 2007), adapted from (Watson, Dietrich, Busto, Wachtel, & Ginsberg, 1985). Mice were anesthetized with 2.5% isoflurane in O_2 and mounted onto a stereotaxic frame. Once anesthetized, a dose of 10mg/ml of Rose Bengal (Tocris) was injected intraperitoneally (*i.p.*). Immediately following the injection of the dye, a small portion of skin on the head of the animal was cut and retracted along the midline of the sagittal plane in order to expose bregma. Using the stereotaxic device, a 520nm laser (~20mW; Beta Electronics) was positioned 3cm above the sensorimotor cortex (+0.7 AP, +2.0 ML) and turned on for 10mins. The incision was closed using Vetbond (3M) tissue adhesive and animals were administered a dose of 2% bupivacaine (Chiron Compounding Pharmacy Inc.) transdermally immediately following the procedure, as well as 4 to 6hrs later.

4.3.2 Cortical endothelin-1 stroke

Cortical endothelin-1 (ET-1) strokes were induced as previously described (Wang, Jin, & Greenberg, 2007). Mice were anesthetised with 2.5% isoflurane in O_2 and mounted onto a stereotaxic frame. A small portion of skin on the head of the animal was cut and retracted along the midline of the sagittal plane in order to expose the cranium and allow for visualisation of the main cranial sutures. For cortical strokes, injection site coordinates (from bregma) were: 1) AP +0.0, ML +2.0, DV -1.6; 2) AP +0.2, ML +2.0, DV -1.4; 3) AP +0.4, ML +2.0, DV -1.3. Using the stereotaxic device, a craniotomy was performed at each site prior to injecting 1uL of 2µg/µL human, porcine ET-1 (Abcam) dissolved in 2.7µg/µL L-NAME (Abcam) over 5mins, with a 28G 10µL Hamilton syringe to induce a transient ischemic stroke (Wang, Jin, & Greenberg, 2007). The incision was closed using Vetbond (3M) tissue adhesive. Animals were administered

a dose of 2% transdermal bupivacaine (Chiron Compounding Pharmacy Inc.), as well as 0.1mg/kg buprenorphine subcutaneously immediately following the procedure as well as 4 to 6hrs later. Mice were observed 24hrs after the procedure and administered 2% transdermal bupivacaine as necessary.

4.3.3 Intracranial cortical injection of Adeno Associated Virus (AAV)

Mice were anesthetized with 2.5% isoflurane in O_2 and mounted onto a stereotaxic apparatus. A small portion of skin on the head of the animal was cut and retracted along the midline of the sagittal plane in order to allow for visualisation of the cranial sutures. Using the stereotaxic device, a 28G 10µL Hamilton syringe was positioned at bregma and from its coordinates, two injection points were measured: 1) AP +1.2, ML +2.0, DV -0.5; 2) AP +0.2, ML +2.0, DV -0.5. These coordinates were selected to ensure transduction of cells in and around the PT stroke region. Once the needle had been placed at the correct coordinates, a craniotomy was performed below each of the two injection sites. Subsequently, 0.5µL of 10^{-12} PFU/ml (plaque forming units) of either AAV-WT-GluN1 or AAV-A714L-GluN1 were injected over 5mins at each site at a rate of 0.1µL/min. After 3mins, the needle was removed from the brain and inserted into the next infection site. The incision was closed using Vetbond (3M) tissue adhesive. Animals were administered a dose of 2% transdermal bupivacaine (Chiron Compounding Pharmacy Inc.), as well as 0.1mg/kg buprenorphine subcutaneously 4–6hrs following the procedure.

4.3.4 Medial pre-frontal cortex endothelin-1 stroke

Medial pre-frontal cortex (mPFC) endothelin-1 (ET-1) strokes were induced with slight modifications (Vahid-Ansari, Lagace, & Albert, 2016). Mice were anesthetised with 2.5% isoflurane in O_2 and mounted onto a stereotaxic frame. A small portion of skin on the head of the

animal was cut and retracted along the midline of the sagittal plane in order to expose the cranium and allow for visualisation of the main cranial sutures. For cortical strokes, injection site coordinates (from bregma) were: 1) AP +2.0, ML +0.5, DV -2.4; 2) AP +2.0, ML +0.5, DV -2.6. Using the stereotaxic device, a craniotomy was performed at each site prior to injecting 0.5uL of 2µg/µL human, porcine ET-1 (Abcam) dissolved in water at a rate of 0.2µl/min, with a 28G 10µL Hamilton syringe to induce a transient ischemic stroke. The incision was closed using Vetbond (3M) tissue adhesive. Animals were administered a dose of 2% transdermal bupivacaine (Chiron Compounding Pharmacy Inc.), as well as 0.1mg/kg buprenorphine subcutaneously immediately following the procedure as well as 4 to 6hrs later. Mice were observed 24hrs after the procedure and administered 2% transdermal bupivacaine as necessary.

4.3.5 2 Vessel occlusion model of global ischemia

Global ischemia was induced using the 2-vessel occlusion model (2VO) (Jiwa, Garrard, & Hainsworth, 2010; Pontarelli, Ofengeim, Zukin, & Jonas, 2012; Yang, Kimura-Ohba, Thompson, & Rosenberg, 2016). 2VO was performed aseptically in a sterile field, under a microscope. The animal was placed supine in the sterile surgical field, where a midline incision in the neck was made with scissors. The thyroid glands were separated onto their respective sides with Q-tips to allow visualization of the oesophagus. The left common carotid artery was isolated from the vagus nerve and surrounding tissue before a 6-0 polypropylene filament was placed below the carotid artery to allow quick localization of the artery. The same procedure was repeated on the right common carotid artery. Once both carotid arteries had been isolated, they were occluded with vascular clamps (FST) for 30 mins. Following the occlusion, clamps were removed, and the incision was closed with 1-2 surgical autoclips. Animals were administered 0.1mg/kg buprenorphine subcutaneously one hour prior to surgery as well as at 6hrs post surgery. A dose

of 2% transdermal bupivacaine was also administered over the incision at close. Surgical autoclips were removed one-week post surgery.

4.3.6 Laser doppler flowmetry and photothrombosis

Laser Doppler Flowmetry (LDF) recordings following PT were done as described by (Toussay, Tiberi, & Lacoste, 2019). Mice were anesthetized with an *i.p.* injection of 0.01ml/g of a cocktail consisting of 120mg/kg ketamine and 10mg/kg xylazine, then mounted onto a stereotaxic apparatus. Following a small incision to expose the skull, the laser probe (Transonic Systems) was positioned above the thinned skull, over sensory motor cortex (+0.7AP; +2.0ML) and recorded baseline activity for 5mins. The laser probe was replaced with a 520nm laser (~20mW; Beta Electronics) to induce PT stroke, as described above. Following PT, the laser probe was removed, and recordings were performed for an additional 30mins. The incision was closed using Vetbond (3M) tissue adhesive and animals were administered a dose of 2% bupivacaine (Chiron Compounding Pharmacy Inc.) transdermally immediately following the procedure, as well as 4 to 6hrs later.

4.4 Histology and microscopy

4.4.1 Brain tissue preparation

For both Cresyl Violet (CV) and FluoroJade C (FJC) staining, brains were processed as follows. Forty-eight hours post-stroke, mice were deeply anesthetized with 5% isoflurane in O_2 and then transcardially perfused with 1X PBS, followed by 4% PFA in 1X PBS. Brains were collected and post-fixed in 4% PFA in 1X PBS overnight and then incubated in increasing concentrations of sucrose in 1X PBS (15% and 30%) until they sank to the bottom of the falcon tube. Brains were embedded in Cryomatrix (Shandon) then frozen in -80°C 2-methylbutane (Sigma Aldrich)

for 3mins and stored at -80°C. Serial 25µm thick coronal sections were cut on a cryostat (Microm HM500) at -25°C, collecting sections at 500µm intervals onto positively charged Superfrost Plus Microscope Slides (Fisher Scientific).

4.4.2 Quantification of stroke volume - Magnetic resonance imaging

In vivo mouse brain MRI was performed at the University of Ottawa pre-clinical imaging core using a 7 Tesla GE/Agilent MR 901. Mice were anaesthetized for the MRI procedure using isoflurane in O_2: induction at 3%, maintenance at 1.5% . A 2D fast spin echo sequence (FSE) pulse sequence was used for the imaging, with the following parameters: slice thickness = 0.5mm, spacing = 0mm, field of view = 2.5cm, matrix = 256 x 256, echo time = 41ms, repetition time = 7000ms, echo train length = 8, bandwidth = 16 kHz, fat saturation. Stroke lesions demonstrated hyperintensity.

4.4.3 Quantification of stroke volume - Triphenyltetrazolium chloride

Stroke volume quantification was performed using triphenyltetrazolium chloride (TTC; Sigma; (Benedek et al., 2006; Hatfield, Mendelow, Perry, Alvarez, & Modha, 1991), which stains all live tissue bright red, while leaving dead tissue white. Forty-eight hours post-stroke, mice were deeply anesthetized with 5% isoflurane in O_2 before decapitation. Brains were removed and placed on a vibratome (Leica) in cold ACSF to be sliced into 0.5mm thick coronal slices. Slices were incubated in 2% TTC at 37°C for 10-15mins, then transferred to 4% PFA at 4°C. To measure stroke volume, brain slices were imaged on the Zeiss Stereo Discovery V20 stereo microscope at 1X magnification from both sides.

4.4.5 Quantification of stroke volume - Cresyl violet

Cresyl violet (CV) staining was accomplished by first immersing 25uμm thick slices mounted on Superfrost Plus Microscope Slides (Fisher) in xylene for 5mins and then slowly rehydrated in decreasing concentrations of ethanol (95% EtOH for 5mins and 70% EtOH for 3mins) before being placed in double distilled water (ddH_2O) for 3mins. Once rehydrated, slides were stained with CV solution for 6-8mins and then placed in ddH_2O for 3mins. Following this step, slides were slowly dehydrated in increasing concentrations of ethanol (70% EtOH for 2 mins, 95% EtOH for 1min, 100% EtOH - 2 dips) before being immersed in xylene for 5mins. Slides were then removed from xylene and mounted with DPX mounting media. Images of CV-stained slices were acquired with the EVOS FLAuto2 inverted epifluorescence microscope at 10X magnification and a transillumination light source.

4.4.6 Stroke volume measurements and analysis

Surface area of the infarct regions in the 0.5mm thick TTC stained slices were measured for each slice on Fiji (ImageJ.com) and multiplied by the thickness of the slice to obtain a final volume. For CV-stained slices, surface area of the infarct regions was multiplied by the distance between each collected slice (500μm) to obtain a volume. The sum of all slices was used to obtain a final stroke volume per brain. For CUBIC cleared brains imaged with the light sheet microscope, infarct volume was automatically measured using a deep learning segmentation model (see below for more information).

4.4.7 Quantification of neuronal loss - FluoroJade C

FluoroJade C (FJC; EMD Millipore) staining was done as described by (Ehara & Ueda, 2009**)**. 25um thick slides were first immersed in 80% ethanol in 1% sodium hydroxide solution for 5mins. Following this step, slides were transferred to 70% ethanol for 3mins and then to ddH_2O for 3mins before being incubated in a 0.06% potassium permanganate ($KMnO_4$; Sigma Aldrich) solution for 10mins. Slides were rinsed in ddH_2O for 1.5min before incubation in a 0.0001% FJC solution dissolved in 0.1% acetic acid (in water) and combined with 0.0001% DAPI (Santa Cruz Biotechnology). Following this, slides were rinsed in ddH_2O and left to air dry for 3 to 4hrs. Once dry, slides were immersed in xylene for 1min and mounted with FluoroMountG (Sigma Aldrich). Slides were imaged with the *Zeiss AxioObserver Z1* inverted epifluorescence microscope using 10X magnification and GFP (488/509nm) and DAPI (359/461nm) filters.

4.4.8 Quantification of neuronal loss - FluoroJade C analysis

Analysis of the total number of degenerating neurons was performed using IMARIS (Bitplane). IMARIS was set to detect and count all green (representing degenerating neurons) and blue (representing nuclear DNA) spots on each image and then calculate how many green and blue spots were colocalized. The cells having been tagged by both DAPI and FJC were counted as FJC positive neurons. Following analysis, each image was manually verified for any false positives and/or false negatives, which were then removed and/or added accordingly.

4.4.9 Immunohistochemistry

Mice were deeply anaesthetized with 5% isoflurane in O_2 and intracardially perfused with 4% (w/v) paraformaldehyde (PFA) in phosphate buffered saline (PBS). The brain was removed,

incubated in sucrose, then frozen in -30°C isopentane before 50μm thick coronal slices were cut with a cryostat (Leica CM 3050S, Houston, TX, USA). Antigen retrieval was performed in 10mM citric acid buffer at 95°C for 15mins. All slices were washed 3x for 5mins in PBS, before being blocked and permeabilized for 4x 10mins in 0.5% Bovine gelatin + 0.2% Triton X-100 in 1xPBS (PBS-GT). Slices were incubated in primary antibodies in PBS-GT for 48hrs at room temperature. Slices were then blocked for 4x 10mins in PBSGT before being incubated in secondary antibodies for 1hr at room temperature. Following this, slices were rinsed, air dried overnight, then mounted onto slides with FluoromountG mounting media.

4.5 A714L mutation generation, viral packaging, and quantification

4.5.1 Generation of WT and A714L constructs

We amplified the GluN1 coding region from the SuperEcliptic Phlourin (SEP)-tagged GluN1 construct (Addgene #23999) with the primer pairs NheIGluN1-F and EcoRVGluN1-R using the high-fidelity polymerase, Phusion (NEB). The PCR product was then cloned into pDrive (pDrive cloning vector, Qiagen). We used this as a template to create a shRNA resistant GluN1 using primers GluN1Shres2-F and GluN1 Shres2R following the standard site directed mutagenesis with Phusion (NEB) (Table 2). We then created A714L mutant clone again using site-directed mutagenesis with the primer pairs A714L-F and A714L-R. Briefly, the site-directed mutagenesis was performed using Phusion following the manufacturer's instructions. The PCR product was then digested with DpnI to specifically target the template DNA. Next, the PCR product was ligated and transformed into stbl3 cells (NEB). We verified the entire coding sequence of GluN1 in the GluN1-WT and the GluN1-A714L clones for the desired mutations (Table 2). We additionally constructed a shRNA resistant GluN1 as we had envisaged using GluN1 shRNA to

inhibit the effect of WT GluN1 molecules *in vivo*. However, we found a robust behavior and GINI phenotype in *ex vivo* slices without the use of shRNA. Therefore, we did not utilise it.

4.5.2 Sub-Cloning into pcDNA3.1

The GluN1-WT and GluN1-A714L inserts were prepared by digesting the pDrive clones (GluN1-WT, GluN1-A714L) with NheI and BamHI, and gel isolated. The vector was prepared by digesting pcDNA3.1 vector (Addgene #82612) with NheI and BamHI to drop out the mCherry and then gel isolated. The inserts and the vector were then ligated, and the ligation product used to transform stbl3 cells (NEB). These clones had the GluN1 gene variants with a CMV promoter. The constructs were transiently transfected into HEK293t cells along with an equimolar ratio of GluN2A. Whole-cell patch-clamp recordings were performed on these HEK293 cells 24–48hrs after transfection using TransIT2020, demonstrating that this construct results in functional NMDARs.

4.5.3 *In vivo* viral constructs

The pDrive GluN1-WT and GluN1-A714L clones were sub-cloned into the pAAV vector, CW3SL, tagged with GFP (Addgene #61463). The CW3SL vector was digested with EcoRI, blunt ended and then subsequently digested with NheI to drop out the eGFP. The vector was then gel isolated. The insert fragment was derived by digesting the pDrive clones with NheI and EcoRV, followed by gel isolation and was then ligated to the vector. This resulted in constructs in which GluN1 was driven off the CamKIIa promoter; stbl3 cells were transformed with the ligation product, which was then verified for the integrity of the ITR sites by a diagnostic digest

using SmaI (each of the ITR sites contained two SmaI sites). Viral constructs were packaged with plasmid AAV2/9 at the University of Laval.

4.5.4 Viral spread quantification

Three weeks following cortical infection, mice were deeply anesthetized with 5% isoflurane and then transcardially perfused with 1X PBS, followed by 4% PFA. Brains were collected and post-fixed in 4% PFA overnight then sliced at 500um the next day with the vibratome (Leica). Slices were cleared according to the SeeDB protocol (Ke, Fujimoto, & Imai, 2013) which involved incubations in increasing concentrations of fructose α-thioglycerol (Sigma Aldrich) over four days. Briefly, slices were transferred from 20% (8 hours), to 40% (overnight), to 60% (8 hours), to 80% (overnight), to 100% (24 hours), to 115% (24 hours). Images of the viral spread in each slice were acquired with the Zeiss LSM800 AxioObserverZ1 mot Confocal Microscope at 10X magnification. GFP fluorescence was excited using a confocal argon laser set at 488ex/515em. Fluorescent areas of each scan were manually traced using ImageJ and summed to obtain a total volume.

4.6 NMDAR internalization quantification

4.6.1 HEK293 cells maintenance, transfection, and whole-cell electrophysiology

HEK293 cells were grown in a humidified 37°C, 5% CO_2 incubator and passaged every 3–4 days using trypsination. For all experiments, HEK293 cells were plated at a density of ~0.2×10^6 cells/mL on 15mm Thermanox plastic coverslips (Thermo Fisher Scientific) in 12-well plates. The HEK293 cells were then transiently transfected with either pHluorin-GluN1-WT or pHluorin-GluN1-A714L cDNAs together with the fluorescent marker cDNA, GluN2A in a 1:1

molar ratio using TransIT-2020 transfection reagent (Mirus) according to manufacturer's instructions. Following transfection, the HEK293 cells were grown in the presence of the selective NMDAR antagonist, 100mM D-APV (Tocris Bioscience) to prevent over-activation and cell death (von Engelhardt, J., Doganci, B., Seeburg, P. H., & Monyer, H, 2009). D-APV was washed off HEK293 cells prior to electrophysiology recordings, which were done 24–48hrs after transfection. Individually transfected HEK293 cells were then visually identified for whole-cell patch clamp recordings using fluorescence microscopy. NMDAR currents were evoked using pressure ejection (10psi) from a picospritzer micropipette filled with 10μM glycine and 1mM glutamate (Sigma-Aldrich) for a duration of 25–50ms every 20s at a membrane potential of -60mV. HEK293 cells were recorded in an external low magnesium solution containing (mM): 150 NaCl, 3 KCl, 0.13 $MgCl_2$, 3.5 $CaCl_2$, 10 HEPES, and 10 glucose (pH adjusted to 7.2 with NaOH, and the osmolality to 300mOsm using sucrose). Thick-walled borosilicate glass electrodes (1.5mm OD, 0.9mm ID) were filled with a K^+-gluconate recording solution containing (mM): 115 K^+-gluconate, 20 KCl, 10 HEPES, 4 Mg^{2+}-ATP, 0.5 GTP, and 10 Na-phosphocreatine (280–290mOsm, pH 7.2).

4.6.2 NMDAR internalization imaging in HEK cells

For all experiments, HEK293 cells were plated at 50-60% confluency in an 8-well chambered coverslip (Ibidi). The HEK293 cells were then transiently transfected with either the fluorescent marker cDNA pHluorin-GluN1-WT or pHluorin-GluN1-A714L together with, the GluN2A cDNAs, in an equimolar ratio using TransIT-2020 transfection reagent (Mirus) according to manufacturer's instructions. Following transfection, the HEK293 cells were grown in the presence of the selective NMDAR antagonist, 100mM D-APV (Tocris Bioscience) to prevent

over-activation and cell death. D-APV was washed off HEK293 cells prior to imaging experiments which were done 24-48hrs after transfection. Individually transfected HEK293 cells were visually confirmed by positive GFP signal (488nm) under epifluorescent illumination.

Imaging experiments were performed in a modified HEPES buffer containing (mM): 150 NaCl, 3 KCl, 0.13 MgCl2, 3.5 CaCl2, 10 HEPES, 10 glucose, and 1 Glutamate (pH adjusted to 7.4 with NaOH, and the osmolality to 290mOsm using sucrose). The cell impermeable, 647nm-tagged FluoTag®-X4 anti-GFP (red; 1:250-1:500; NanoTag Biotechnologies) was added to the well before identifying a positively transfected cell (green; GFP^+). 10μM glycine was then added to the well prior to the addition of an internalizing dose of glycine (1mM). Cells were then imaged every 3mins, over the course of 10mins using an LSM880 Confocal Microscope with Airy Scan (Zeiss) at 63X magnification. Internalization was deemed to have occurred when the cell impermeable NanoTag (red) was observed within the cell.

4.7 Light Sheet Fluorescence Microscopy

4.7.1 Imaging and segmentation

Imaging was performed using our custom-built light sheet microscope. CUBIC-cleared brains were imaged using 2.5X objective (NA0.07), 488nm excitation laser line and 5μm steps. Each sample was scanned as a series of tiles, then stitched into a single image using TeraStitcher, as it allowed for automated, batch processing on a standard desktop (16GB RAM). The stitched scans were then run through AIVIA 9 to segment and create 3D reconstructions of the vascular network. Properties of each vessel (diameter and length) were automatically calculated by

AIVIA 9, and then exported for analysis. The results of segmentation were validated by comparing the output against manual measurements in ImageJ.

4.7.2 Automated stroke volume measurement

Stroke volume in cleared tissue was calculated as follows: the areas representing stroke in each slice were identified, multiplied by their z-depth (thickness), then summed to obtain a total volume. The stroke regions were identified in each slice using a deep convolutional neural network (Biswas & Barma, 2020; Kermany et al., 2018) based on the architecture proposed by Yu et al., 2018 (Yu et al., 2018). This neural network segmented each slice into three regions: stroke, normal tissue, and background. The network was first pre-trained on a large dataset (Deng et al., 2009), then further trained using 906 samples from scans taken in-house. The network achieved a 98% pixel-wise accuracy following validation on an additional 225 samples. Statistical significance of stroke volume was determined using a student's t-test. A p-value of < 0.05 was considered statistically significant. All values are expressed as mean ± SEM.

4.7.3 Post-stroke vascular morphology quantification

For analysis of vascular morphology in the peri-infarct region, transcardial FITC-BSA staining was paired with CUBIC brain clearing to allow for light sheet imaging. We developed our own protocol to do so. Forty-eight hours post PT stroke, mice were deeply anesthetized with 5% isoflurane in O_2 and transcardially perfused with 20ml 1XPBS, then 20ml 4% PFA. Mice were then submerged in a 37°C water bath, facing down at an angle of 30° before being injected with 10ml of 0.5% FITC-BSA (Sigma AG77i4G), in 2% gelatin at a rate of 10ml/min. Mice were submerged in an ice bath for 30mins before the brain was dissected out (P. S. Tsai et al., 2009).

Brains were collected and post-fixed in 4% PFA in 1X PBS overnight, then cleared following the CUBIC tissue clearing protocol (Matsumoto et al., 2019). Following tissue clearing, brains were imaged with the light sheet microscope using 2.5X objective, 488nm excitation laser line and 5µm steps. A 1.125mm^3 ROI lateral to the stroke site was manually selected, then analyzed using AIVIA (DRVISION Technologies).

4.8 Tissue clearing for Light Sheet Fluorescence Microscopy

4.8.1 CUBIC$_{2019}$ tissue clearing

Tissue clearing was done according to the CUBIC protocol described by (Matsumoto et al., 2019). Following perfusion, the tissue was post-fixed overnight in 4% PFA, then washed in 1xPBS every 2hrs at least 3 times the following day. Following washes, tissue was submerged in 10ml of ½ diluted CUBIC-L (1:1, CUBIC-L:Water) at 37°C with gentle shaking overnight. Tissue was submerged in 10ml of CUBIC-L (10%(wt/v) Tx-100, 10%(wt/v) N-Butyldiethanolamine in ddH_2O) at 37°C with gentle shaking over 10 days, changing the solution every 48hrs. Tissue was then washed in 1xPBS (>20ml) every 2hrs at least 3 times before being submerged in 4ml of ½ diluted CUBIC-R$^+$(M) (1:1, CUBIC-R$^+$(M) : Water) overnight at room temperature, with gentle shaking. Tissue was submerged in 4ml of CUBIC-R$^+$(M) the following day, then replaced with fresh CUBIC-R$^+$(M) 24hrs later. Tissue was imaged with the light sheet microscope in a refractive index matched imaging solution consisting of a mixture of HIVAC-4 with mineral oil. This protocol was used for vascular imaging with our light sheet microscope.

4.8.2 CUBIC$_{2015}$ tissue Clearing

Tissue clearing was done according to the CUBIC protocol described by (Susaki et al., 2015).Following perfusion, tissue was post-fixed overnight in 4% PFA, then washed in 1xPBS every 2hrs at least 3 times the following day. Following washes, tissue was submerged in 10ml of ½ diluted CUBIC-R1 (1:1, CUBIC-R1:Water) at 37°C with gentle shaking overnight. Tissue was submerged in 10ml of CUBIC-R1 (25%(wt/v) Urea, 25%(wt/v) Sucrose, 15%(wt/v) Tx-100, in ddH_2O) at 37°C with gentle shaking over 10 days, changing the solution every 48hrs. Tissue was then washed in 1xPBS (>20ml) every 2hrs at least 3 times before being submerged in 4ml of ½ diluted CUBIC-R2 (1:1, CUBIC-R2:Water) overnight at room temperature, with gentle shaking. Tissue was submerged in 10ml of CUBIC-R2 (25%(wt/v) Urea, 50%(wt/v) Sucrose, 10%(wt/v) 2,20,20'-nitrilotriethanol, 0.1% (wt/v) Tx-100, in ddH_2O) the following day, then replaced with fresh CUBIC-R2 24hrs later. Tissue was imaged with the light sheet microscope in CUBIC-R2.

4.8.3 Scale A2 tissue clearing

Tissue clearing was done according to the Scale *A2* protocol described by (Hama et al., 2011). Following perfusion, tissue was post-fixed overnight in 4% PFA, then washed in 1xPBS every 2hrs at least 3 times the following day. Following washes, tissue was submerged in Scale A2 solution (4 M urea, 10% (wt/vol) glycerol and 0.1% (wt/vol) Triton X-100, in ddH_2O) for one month at room temperature. Tissue was imaged with the light sheet microscope in Scale A2.

4.8.4 Scale S4 tissue clearing

Tissue clearing was done according to the Scale *S4* protocol described by (Hama et al., 2011). Following perfusion, tissue was post-fixed overnight in 4% PFA, then washed in 1xPBS every 2hrs at least 3 times the following day. Following washes, tissue was submerged in Scale A2 solution (40%(wt/v) D-Sorbitol, 4M urea, 10% (wt/vol) glycerol and 0.2% (wt/vol) Triton X-100, 20% D-Methyl-Sulfoxide, in ddH_2O; pH7.9) for one month at room temperature. Tissue was imaged with the light sheet microscope in Scale S4.

4.8.5 SeeDB tissue clearing

Tissue clearing was done according to the SeeDB protocol described by (Ke et al., 2013; Ke & Imai, 2014). Following perfusion, tissue was post-fixed overnight in 4% PFA, then washed in 1xPBS every 2hrs at least 3 times the following day. Following washes, tissue was submerged for 8hrs in increasing concentrations of fructose + α-thiolglycerol over one week in the following order: 20%, 60%, 100%, 115%. Tissue was imaged with LSM800 Confocal Microscope (Zeiss) in 115% fructose.

4.8.6 PEGASOS tissue clearing

Tissue clearing was done according to the PEGASOS protocol described by (Jing et al., 2018). Following perfusion, tissue was post-fixed overnight in 4% PFA then submerged in 25%(wt/v) Quadrol at 37°C for 48hrs. Tissue was then incubated in increasing concentrations of tert-butanol (30%, 50%, 70%) +3% Quadrol at 37°C for 4hrs, 6hrs, and 24hrs respectively. Tissue was then dehydrated in 70%(v/v) tert-butanol + 30% (v/v) PEG-MMA-500 + 3%(wt/v) Quadrol in ddH_2O at 37°C for 48hrs, refreshing the solution after 24hrs. Finally, tissue was rinsed in ddH_2O before

being submerged in 75%(v/v) Benzyl Benzoate + 25% (v/v) PEG-MMA-500 + 3%(wt/v) Quadrol in dH2O at 37°C for 24hrs. Tissue was imaged with the light sheet microscope in the same solution.

4.8.7 iDISCO^{+} tissue clearing

Tissue clearing was done according to the CUBIC protocol described by (Renier et al., 2014). Following perfusion, tissue was post-fixed overnight in 4% PFA, then washed in 1xPBS for 1hour. Tissue was submerged for one hour in 5ml of increasing concentrations of methanol (20%, 40%, 60%, 80%, 100%, 100%; MeOH) at room temperature. Tissue was then delipidated with 1hour + 2x 15mins incubations in 5ml dichloromethane (DCM). Tissue was subsequently placed in 25ml ethyl cinnamate overnight, then 5ml of fresh ethyl cinnamate the following morning. Tissue was imaged with the light sheet microscope in ethyl cinnamate.

4.9 Behavioural tests and statistical analysis

4.9.1 Habituation to behavioural testing

One week prior to beginning behavioural testing, mice were placed into new cages and transferred to the quieter animal housing room. Mice were then handled daily for 5mins to allow for habituation to the experimenter. Mice were left undisturbed in the experimental room for 30-60min prior to the start of each behavioural task.

4.9.2 Adhesive removal test

The adhesive removal test was performed as described by (Bouet et al., 2009). A single mouse was first given 1min of habituation to an empty home cage, before one experimenter restrained

the mouse while the other quickly placed the strips of adhesive onto both forepaws, applying equal pressure to both pieces of adhesive. The mouse was then placed back in the cage for a maximum of 2mins following the application of the adhesive tapes. During the 5 days of training sessions, the mice were put back in their home cages with the tape still attached if they failed to remove the adhesive after the allotted time. However, during the 2 days of post-stroke testing, if the mice failed to remove both adhesive strips in the allotted time, the tape was removed by one of the experimenters and the mouse was given a time of 2mins for that trial, the maximum period attributable. The times to contact and remove the pieces of adhesive tapes were compared per paw, before and after stroke. The times of the 2 last days of pre-stroke training were compared to the 2 days post-stroke and were analyzed using a two-way ANOVA with repeated measures, and a Bonferroni *post hoc* test. A value of $p < 0.05$ was considered to be statistically significant.

4.9.3 Horizontal ladder test

The horizontal ladder test was performed based on protocols described previously (Farr, Liu, Colwell, Whishaw, & Metz, 2006; Metz & Whishaw, 2009) with slight modifications. The horizontal ladder test apparatus was set up by placing small rungs through 2 pieces of transparent plastic at random intervals. The width between both pieces of plastic was set at 1cm wider than the mouse. The assembled ladder was placed atop 2 cages. A neutral cage was placed at the beginning of the ladder and the animal's home cage was placed at the end. The mice always crossed the ladder in the same direction and were gently nudged along with a toothbrush if they stopped or attempted to turn around on the ladder.

Mice underwent 1 day of training prior to stroke testing to allow both acclimatization to the ladder apparatus and reduction of stress and anxiety. During the training day, mice walked across the ladder until they had completed 2 consecutive satisfactory runs. In the pre-stroke trials, mice crossed the ladder as often as needed until they had performed 2 acceptable runs. In turn, during the post-stroke trials, mice had only 3 attempts to cross the ladder, 2 of which were scored. Each trial was recorded with a video camera positioned slightly below the ladder to ensure all limbs were always visible.

Scoring and analysis were performed by a single experimenter who was blind to the conditions being tested to avoid bias. The video recordings of the best 2 trials from each mouse were analyzed frame-by-frame with Noldus Observer XT program. Each step was scored as either "correct", "partial" or "miss". The percentage of missed steps pre- and post-stroke were compared. The scores obtained by each limb pre- and post-stroke were compared using two-way ANOVA with repeated measures and Bonferroni pairwise *post hoc* test. A value of $P < 0.05$ was considered to be statistically significant. All values are expressed as mean ± SEM.

4.9.4 Cylinder test

The cylinder test was performed based on protocols described in (Balkaya, Krober, Gertz, Peruzzaro, & Endres, 2013; Schallert, Fleming, Leasure, Tillerson, & Bland, 2000) with slight modifications. Mice were placed in a transparent cylinder and filmed with an overhead camera until they reared 22 times. A rear was considered to be when a mouse got up on its hind limbs and used its forelimbs to support itself along the wall of the cylinder. With each rear, three types of behaviours could occur: (A) right paw is exclusively weight bearing; (B) left paw is

exclusively weight bearing; (C) both paws are weight bearing at the same time. During each rear, the first paw to make contact with the wall was scored as an independent forelimb placement, be it left or right. If the second paw made contact with the wall while the first paw was still in use, the behaviour was scored as a "both" placement from the moment the second paw made contact with the wall. The same principle was applied if both paws were in use and the animal removed one paw from the wall. Those behaviours were scored as "both" and then either "left" or "right" as soon as the second forelimb was removed from the wall of the cylinder.

Scoring and analysis was always done by a single experimenter blind to the conditions being tested to avoid any bias. The first 20 visible weight bearing forelimb contacts to the wall of the cylinder were recorded for duration in seconds. Any forelimb contacts to the wall which were not fully visible to the person scoring were excluded. Noldus Observer XT program was used to score the length and frequency of the different behaviours. The behaviours were expressed per paw as an average time in relation to the sum of the independent left and right behaviours. For statistical analysis, the average time spent on the impaired paw (right) was calculated for both the pre-stroke and post stroke trials. The difference between pre-stroke and post stroke times were calculated and were compared per treatment group with a t-test in which a value of $p<0.05$ was considered to be a statistically significant difference in right paw use. All values are expressed as mean ± SEM.

4.9.5 Morris water maze (MWM)

The Morris Water Maze was performed based on protocols first described in (Morris, 1984) on mice having been induced an ET-1 stroke in the left mPFC to evaluate spatial learning and memory. In this test, the animals learned to find a platform hidden 1cm below the water, using

external visual cues placed on the walls of the testing room. EthoVision (Noldus) software was connected to a video camera to track the movements of the mice within the pool (132 cm diameter; 91.5cm depth). A non-toxic white paint was added to the water (24°C) daily to ensure detection of mice in the pool and to keep the platform hidden. Mice were given four daily training sessions (60s) over 5 days, with a 30min inter-trial interval. During each training session, mice were placed in the pool from alternating quadrants and removed once they had either found and stayed on the platform for 5s, or 60s had elapsed. If mice failed, they were shown the platform after 60s. Mice were taken in and out of the pool with a towel and placed back into their home cages between trials. Once mice had learned the task, mice underwent a probe trial. During the probe trial, the platform was removed and the amount of time the mouse spent in the quadrant where the platform used to be was calculated. The difference between pre-stroke and post stroke times were calculated and were compared per treatment group with a mixed model ANOVA in which a value of $p<0.05$ was considered to be a statistically significant difference in time spent in the target quadrant. All values are expressed as mean ± SEM.

4.9.6 Forced swim test

The forced swim task was performed based on protocols described in (Can et al., 2012)on mice having been induced ET-1 stroke in the left mPFC to evaluate depressive phenotypes. Animals were placed in a clear 22cm diameter cylinder filled with 4L of 21°C water for 6 minutes. The task was performed under red lighting and EthoVision (Noldus) software was connected to a video camera to track and quantify the duration of mobility and immobility of the mice in the water. The difference between time spent mobile and immobile were calculated and were compared per treatment group with a t-test in which a value of $p<0.05$ was considered to be a statistically significant difference in mobility. All values are expressed as mean ± SEM.

4.9.7 Open field test

The open field test was performed based on protocols described by (Seibenhener & Wooten, 2015). EthoVision Noldus software connected to a video camera was used to track the movements of the mice within the arenas. The arenas were white opaque plastic boxes (50 cm x 50 cm, and 50 cm high). The arenas and objects were cleaned with 70% EtOH between each trial and before the first trial. All testing was performed at 300Lux. Mice were placed into the center of the empty arena and allowed to explore for 15 mins. Time spent exploring the corners of the areas was compared to the time spent exploring the center of the arenas. Total distance covered as well as velocity of movements were recorded and were compared per treatment group with a t-test in which a value of $p<0.05$ was considered to be a statistically significant difference. All values are expressed as mean ± SEM.

4.9.8 Novel object test

The novel object test was performed based on work described by (Leger et al., 2013). EthoVision Noldus software connected to a video camera was used to track the movements of the mice within the arenas. The arenas were white opaque plastic boxes (50 cm x 50 cm, and 50 cm high). The arenas and objects were cleaned with 70% EtOH between each trial and before the first trial. Objects used were red cups in arena 1 and funnels in arena 2. 30 mins of habituation was allowed in a separate room with the lights on before each day of testing. All NOR testing was performed in the dark, with the red lights on.

Mice were placed into the empty arenas and allowed to explore for 10 mins. 24 hours later, mice explored 2 identical objects placed in the arena 25 cm from the edge and 5 cm apart for 10 mins.

3 hours later, one object (left and right objects were alternated) was replaced with a novel object and mice were returned to the arena for 10 mins. Time spent exploring each object and frequency of visits to each object were recorded. Mice were considered to be exploring if their snout was within 1cm of the object. Recognition memory was calculated by dividing the time spent exploring the novel object by the total time spent exploring both objects. The cumulative in zone nose-point interaction time in seconds was used for those calculations. Times and index scores were compared per treatment group with a t-test in which a value of $p<0.05$ was considered to be a statistically significant difference. All values are expressed as mean ± SEM.

4.10 Electrophysiology

4.10.1 Hippocampal brain slice preparation

Whole-cell electrophysiological recordings were obtained from CA1 pyramidal cells *in situ* in coronal hippocampal brain slices (300μm thick) as previously described (Martina et al., 2004). In brief, animals were anaesthetized using an isoflurane vaporizer (Stoelting, Wood Dale, IL, USA; 2–5% isoflurane in air, with a flow rate of 1 L/min) prior to decapitation. The brain was removed and placed in ice-cold oxygenated (95% O_2/5% CO_2) *N*-methyl-D-glucamine (NMDG) based cutting solution at 4°C containing (in mM): 92 NMDG, 20 HEPES, 25 glucose, 30 $NaHCO_3$, 1.2 NaH_2PO_4, 2.5 KCl, 5 Na-L-ascorbate, 3 Na-pyruvate, 2 thiourea, 10 $MgSO_4$ and 0.5 $CaCl_2$ (300mOsm, pH 7.2). Acute brain slices were cut with a vibratome (Leica System, VT 1000S, Wetzler, Germany) then were allowed to recover for 1hr at room temperature (RT) in oxygenated artificial cerebrospinal fluid (ACSF) containing (in mM): 119 NaCl, 2.5 KCl, 2.5 $CaCl_2$, 1.3 $MgSO_4$, 1 NaH_2PO_4, 26 $NaHCO_3$, and 11 glucose (300 mOsm, pH 7.2).

4.10.2 Whole-cell electrophysiology on hippocampal slices

Whole-cell voltage-clamp recordings were obtained from visually identified CA1 pyramidal cells from acute hippocampal slices using differential interference contrast optics and infrared video microscopy (IR-DIC: Leica DMLFSA, Wetzler, Germany). The recordings were performed at RT and cells were voltage-clamped at -65mV. Postsynaptic currents were evoked by electrical stimulation of the Schaffer collaterals with a bipolar stimulating electrode positioned in the *stratum radiatum*. Borosilicate glass electrodes were filled with an internal solution containing (mM): 115 Cs-methane-sulfonate, 0.4 EGTA, 5 TEA-Cl, 6.6 NaCl, 20 HEPES, 4 Mg-ATP, 0.5 GTP, 10 sodium Na-phosphocreatine, and 5 QX-314 bromide, and the pH was adjusted to 7.2 (280–290mOsm). The recording electrodes had a resistance of 4–6MΩ when filled with this solution. The series resistance was monitored during the experiment and the data were discarded when the series resistance changed more than 15% of the original level or exceeded 30MΩ. The intensity of the stimulation was adjusted to obtain evoked excitatory postsynaptic currents (EPSCs) in the amplitude range of 100–150pA at a membrane potential of -65mV. The stimulation protocol consisted of single 100μs current pulses (10–200μA) evoked every 12s. For the train stimulation protocol, 10 current pulses (100μs long) were evoked at 50Hz for 200ms and then repeated once every 20s.

To isolate the NMDAR-EPSC, an ACSF was used with a low concentration of $MgCl_2$ (0.13mM) and containing (μM): 5 NBQX, and 50 picrotoxin (Tocris Bioscience), with the $CaCl_2$ increased to 3.5mM to maintain cation balance. When required, additional drugs were applied including various concentrations of D-serine and glycine (Millipore Sigma). The clathrin-mediated endocytosis inhibitor, 100μM dynasore (Millipore Sigma), was included in the internal solution.

4.10.3 Sniffer-patch technique

To detect glycine release, we used the "sniffer patch" technique (Allen, 1997; Aubrey et al., 2007; C. J. Lee et al., 2007; Scain et al., 2010). A Chinese Hamster Ovary (CHO) cell line were generated and stably transfected with the α2 subunit of the glycine receptor (GlyR)(Mangin et al., 2003). Outside-out membrane patches were excised from the CHO cells using thick-walled borosilicate glass pipettes filled with a cesium chloride internal solution. Following patch excision, the electrode was placed in the *stratum radiatum* of the CA1 region of the hippocampus to detect glycine release and allow channel activation. Channel open probability (P_{open}) was derived by measuring the mean open time of all the single channel events during the recording window, then dividing by the sum of the mean open and shut times. Multiple channel openings were set as a $P_{open} = 1$ for that particular time period. All values are expressed as mean ± SEM.

4.10.3 Oxygen-glucose deprivation paradigm

To mimic ischemia, the acute slices were challenged by an oxygen-glucose deprivation paradigm (OGD) modified from Rossi *et al.(Rossi, Oshima, & Attwell, 2000)*. In this paradigm, external glucose was replaced with 7mM sucrose, and the external solution was saturated with 95% N_2 / 5% CO_2 instead of 95% O_2 / 5% CO_2. Iodoacetate and cyanide were also added to the OGD external solution to block glycolysis and oxidative phosphorylation.

5. RESULTS

5.1 High concentrations of glycine induce NMDAR internalization, *in vitro*

We first demonstrated the effects of various glycine concentrations on stimulation-evoked NMDAR-EPSCs recorded in CA1 pyramidal neurons from acute hippocampal brain slices. At glycine concentrations below 250μM, NMDAR-ESPC amplitudes were potentiated in a dose-dependent fashion. However, increasing the glycine concentration to 1mM resulted in a significant decrease in NMDAR-EPSC amplitude. (Suppl. Fig. 1A-B). To confirm that this decrease in EPSC was a result of glycine induced NMDAR internalization (GINI), we applied 1mM glycine in the presence of 100μM dynasore, a cell-permeable inhibitor of both dynamin-1 and dynamin-2, to block internalization. We found that the decrease in NMDAR-EPSC amplitudes generated by 1mM glycine no longer occurred in the presence of 100μM dynasore (Suppl. Fig. 1C) suggesting glycine was responsible for inducing NMDAR internalization.

5.2 Glycine is released during oxygen-glucose deprivation paradigm

We next questioned if these high levels required to trigger GINI could be released endogenously. During physiological conditions, GlyT1's maintain synaptic glycine levels far below the level that would induce GINI. However, we hypothesised that depolarization of glutamatergic CA1 pyramidal neurons during a modified oxygen-glucose deprivation (OGD) paradigm could result in detectable local glycine release. In order to detect glycine release during an OGD paradigm, we used the sniffer-patch technique, wherein activation of glycine receptor α2 subunit indicated glycine release. When the modified OGD paradigm was initiated and applied to the slice, there was a marked increase in the frequency of glycine receptor α2 opening in the patch and a significant increase in P_{open}, compared to control (Suppl Fig. 1D). To further confirm that glycine

was released, we repeated the experiment in the presence glycine oxidase (GO) and no longer observed increases in P_{open} (Suppl. Fig. 1E). Overall, these results indicate that glycine is released into the CA1 extracellular space during OGD conditions.

5.3 Genetic elevation of brain glycine reduces infarct size following photothrombotic stroke

Altogether, these *in vitro* data demonstrate that GINI is induced by high concentrations of glycine. Such levels have been shown to occur during pathological conditions such as ischemia, therefore, we speculated that GINI could also be triggered, *in vivo* during stroke. To determine such, we utilised the photothrombotic (PT) model of focal ischemia in the transgenic GlyT1$^{+/-}$ mouse line which have chronically elevated glycine levels. Since increased glycine levels resulted in NMDAR internalization, we hypothesized that the stroke volume in GlyT1$^{+/-}$ mice would be smaller than that observed in WT mice. Indeed, there was a statistically significant ~75% decrease in stroke volume in the GlyT1$^{+/-}$ mice compared to WT (Fig. 7A; middle). In contrast, in transgenic SR$^{-/-}$ mice, which have chronically low levels of endogenous D-serine, a co-agonist of the glycine binding site on the NMDAR, stroke volumes were ~40% larger than WT mice (Fig. 7A; right) but this was not a significant change.

5.4 Pharmacological elevation of brain glycine reduces infarct size and improves motor behavioural deficits following photothrombotic stroke

Next, we were interested to know if pharmacologically increasing glycine levels in WT mice could produce results similar to those observed in the GlyT1$^{+/-}$ mice. To do so, we treated animals with NFPS, a glycine transporter antagonist which elevates brain glycine levels, 24 hrs

prior to inducing stroke. Then, 48 hours following PT stroke, stroke volumes were quantified using 2,3,5-triphenyltetrazolium chloride (TTC; Fig. 7B). Figure 7B's box-and-whisker plot shows a statistically significant ~50% decrease in median stroke volume in the NFPS-treated mice compared to the saline-treated mice.

Although encouraging, a decrease in stroke volume does not necessarily correlate with a decrease in post-stroke behavioural deficits. To determine if NFPS administration could minimize post-stroke behavioural deficits, we measured motor deficits using a well-established behavioural test of motor function, the adhesive removal test. Prior to stroke induction, the time to contact and time to remove the adhesive sticker from both paws was comparable (Fig. 7C). Following PT, a significant attenuation of post-stroke deficits was observed in the mice treated with NFPS in both times to contact and remove in the impaired paw, with no significant stroke or drug effect in the unimpaired paw, demonstrating a substantial attenuation of post-stroke motor behavioural deficits (Fig. 7C). The cylinder test was also performed yet revealed no post-stroke differences in impaired paw use in NFPS-treated mice compared to saline-treated mice (Fig. 7D).

Finally, FluoroJade C (FJC) experiments demonstrated that the NFPS-treated mice have significantly decreased levels of neuronal cell death compared with the saline-treated mice following PT stroke (Fig. 7E). Therefore, both genetic and pharmacological approaches which increased brain glycine levels prior to ischemic stroke resulted in reduced infarct volumes. Interestingly, this decrease in stroke volume was recapitulated when NFPS was administered up to 30mins post-stroke (Fig. 7J). Furthermore, recording the body temperatures of mice treated

with NFPS or saline in the hours and days following PT stroke demonstrated that hypothermia did not contribute to the effect of NFPS (Suppl. Fig. 2A).

5.6 Pre-stroke administration of NFPS decreases stroke volume and improves motor behavioural deficits following endothelin-1 stroke

The decrease in infarct volume following NFPS treatment is consistent with what has been previously observed in the transient middle cerebral artery occlusion (tMCAO) model of ischemic stroke (B. Huang et al., 2016). However, the PT stroke or the tMCAO models does recapitulate all clinical aspects of ischemia. Therefore, to ensure that the observed decrease in stroke volume and attenuation of behavioural deficits was not an artefact of our stroke model, we repeated the experiments using a second known model of focal stroke, the endothelin-1 (ET-1) model. As the vasoconstricting agent, ET-1, is metabolized, reperfusion of the ischemic site occurs gradually and creates a penumbra area which is a phenomenon often seen occurring in human clinical stroke (Dojo Soeandy et al., 2019).

We first confirmed that this model induced consistently sized infarcts (Suppl. Fig. 2B), and sensory and motor deficits with the adhesive removal task (Suppl. Fig. 2C). Once confirmed, mice were treated with NFPS 24hrs pre-ET-1 stroke and subsequently underwent a battery of motor behavioural tasks, then infarct volume tracing. Similar to what was observed in the PT stroke paradigm, NFPS-treated mice showed a significant ~43% decrease infarct volume (Fig. 7F) compared to saline-treated mice. Furthermore, NFPS-treated mice showed significant attenuation of post-stroke motor behavioural deficits in the adhesive removal task (Fig. 7G), but not in the cylinder task, where they performed similarly to non-treated mice (Fig. 7H). Additionally, NFPS-treated mice showed an attenuation in behavioural deficits in the horizontal

ladder test in the ET-1 stroke paradigm (Fig. 7I; left) and these deficits seemed to be localized to the impaired hindlimb (Fig. 7I; right).

Taken together, either genetic or pharmacological elevation of brain glycine resulted in a significant decrease in stroke volume in two well established models of focal ischemia. These behavioural data also reveal that pre-treatment with NFPS significantly attenuated post stroke behavioural deficits.

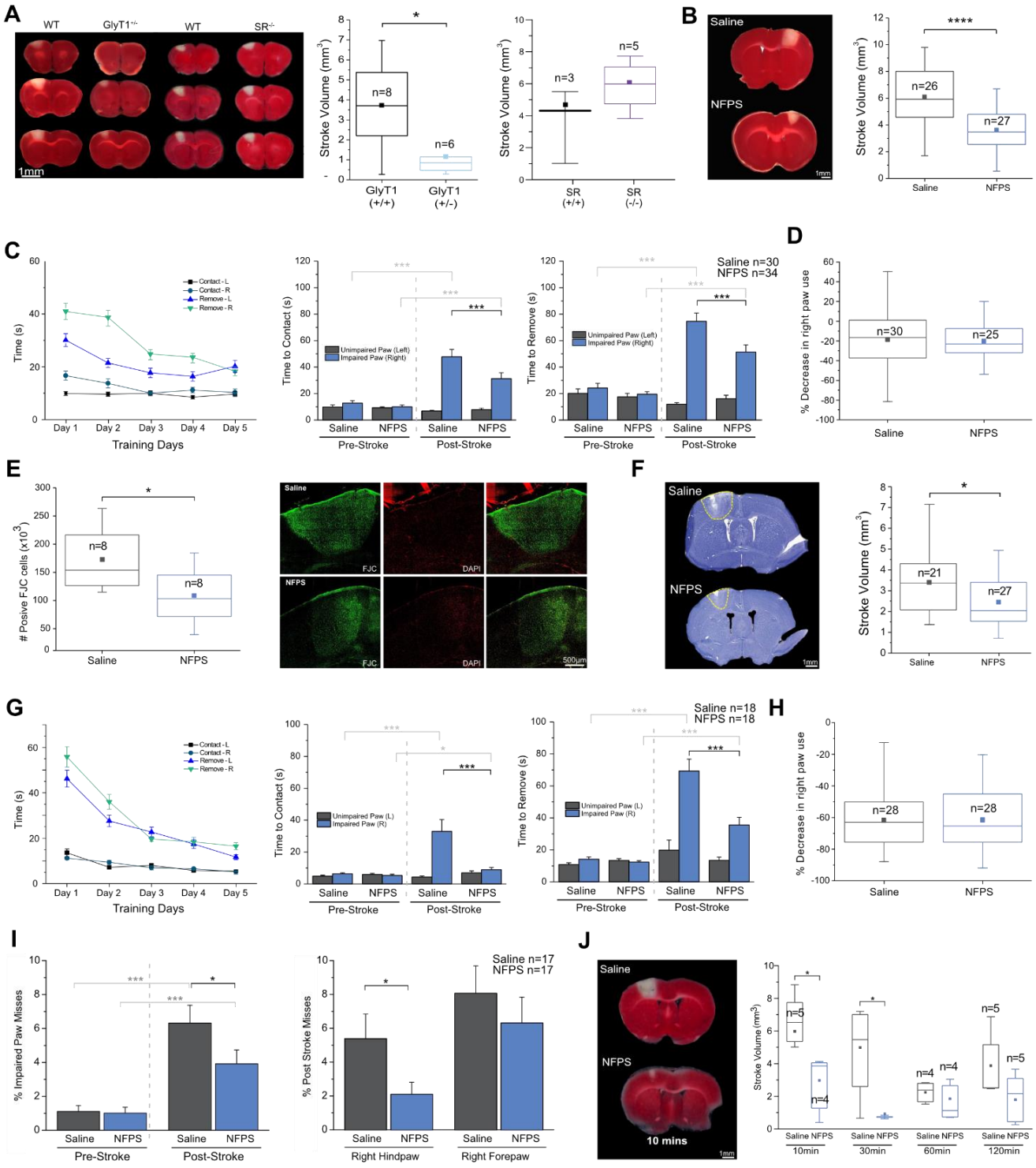
A
WT
GlyT1+/-
WT
SR-/-
1mm
Stroke Volume (mm3)
n=8
n=6
GlyT1 (+/+)
GlyT1 (+/-)
n=3
n=5
SR (+/+)
SR (-/-)
B
Saline
NFPS
1mm
****
n=26
n=27
Saline
NFPS
C
Contact - L
Contact - R
Remove - L
Remove - R
Time (s)
Day 1
Day 2
Day 3
Day 4
Day 5
Training Days
Time to Contact (s)
Unimpaired Paw (Left)
Impaired Paw (Right)
Saline
NFPS
Pre-Stroke
Post-Stroke
Time to Remove (s)
Saline n=30
NFPS n=34
D
% Decrease in right paw use
n=30
n=25
E
# Posive FJC cells (x10^3)
n=8
n=8
Saline
NFPS
FJC
DAPI
500µm
F
Saline
NFPS
1mm
Stroke Volume (mm3)
n=21
n=27
G
Contact - L
Contact - R
Remove - L
Remove - R
Time (s)
Training Days
Time to Contact (s)
Unimpaired Paw (L)
Impaired Paw (R)
Time to Remove (s)
Saline n=18
NFPS n=18
H
% Decrease in right paw use
n=28
n=28
I
% Impaired Paw Misses
Pre-Stroke
Post-Stroke
% Post Stroke Misses
Saline n=17
NFPS n=17
Right Hindpaw
Right Forepaw
J
Saline
NFPS
10 mins
1mm
Stroke Volume (mm3)
n=5
n=4
n=4
n=4
n=5
n=5
Saline NFPS
10min
30min
60min
120min

Figure 7. Elevation of extracellular glycine results in a smaller infarct volume and decreased motor behavioural deficits following photothrombotic and endothelin-1 stroke. **A)** 500µm thick coronal sections of TTC stained mouse brain sections and box and whisker plots representing infarct volume when measured 48hrs post PT stroke in GlyT1+/- and SR-/- mice relative to respective WT littermates. **B)** Representative 500µm thick TTC stained mouse brains sections and box and whisker plot representing infarct volume in saline-treated (grey) and NFPS-treated (blue) mice 24hrs prior to PT stroke induction. **C)** The effect of NFPS (blue) administration on post-PT stroke time to contact and time to remove in the adhesive removal task compared with saline (grey) treatment. **D)** A box and whisker plot demonstrating the effect of NFPS (blue) administration on post-PT stroke time spent on impaired paw (right) in the cylinder test compared with saline (black) treated mice. **E)** Box and whisker plot showing the effect of NFPS on cell death in NFPS treated mice (blue) compared to saline treated mice (grey) using FluoroJadeC stain, with representative images. **F)** Representative cresyl violet sections (25µm thick) obtained from saline-treated and NFPS-treated mice; infarct is shown by the yellow border. A box and whisker plot depicting infarct volume observed in mice treated with NFPS (blue) compared with saline (grey). **G)** The effect of NFPS (blue) administration on post-ET-1 stroke time to contact and time to remove in the adhesive removal task compared with saline (grey) treatment. **H)** A box and whisker plot demonstrating the effect of NFPS (blue) administration on post-ET-1 stroke time spent on impaired paw (right) in the cylinder test compared with saline treated mice (grey). **I)** The effect of NFPS (blue) administration on post stroke performance on the horizontal ladder task post ET-1 stroke compared to saline (grey) administration. **J)** 500µm thick coronal sections of TTC stained mouse brain sections and box and whisker plot representing infarct volume when measured 48hrs post PT stroke in mice having been treated with NFPS (blue) or saline (grey) at 10, 30, 60, 120mins post stroke. Data is mean ± SEM; statistical significance $p < 0.05$ *, $p < 0.001$ *** and $p < 0.0005$ ****.

5.7 Blocking NMDAR internalization abolishes the effect of NFPS

We next aimed to confirm that our stroke volume and behaviour data observed following treatment with NFPS was occurring due to GINI, as we hypothesized. We therefore introduced a point mutation into the NMDAR GluN1 subunit (A714L), which was shown to abolish glycine-mediated NMDAR internalization *in vitro* (Han et al., 2013). GINI is mediated by A714 on the CTD of GluN1, therefore this residue is necessary for priming of NMDARs containing either GluN2A or GluN2B in recombinant systems (Han et al., 2013).

We first assessed the functionality of this mutation in HEK cells. To do so, we transiently transfected GluN1-WT or GluN1-A714L together with WT GluN2A subunits into HEK293 cells to create a functional NMDAR. As seen in Suppl. Fig. 3A, application of a known NMDAR antagonist, D-APV, blocked NMDAR-EPSCs in cells expressing either GluN1-WT or GluN1-A714L. In the subsequent experiment, we applied 1mM glycine in cells expressing GluN1-WT and observed a significant decrease in the amplitude of the NMDAR-EPSCs similarly to what was observed in acute slice recordings (Suppl. Fig. 1A-B). However, in cells expressing GluN1-A714L this concentration of glycine significantly increased the NMDAR amplitude (Suppl. Fig. 3B) indicating no internalization occurred in these cells. To visually confirm the occurrence of GINI, the movements of NMDARs were tracked over time by live-cell imaging following application of 1mM glycine to HEK cells. We first transfected HEK cells with GFP-expressing NMDARs (green) and then additionally stained them with a cell-impermeable nanobody (red) to tag extracellular NMDARs. By utilizing a cell-impermeable nanobody, we ensured that when tagged-NMDARs (red) were seen to move into the cell, it would be exclusively due to internalization. In cells expressing GluN1-WT, extracellularly tagged NMDARs (red) are seen to

move into the cell following application of an internalizing dose of glycine. However, in cells expressing GluN1-A714L, extracellularly tagged NMDARs remain on the cell surface following application of glycine (Fig. 8A; Suppl Fig. 3D; Video S1 and S2).

Once the functionality of the mutation was established, we packaged GluN1-WT as well as GluN1-A714L into an adeno-associated virus (AAV2/9) and stereotaxically injected into the sensory-motor cortex of mice. The functionality of the mutation was then re-assessed in acute slices. Again, a dose of 1mM glycine decreased the NMDAR-EPSC amplitudes in cells infected with AAV-GluN1-WT while this dose of glycine did not change the NMDAR-EPSC amplitudes in cells infected with the AAV-GluN1-A714L (Suppl. Fig. 3C) indicating GINI was abolished in AAV-GluN1-A714L infected cells. We then ensured that the spread of the virus occupied a volume that was comparable to the PT stroke (Fig. 8B; Video S3). Following these control experiments, we investigated the effect of NFPS on PT stroke volume in mice infected with either the AAV-GluN1-WT or the AAV-GluN1-A714L. There were no significant differences in the PT-induced stroke volume between the mice infected with either the AAV-GluN1-WT or the AAV-GluN1-A714L constructs alone. However, there was a significant decrease in stroke volume following pre-treatment with NFPS in mice infected with AAV-GluN1-WT. Interestingly, NFPS administration no longer had an effect on stroke volume in the mice infected with AAV-GluN1-A714L (Fig. 8C) suggesting GINI is crucial in the observed effects of NFPS on post stroke outcomes.

To further confirm the importance of GINI, the adhesive removal test was repeated on mice infected with either the AAV-GluN1-A714L mutation or the AAV-GluN1-WT. NFPS-treated

mice infected with AAV-GluN1-WT had a significant decrease in post-stroke time to contact and time to remove in the impaired paw (Fig. 8D). Interestingly, NFPS-treated mice infected with AAV-GluN1-A714L (Fig. 8E), there was no significant change in time to contact and time to remove following stroke. Data illustrated in supplemental figure 3E confirm that the injections of the AAV-GluN1-WT or -GluN1-A714L alone had no effect on behaviour. It is worth noting that we also generated a shRNA resistant GluN1 as we had envisaged using GluN1 shRNA to inhibit the effect of WT GluN1 *in vivo*. However, as we found a robust behavior and GINI phenotype in slices and behavioural studies without the use of shRNA, we did not require it. Taken together, these data confirm that GlyT1-A administration induces neuroprotection *in vivo*, *via* GINI.

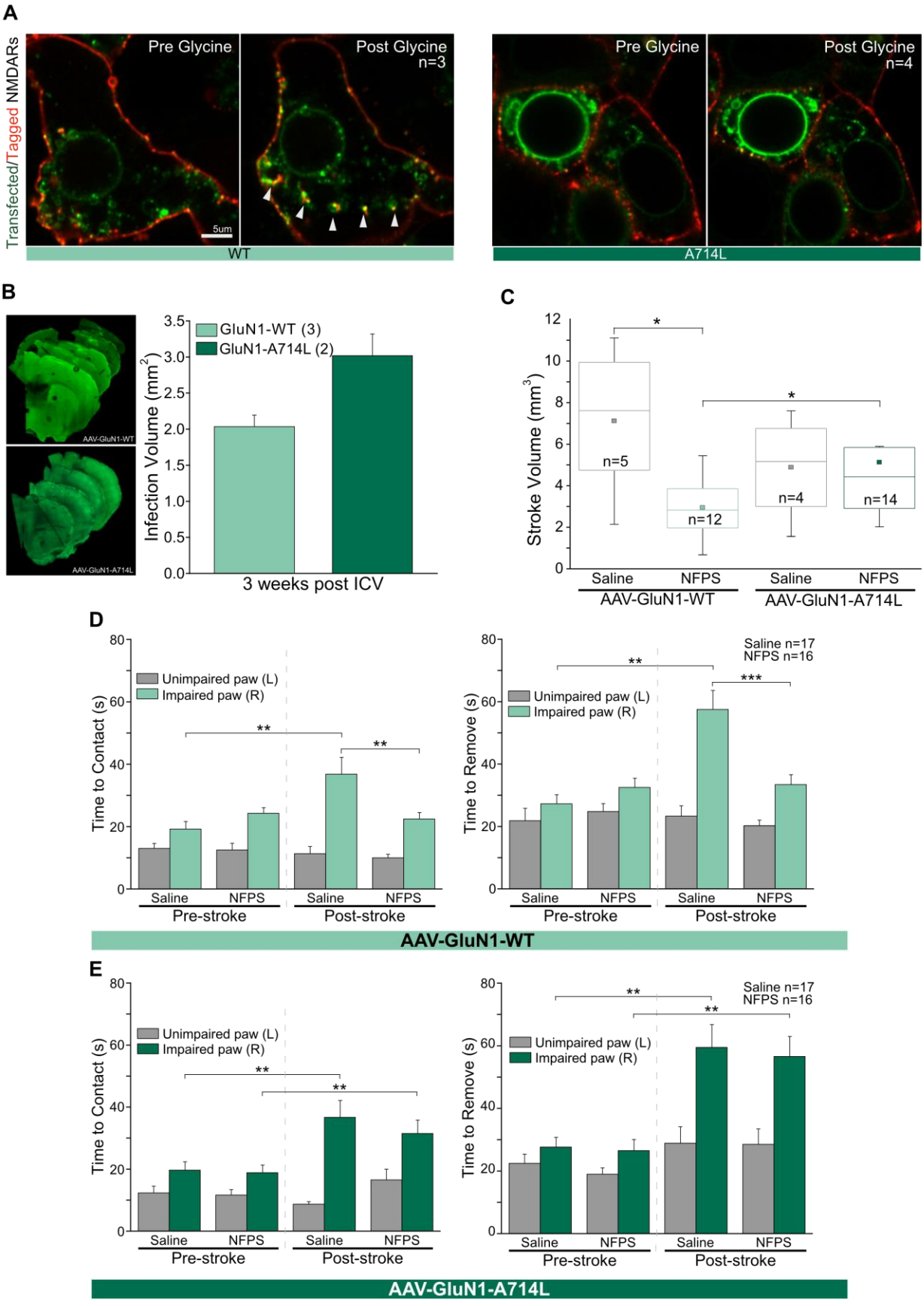
A
Transfected/Tagged NMDARs
Pre Glycine
Post Glycine
n=3
5um
WT
Pre Glycine
Post Glycine
n=4
A714L
B
AAV-GluN1-WT
AAV-GluN1-A714L
GluN1-WT (3)
GluN1-A714L (2)
Infection Volume (mm2)
3 weeks post ICV
C
Stroke Volume (mm3)
n=5
n=12
n=4
n=14
Saline
NFPS
Saline
NFPS
AAV-GluN1-WT
AAV-GluN1-A714L
D
Unimpaired paw (L)
Impaired paw (R)
Time to Contact (s)
Time to Remove (s)
Saline n=17
NFPS n=16
Pre-stroke
Post-stroke
AAV-GluN1-WT
E
Unimpaired paw (L)
Impaired paw (R)
Time to Contact (s)
Time to Remove (s)
Saline n=17
NFPS n=16
Pre-stroke
Post-stroke
AAV-GluN1-A714L

Figure 8: Infection of the stroke site with the non-internalizing GluN1-A714L mutation abolishes the protective effect of elevating extracellular glycine on stroke volume and during a behavioural task. A) Visual representation of NMDAR internalization in GluN1-WT or GluN1-A714L transfected HEK293 cells following application of 1mM glycine. Transfected NMDARs are labeled in green, while extracellular NMDARs are additionally labeled with red cell impermeable nanobody staining. **B)** 2D coronal sections from representative images demonstrating the extent of the viral spread in the mouse brain following infection with AAV-GluN1-WT or AAV-GluN1-A4714L. **C)** 500μm thick representative coronal sections of infarct volumes as well as box and whisker plot demonstrating infarct volumes in AAV-GluN1-WT or AAV-GluN1-A4714L infected mice treated with NFPS (green) or saline (grey) 24hrs pre-PT stroke. **D)** The effect of NFPS versus saline administration on the post-PT stroke performance in the adhesive removal task, in mice infected with the AAV-GluN1-WT. **E)** The effect of NFPS versus saline administration on the post-PT stroke performance in the adhesive removal task, in mice infected with AAV-GluN1-A714L. Data is mean ± SEM; statistical significance $p < 0.05$ *, $p < 0.01$** and $p < 0.001$ ***.

5.8 NFPS and animal models of cognitive impairment

Given the efficacy demonstrated in ameliorating motor deficits and having confirmed the involvement of GINI in the neuroprotection offered by NFPS administration, we were interested in ascertaining if NFPS could also be protective against cognitive deficits and mood changes, which are often reported by stroke patients. We first required a suitable model of cognitive deficits. We investigated three: ET-1 strokes in the CA1 or DG region of the hippocampus, 2 vessel occlusion, and ET-1 strokes in the left medial pre-frontal cortex (mPFC).

Injecting ET-1 directly into the CA1 or DG regions of the hippocampus was not a viable option as a visible infarct was only achieved in a singular mouse (Fig. 9A). In fact, following several attempts in which the dose and volume of ET-1 injected was altered, mice either died during surgery or had infarcts which were too small to be detected by MRI. Therefore, we turned to the two-vessel occlusion model of global ischemia (Fig. 9B). This model induced very minimal damage to the hippocampus (Fig. 9C), had a significantly higher mortality rate following surgery, and did not induce deficits in the novel object recognition task when tested 7days following surgery (Fig. 9D).

Finally, we sought to reproduce the mPFC ET-1 stroke model established by Dr. Paul Albert's lab (Vahid-Ansari et al., 2016). Again, we first tested whether this model induced deficits by comparing animals having been induced ET-1 strokes to animals receiving a sham intracranial injection of saline. Following completion of a battery of behavioural tests, mice were collected, and brain tissue underwent cresyl violet staining to assess infarct volume. However, no infarcts were detectable, likely due to the duration of the behavioural testing (Fig. 9E). Behavioural

testing revealed no significant impairment induced by ET-1 stroke in the Morris water maze (Fig. 9F) or the forced swim test (Fig. 9G). However, this paradigm did induce deficits in the novel object task (Fig. 9H). Here, mice having received saline injections (sham stroke) visited the novel object more frequently than the familiar object while ET-1 injected mice visited both objects equally. Finally, the open field test indicated that the stroke paradigm did not induce any motor deficits (Fig. 9I) as both groups explored equally. Thus, this paradigm only induced cognitive deficits in one of the three behavioural tests performed. It would be worthwhile repeating this paradigm in the future.

Prior to repeating this experiment, we hypothesized that incorporating L-NAME into the ET-1 may produce more severe impairments while inducing similarly sized infarcts as the previously used ET-1 in water. Figure 9J shows similar infarct volumes in both conditions when assessed using MRI, however behavioural experiments were not repeated. Taken together, NFPS may improve cognitive deficits, however a suitable model of cognitive deficits must first be established.

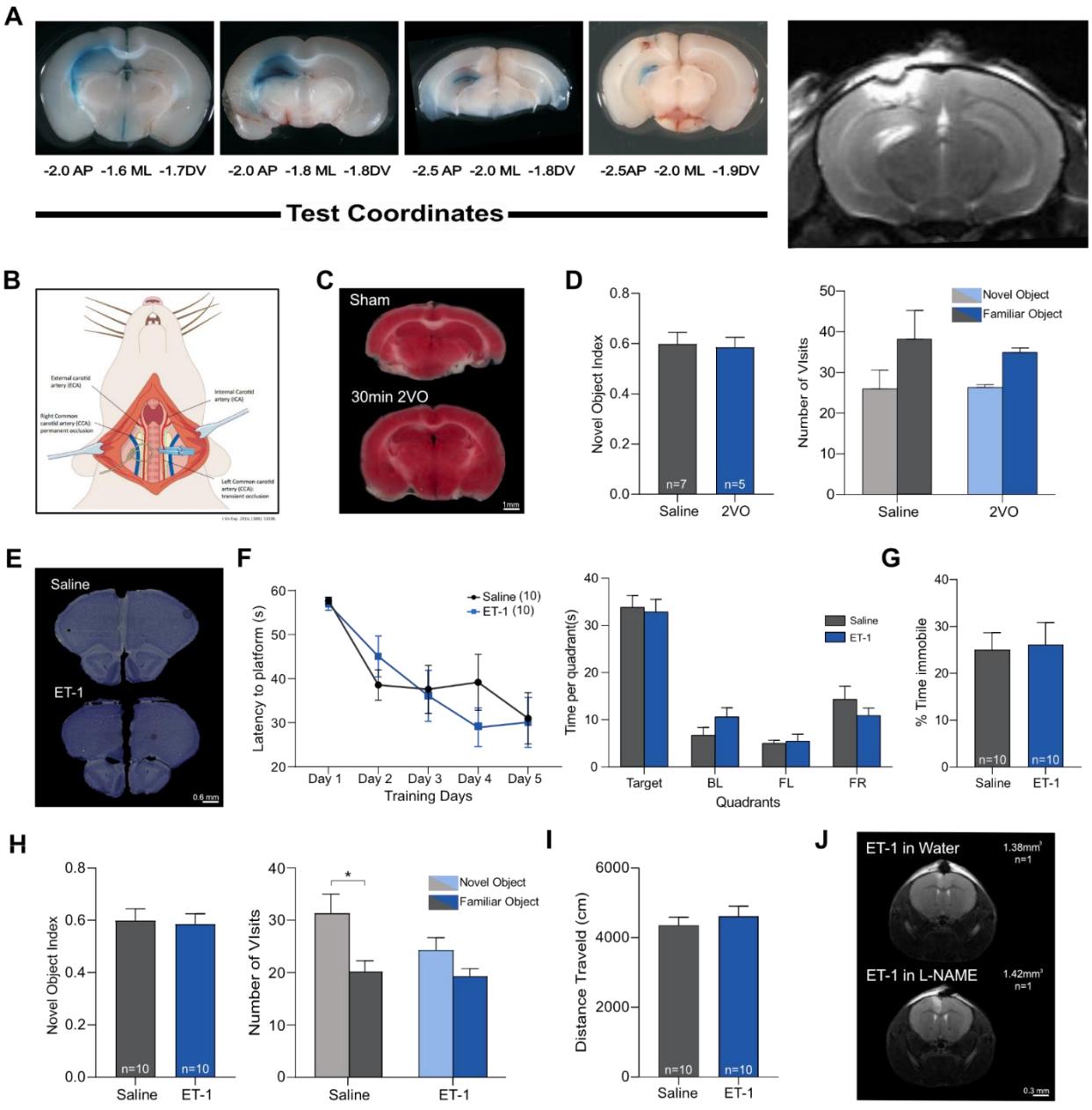
A
-2.0 AP -1.6 ML -1.7DV
-2.0 AP -1.8 ML -1.8DV
-2.5 AP -2.0 ML -1.8DV
-2.5AP -2.0 ML -1.9DV
Test Coordinates
B
External carotid artery (ECA)
Internal Carotid artery (ICA)
Right Common carotid artery (CCA): permanent occlusion
Left Common carotid artery (CCA): transient occlusion
C
Sham
30min 2VO
1mm
D
Novel Object Index
n=7
n=5
Saline
2VO
Number of VIsits
Novel Object
Familiar Object
Saline
2VO
E
Saline
ET-1
0.6 mm
F
Latency to platform (s)
Saline (10)
ET-1 (10)
Day 1
Day 2
Day 3
Day 4
Day 5
Training Days
Time per quadrant(s)
Saline
ET-1
Target
BL
FL
FR
Quadrants
G
% Time immobile
n=10
n=10
Saline
ET-1
H
Novel Object Index
n=10
n=10
Saline
ET-1
Number of VIsits
*
Novel Object
Familiar Object
Saline
ET-1
I
Distance Traveld (cm)
n=10
n=10
Saline
ET-1
J
ET-1 in Water
1.38mm³
n=1
ET-1 in L-NAME
1.42mm³
n=1
0.3 mm

Figure 9. Assaying ischemic models of cognitive deficits. A) 500μm thick representative coronal brain slices demonstrating various coordinates tested using alcian blue dye intracranial injections; Representative MRI image demonstrating lesion in DG region of hippocampus, 48hrs post ET-1 stroke. **B)** Representative image of the two-vessel occlusion model of global ischemia **C)** 500μm thick TTC stained representative coronal brain sections demonstrating infarct volume in hippocampus following sham surgery (top) or 30min 2 vessel occlusion (bottom). **D)** Bar graph demonstrating the effect of 30min vessel occlusion (blue) surgery compared to sham (grey) surgery on the novel object task. **E)** Representative cresyl violet sections (25μm thick) obtained from saline and ET-1 injections into the left mPFC, where the infarct is not visible. The effect of ET-1 (blue) and saline (grey) injections into the mPFC on the post stroke performance in the: **F)** Morris Water Maze; **G)** Forced Swim Test; **H)** Novel Object Task; **I)** Open Field Task. **J)** Representative MRI images demonstrating stroke volume resulting from injections of ET-1 in water and ET-1 in L-NAME into the left mPFC, when observed 48hrs post stroke. Data is mean ± SEM; statistical significance $p < 0.05$ *.

5.9 Pre-stroke administration of NFPS is beneficial to post-stroke vascular health

Stroke is primarily characterized as a vascular disease; therefore, we evaluated the impact of NFPS on vascular function and morphology following PT stroke. Using Laser Doppler flowmetry (LDF; Fig. 10A; right), we showed that pre-treatment with NFPS abolished the decrease in blood flow immediately following PT stroke compared to saline-treated mice (Fig. 10A; right). We further demonstrated that the degree of protection on vascular function following stroke was proportional to brain glycine levels. Mice treated with NFPS showed the highest degree of preserved blood flow post-stroke, $GlyT1^{+/-}$ had an intermediate degree of blood flow and $SR^{-/-}$ showed the most drastic decrease in blood flow (Fig. 10B).

Having established that NFPS improved post-stroke vascular function, we next assessed whether NFPS could modify vascular morphology by pairing transcardial perfusions of a fluorescent dye with tissue clearing and light sheet fluorescence microscopy (LSFM). We first constructed a home-made light sheet microscope (Suppl. Fig. 4A) and assayed various tissue clearing methods such as SeeDB, ScaleA2, PEGASOS, and iDISCO+ (Suppl. Fig. 4B). These methods were all unsuccessful due to limitations on tissue volume able to be cleared, poor transparency, dangerous organic solvents, and significant tissue shrinkage, respectively. Most notably, methods involving organic solvents such as PEGASOS and iDISCO were incompatible with our 3D printed imaging chambers. Organic solvent-based methods also often resulted in increased light scattering within the tissue leading to a poor signal to noise ratio (Suppl. Fig. 4C) thus making analysis impossible.

The CUBIC method of tissue clearing offered us the best tissue clearing (Suppl. Fig. 4D). Subsequently to determining a successful clearing method, we confirmed that our transcardial injections of fluorescent dye labeled the entire cerebral vascular network, as it was colocalized with collagen IV and CD31 vascular immunostaining (Suppl. Fig. 4E). We then ensured that this pairing of transcardial perfusions of a fluorescent dye with tissue clearing resulted in high quality images when acquired with our LSFM. Figure 10C depicts a maximum projection image of a left hemisphere collected 48hrs post stroke as well as raw images of single planes of the tissue at different depths.

To quantify the effect of NFPS on post stroke vasculature, we repeated the same experimental model as previously described. NFPS was administered 24hrs prior to PT stroke induction and animals were collected 48hrs post-stroke for analysis. We used a deep learning segmentation model to automatically calculate stroke volume from our cleared tissue (Fig. 10D; Video S4). Here, we observed a significant ~40% decrease in stroke volume in NFPS-treated mice compared to saline-treated mice (Fig. 10E). These results were consistent with data illustrated in figure 2B. We further explored the effect of NFPS following PT on vessel properties by using AIVIA (DRVISION) to segment and analyze these data (Fig. 10F). Here we show that the PT-induced-decrease in vascular density was attenuated in NFPS-treated mice compared to saline-treated mice, in the peri-infarct region (Fig. 10G). Furthermore, NFPS treatment lessened the PT-induced loss in vessels of smaller diameter (Fig. 10H) and length (Fig. 10I) compared to saline-treated mice, in the peri-infarct region. Taken together, these data strongly suggest that NFPS is beneficial to post-stroke vascular integrity, however more work is required to ascertain the exact mechanism by which this occurs.

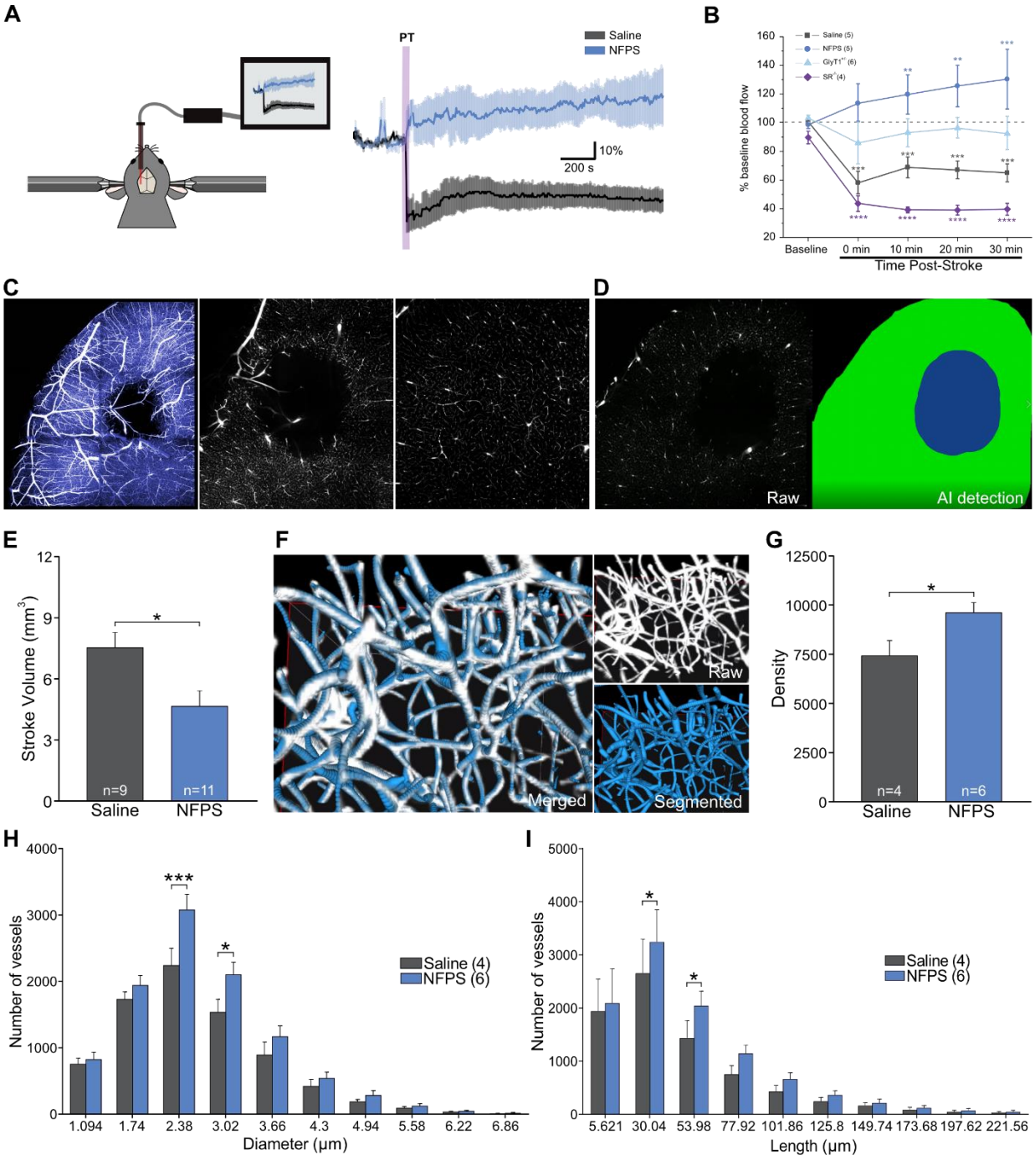
A
PT
Saline
NFPS
10%
200 s
B
% baseline blood flow
Baseline
0 min
10 min
20 min
30 min
Time Post-Stroke
C
D
Raw
AI detection
E
Stroke Volume (mm3)
n=9
n=11
Saline
NFPS
F
Raw
Merged
Segmented
G
Density
n=4
n=6
Saline
NFPS
H
Number of vessels
Saline (4)
NFPS (6)
Diameter (µm)
1.094
1.74
2.38
3.02
3.66
4.3
4.94
5.58
6.22
6.86
I
Number of vessels
Saline (4)
NFPS (6)
Length (µm)
5.621
30.04
53.98
77.92
101.86
125.8
149.74
173.68
197.62
221.56

Figure 10. NFPS has a protective effect on vascular function and morphology. A) Representative cartoon of the Laser Doppler Flow recording method; The effect of NFPS (blue) on cerebral blood flow post PT stroke compared to saline (grey) over 30mins. **B)** The effect of different levels of endogenous or exogenous brain glycine/D-serine levels on cerebral blood flow post PT stroke. **C)** Maximum projection of left hemisphere collected 48hrs post PT stroke (left); 2D section of raw data collected with light sheet microscope (right) at depths of -0.5mm (middle) and -3mm (right). **D)** Depiction of raw data (left) and of AI detection (right) of raw data. **E)** Bar graph representing stroke volume detected by our home-made AI software in NFPS (blue) treated mice compared to saline (grey) treated mice, when measured 48hrs post PT stroke. **F)** A 3D voxel of raw data collected with light sheet microscope, representing blood vessels (top right). Automatic segmentation done by AIVA software of raw data (bottom right) and merged image of raw data, overlayed with automated segmentation demonstrating high degree of accuracy (left). **G)** Bar graph demonstrating differences in vessel density in the peri-infarct region of mice treaded with NFPS (blue) or saline (grey). **H)** Bar graph representing the number of vessels counted per diameter in NFPS (blue) treated mice, compared to saline (grey) treated mice. **I)** Bar graph representing the number of vessels counted per length in NFPS (blue) treated mice, compared to saline (grey) treated mice. Data is mean ± SEM; statistical significance $p < 0.05$ *, $p < 0.01$, $p < 0.001$*** and $p < 0.0005$ ****.

6. DISCUSSION

This thesis highlights the possibility of utilizing GlyT1As as a novel pharmacotherapy for ischemic stroke. Using two different models of ischemia, we show that pre-treatment with our GlyT1-A of interest, NFPS, significantly ameliorates stroke volume, cell death, and behavioural deficits. Based on electrophysiological work performed in the lab, we observed that elevated glycine levels resulted in NMDAR internalization and that glycine was released during ischemic conditions. Therefore, we hypothesized that when administered prior to stroke, the elevation of synaptic glycine levels induced by NFPS would also trigger GINI. By investigating the effect of NFPS in the presence of non-internalizing NMDARs *in vitro* and *in vivo*, we concluded that this strategy does act *via* GINI. Not only did we confirm the mechanism of action to be GINI, but we are the first to show that GINI can and does occur *in vivo* and were able to acquire live cell imaging of GINI. Further, we show that GlyT1-As have beneficial effects on post-stroke vascular function and morphology, however the mechanism by which this occurs remains to be investigated. Overall, this work has a highly translational aspect and stresses the importance of investigating these compounds in the context of stroke.

Following our *in vitro* electrophysiological work, we investigated the effect of elevated glycine levels *in vivo* using the GlyT1$^{+/-}$ transgenic mouse line. These mice have a 50% reduction in levels of GlyT1 which results in chronically elevated levels of synaptic glycine (G. Tsai et al., 2004). Confirming our hypothesis that elevated glycine levels could trigger GINI which could in turn be neuroprotective, GlyT1$^{+/-}$ had significantly smaller stroke volumes than their WT littermates. Seeing as genetic manipulation of the GlyT1 gene is not a feasible treatment option in the human population, we next investigated recapitulating these results using the GlyT1-A,

NFPS. GlyT1-As are a class of drugs which specifically block GlyT1s which results in increased levels of synaptic glycine levels (Aubrey & Vandenberg, 2001; Mallorga et al., 2003). Here, in both models of focal ischemia, mice pre-treated with NFPS consistently demonstrated smaller stroke volumes. Interestingly, this phenotype was observed when NFPS was administered up to 30mins post stroke which highlights the possibility of potentially utilizing it as an acute treatment. However, it seeing as a more robust phenotype was consistently observed when NFPS was administered pre-stroke, it seems more likely these compounds may be used as a prevention measure rather than an acute treatment. For example, it could be prescribed similarly to how aspirin currently is.

We consistently observed reduced motor deficits in the adhesive removal task in NFPS-treated mice. Interestingly, the cylinder task revealed no difference in NFPS-treated mice compared to saline-treated mice in either model, perhaps as this is a simpler task to perform. However, NFPS specifically ameliorated hindlimb deficits in the horizontal ladder task following ET-1 stroke. This may be a direct result of the stroke coordinates chosen for the ET-1 stroke, which impairs a larger area of the cortical hindlimb representation. Alternatively, this may be due to the fact that animals are better able to use their vision to plan paw placement in their forelimbs versus their hindlimbs. In any case, a more pronounced hindlimb effect is a novel finding.

Unfortunately, a suitable model of stroke-induced cognitive deficits was not established and as such changes in post stroke cognition were not able to be evaluated. However, given the body of literature suggesting GlyT1-As involvement in cognition (Christmas et al., 2014; Harvey & Yee, 2013), it is possible NFPS could ameliorate these symptoms *in vivo* as well. It is likely that

further testing and troubleshooting would have resulted in successfully inducing cognitive deficits following ET-1 in the mPFC. It should be noted that the literature on cognitive changes in the human population post stroke suggests that these changes occur not due to the infarct but rather due to the limitations on activities of daily living because of reduced mobility and independence. These aspects are difficult to model in rodent behavioural testing. Therefore, attempting to model these behavioural phenotypes by impairing various regions of the brain to impact some aspects of executive and visuo-spatial function does not entirely capture the changes a human may experience. One alternative way to evaluate how NFPS may impact cognition would be to administer it to healthy animals and observe upward changes in their cognition compared to saline treated animals. Overall, this *in vivo* work strongly implies that elevation of glycine levels prior to or shortly after stroke is a strategy which offers neuroprotection.

Having demonstrated these neuroprotective phenotypes, we next aimed to confirm if NFPS did in fact induce GINI. We accomplished this by investigating the post stroke outcome of NFPS-treated mice in the presence of non-internalizing NMDARs. We first utilized live-cell imaging of HEK cells transfected with either WT-GluN1-containing NMDARs or mutant, non-internalizing A714L-GluN1-containing NMDARs. We utilized a novel strategy of tagging extracellular NMDARs with a cell-impermeable nanobody. Therefore, the only possible way to observe signal from this nanobody from within the cell is when that receptor is internalized. As predicted, WT cells were shown to undergo GINI following application of an internalizing dose of glycine while A714L cells did not. We then packaged this mutation into an AAV and investigated the effects of NFPS in mice having been cortically infected with non-internalizing NMDARs. Again,

NFPS elicited neuroprotection in mice infected with AAV-GluN1-WT as they had smaller stroke volumes and attenuated motor deficits in the adhesive removal task. In mice infected with AAV-GluN1-A714L however, the effect of NFPS was abolished indicating GINI is crucial for eliciting the neuroprotection observed in NFPS treated animals.

Glycine has previously been investigated as a neuroprotective agent. In fact, many studies have successfully elucidated various mechanisms by which glycine affords neuroprotection, however these studies have failed to elevate their work into feasible pre-clinical compounds. Recent work suggests that it is *via* modulation of intracellular pathways, including the phosphatase and tensin homolog (PTEN)/protein kinase B (AKT) signaling pathway (Qin et al., 2019; Zhao et al., 2018), or vascular endothelial growth factor receptor 2 (Z. Chen et al., 2020). Glycine is also thought to exert its neuroprotective effects *via* mediation of non-ionotropic NMDAR function (J. Chen et al., 2017; Z. Chen et al., 2015; Hu et al., 2016), or by promoting microglial polarization (R. Liu et al., 2019). Others have suggested that activation of ionotropic glycine receptors prior to tMCAO are responsible for the neuroprotective phenotype observed in GlyT1-A-treated animals (B. Huang et al., 2016). Moreover, research has demonstrated that the level of extracellular glycine appears to be important in stroke outcome. A low level of glycine, corresponding to increased NMDAR activation, appears to be deleterious. In contrast, an elevated level of glycine appears to be neuroprotective (Yao et al., 2012), as we have also observed. While these mechanisms are reported to occur *in vivo* and offer some degree of neuroprotection, we have strong evidence to suggest that the elevated levels of glycine elicited by GlyT1-A administration trigger GINI which is primarily responsible for neuroprotection following stroke.

Interestingly, glycine has also been shown to influence vasculature in various pathological states. These findings may in part explain some of the observations we made. For example, some recent work indicates that elevated levels of glycine increase vascular endothelial growth factor (VEGF) levels which could in turn increase post-stroke angiogenesis thus ameliorating the revascularization of the infarct area (Guo et al., 2017). Others have implicated GlyR-α2 in improved post-stroke vascular outcomes following treatment with elevated glycine levels (Z. Chen et al., 2020). Overall, it would be interesting to investigate the effect of NFPS on these markers as well as long-term vascular recovery in future work to truly elucidate the mechanism by which the improved vascular phenotype we observed occurred.

As mentioned in the introduction, there has long been interest in pharmaceutically manipulating NMDARs during stroke and many pre-clinical studies showed promising results (Simon et al., 1984). However, these interventions failed as they permanently blocked the proper functioning of the receptor. It is now known that this strategy impedes upon neuronal functioning and communication thus rendering it unusable in clinical settings. Using GlyT1-As, we were able to modulate NMDAR function specifically during stroke. Importantly, this strategy does not directly block NMDARs but rather dynamically and reversibly dampens NMDAR-mediated excitotoxicity exclusively during ischemia while also maintaining basal synaptic activity of NMDARs. As such, this strategy successfully inhibits a major player in the ischemic cascade in a novel way. This thesis has described multiple ways in which these compounds offer neuroprotection in *in vivo* models of stroke. These results are of particular interest given GlyT1-As extensive use in clinical trials. While these clinical trials were largely unsuccessful in improving symptoms of conditions such as schizophrenia, it is important to note that the

compounds were consistently well tolerated with few side-effects reported even when taken chronically over extended periods of time (Harvey & Yee, 2013). This demonstrates the highly translational impact of the work outlined in this thesis and indicates GlyT1-As could be studied for their use in stroke in the human population in the near future.

Overall, our data demonstrate that elevation of glycine with GlyT1-As before or shortly after an ischemic event may provide a rationale for the repurposing of currently approved pharmaceuticals as potential stroke treatments. For example, there is currently a glycine re-uptake blocker being studied for its efficacy in improving vascular dementia by the pharmaceutical company Boehringer Ingelheim. Given the pre-clinical efficacy of this class of drugs in minimizing the deficits induced by PT and ET-1 paradigms described in this thesis and considering that several GlyT1-As have been tested and proven to be safe and well tolerated in human clinical trials, GlyT1 should be tested as a new therapeutic for ischemic stroke.

7. CONCLUSION

In conclusion, this thesis aimed to ascertain if GlyT1-As trigger GINI during ischemic events, and if this strategy could provide neuroprotection. To do so, we employed a multidisciplinary approach including *in vitro* techniques (whole-cell patch-clamp recording, sniffer-patch technique, live cell-imaging), microscopy techniques (light sheet microscopy, tissue clearing, live cell-imaging), point mutation and viral construct transduction/infection, as well as several *in vivo* models of ischemic stroke, several behavioural tasks and laser doppler flowmetry (LDF).

We concluded that when synaptic levels of glycine were elevated *via* the administration of GlyT1-As prior to an ischemic event, GINI was triggered *in vivo*. We then confirmed this strategy provided neuroprotection as animals treated with GlyT1-As showed smaller stroke volumes as well as improved post-stroke behavioural outcomes. Interestingly, we have data supporting this strategy could also be neuroprotective when GlyT1-As are administered post-stroke. Finally, we also observed a robust vascular phenotype in mice pre-treated with GlyT1-As, yet the mechanism supporting this observation remains to be discovered.

Given the lack of currently available pharmacotherapies for both the prevention and acute treatment of ischemic stroke, novel pharmacotherapies are desperately needed. We believe that our data provides a strong rationale to investigate the use of GlyT1-As for stroke. Furthermore, when we take into consideration the fact that GlyT1-As have been repeatedly shown to be safe and well tolerated in human clinical trials, the translational aspect of this work becomes even more apparent and support the possibility of investigating these findings in the context of clinical trials in the near future.

8. TABLES

Primary Antibody	Source	Catalogue Number	Dilution
Rabbit polyclonal anti-CD31	Abcam	ab28364	1:50
Rabbit polyclonal anti-Collagen IV	Abcam	ab19808	1:400
FluoTag®-X4 anti-GFP, conjugated with Alexa Fluor 647	NanoTag Biotechnologies	N0304	1:250-1:500

Secondary Antibody	Source	Catalogue Number	Dilution
Goat Anti-Rabbit IgG H&L (Alexa Fluor® 647)	Abcam	ab150079	1:400

Table 1. List of antibodies.

Primer	Sequence
NhelGluN1-F	5'-AGCTAGCATGAGCACCATGCACCTGCT-3'
EcoRVGluN1-R	5'-AGATATCTCAGCTCTCCCTATGACGGG-3'
A714L-F	5'-ACAATTACGAGAGCCTGGCTGAGGCCATCCA -3'
A714L-R	5'- GCTCTCGTAATTGTGTTTTCCATGTGCCG-3'

Table 2. Primers used for GluN1 variants subcloning into pcDNA3.1. F indicates a forward primer; R indicates a reverse primer.

9. SUPPLEMENTAL FIGURES

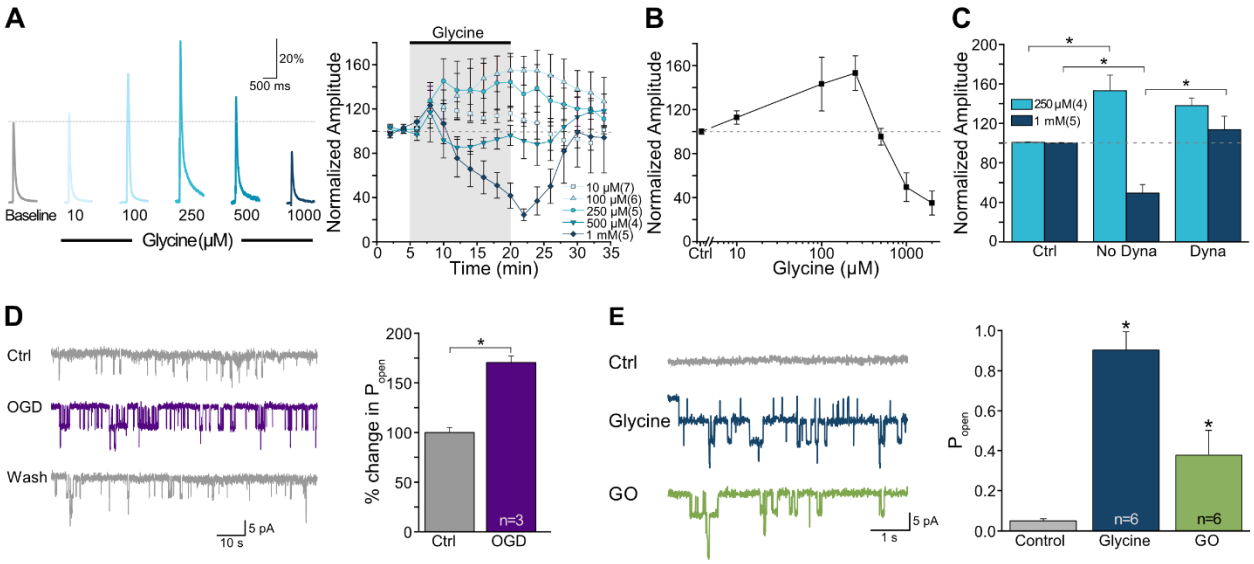

Supplemental Figure 1. Elevated glycine concentrations result in NMDAR internalization and can occur during ischemia. A) Normalized raw traces showing the effect of increasing concentrations of exogenous glycine on Schaffer Collateral NMDAR-EPSCs and mean time-course data showing the effect of a 15mins application of various glycine concentrations. **B)** A dose-response curve of glycine and NMDAR-EPSC amplitudes. **C)** The effect of 250μM and 1mM glycine on NMDAR-EPSC amplitudes in the presence of dynasore. **D)** The effect of oxygen-glucose deprivation (OGD) on P_{open} of homomeric α2 glycine receptors; changes in P_{open} in the presence of OGD alone. **E)** The effect of purified glycine oxidase (GO; an enzyme that catalyzes the breakdown of glycine) with 1μM glycine on P_{open} of homomeric α2 glycine receptors expressed in outside-out patches obtained from CHO cells during OGD. Data is mean ± SEM; statistical significance $p < 0.05$ *.

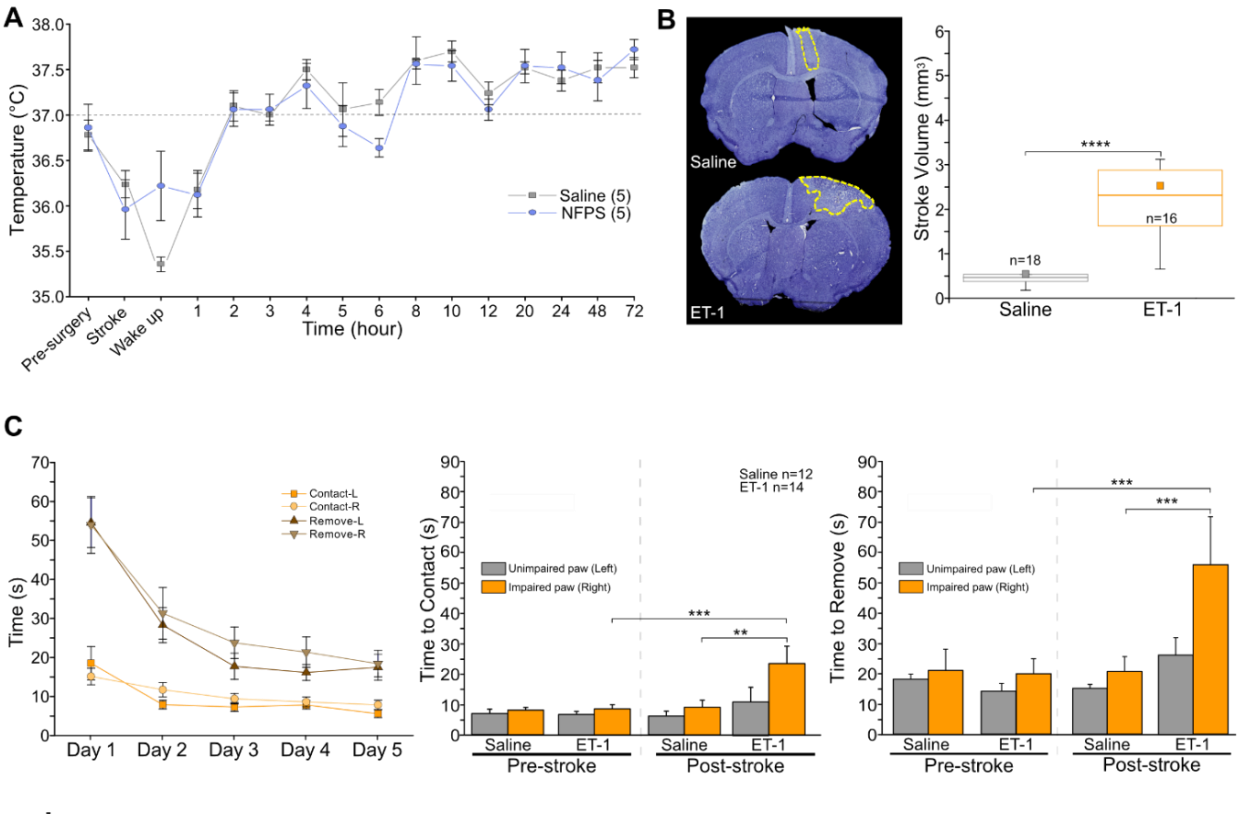

Supplemental Figure 2. *In vivo* control experiments. A) Temperature time-course experiment following photothrombotic stroke, showing no contribution of hypothermia on the therapeutic effect of NFPS. **B)** Representative cresyl violet sections (25µm thick) obtained from saline-treated and ET-1-treated mice, where the infarct is shown by the yellow border. A box and whisker plot depicting infarct volume observed in mice treated with ET-1 (red) compared with saline (black). **C)** The effect of ET-1 stroke on post-stroke time to contact and time to remove in the adhesive removal task compared with saline sham stroke. Data is mean ± SEM; statistical significance $p < 0.05$ *, $P < 0.01$ **, $p < 0.001$ *** and $p < 0.0005$ ****.

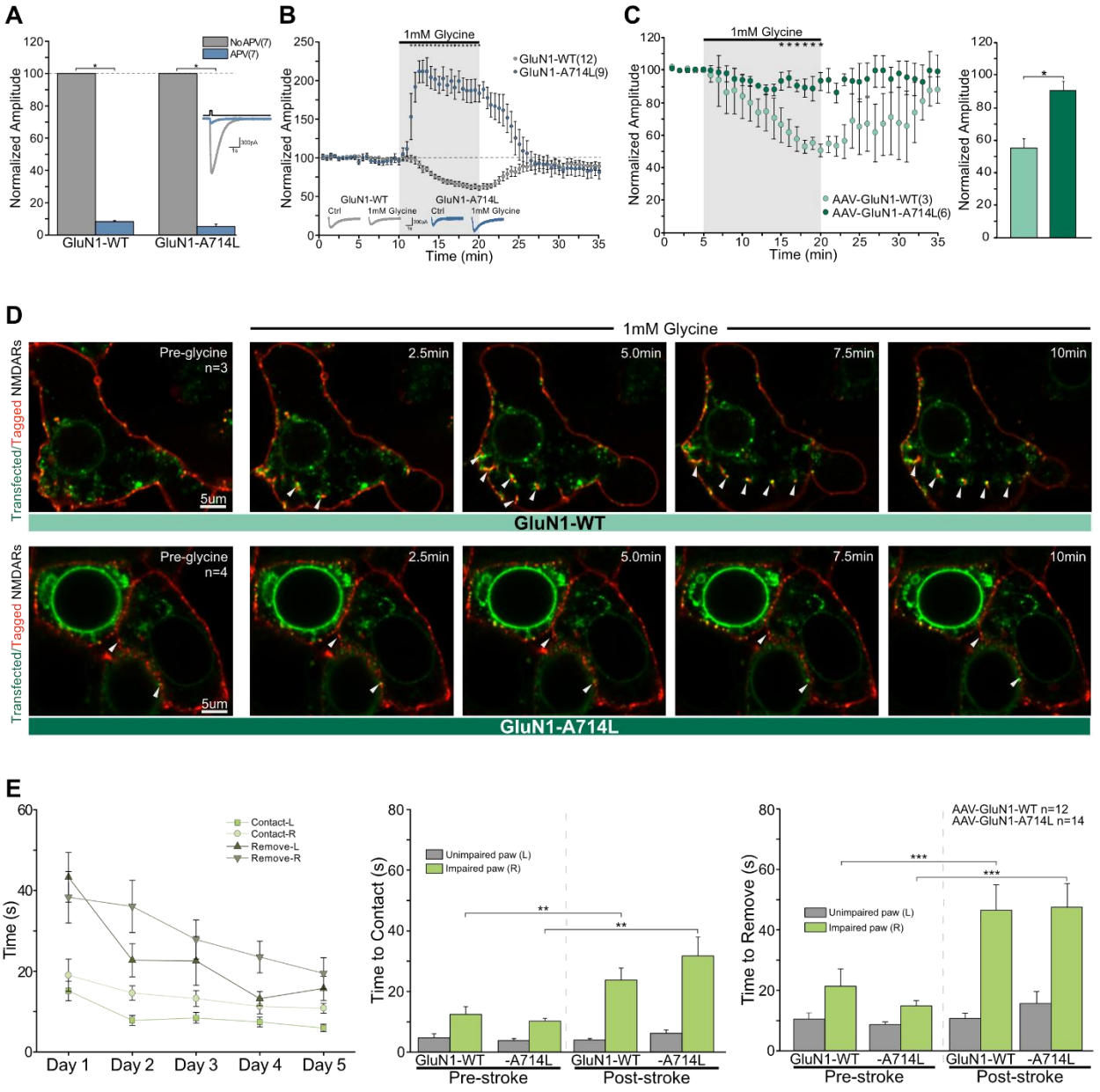

Supplemental Figure 3. GluN1-A714L mutation control experiments. A) Normalized NMDAR-EPSC amplitudes and normalized raw data traces recorded from GluN1-WT and GluN1-A714L transfected HEK293 cells with and without the NMDAR competitive antagonist, APV. **B)** Normalized NMDAR-EPSC amplitudes mean time-course data showing the effect of 1mM glycine application in GluN1-WT and GluN1-A714L transfected HEK293 cells. **C)** Normalized NMDAR-EPSC amplitudes mean time-course data showing the effect of 1mM glycine application in GluN1-WT and GluN1-A714L infected cells from acute hippocampal slice recordings. **D)** Visual representation of the internalization of NMDARs into the cell in GluN1-WT and GluN1-A714L transfected HEK293 cells. Transfected NMDARs are labeled in green, and extracellular NMDARs are additionally labeled in red, with cell impermeable nanobody. **E)** Effect of adeno-associated virus (AAV)-GluN1-WT and AAV-GluN1-A714L intracortical injections alone on post-stroke behavioural performance in the adhesive removal task. Data is mean ± SEM; statistical significance $p < 0.05$ *, $p < 0.01$**, $p < 0.001$ *** and $p < 0.0005$ ****.

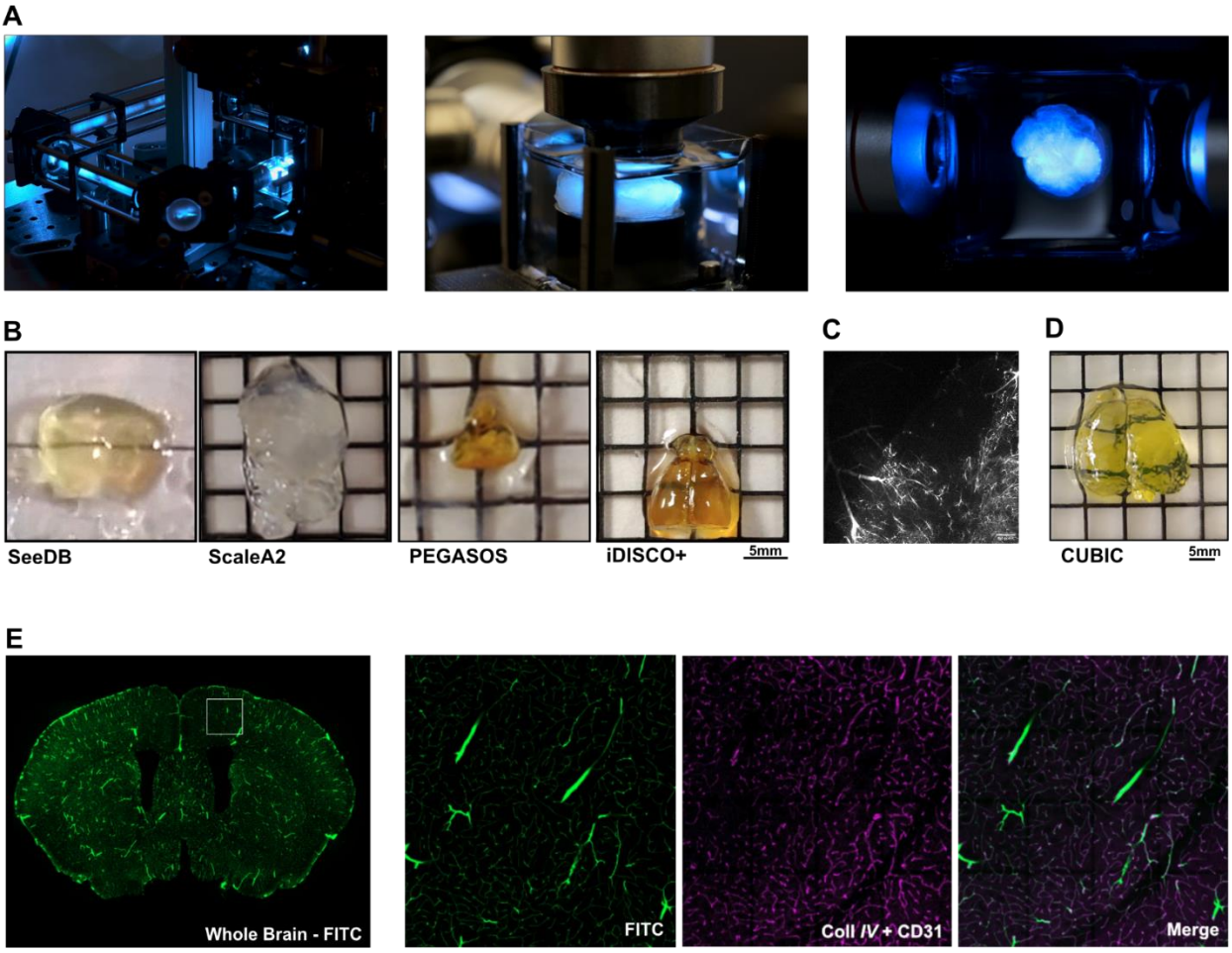

Supplemental Figure 4. Light sheet and tissue clearing control experiments. A) Depiction of our home-made light sheet microscope. **B)** Representative images of four distinct clearing methods; SeeDB, ScaleA2, PEGASOS, iDISCO^{+} respectively. **C)** Example of poor tissue clearing. **D)** Representative image demonstrating clearing method used for all light sheet experiments: CUBIC. **E)** 50μm coronal section of brain perfused with FITC-BSA (left); magnified images from the sensorimotor cortex demonstrating exact colocalization of FITC-BSA perfusion (green) with CD31 and CollIV vascular immunostaining (purple).

10. VIDEOS

https://drive.google.com/file/d/1u3fFBbEQhNADnC-EjOKSdM-kzzVUUa--/view?usp=sharing

11. REFERENCES

Uncategorized References

Allen, T. G. (1997). The 'sniffer-patch' technique for detection of neurotransmitter release. *Trends Neurosci, 20*(5), 192-197. doi:10.1016/s0166-2236(96)01039-9

Ansara, A. J., Nisly, S. A., Arif, S. A., Koehler, J. M., & Nordmeyer, S. T. (2010). Aspirin dosing for the prevention and treatment of ischemic stroke: an indication-specific review of the literature. *Ann Pharmacother, 44*(5), 851-862. doi:10.1345/aph.1M346

Aprison, M. H., & Werman, R. (1965). The distribution of glycine in cat spinal cord and roots. *Life Sci, 4*(21), 2075-2083. doi:10.1016/0024-3205(65)90325-5

Arnett, D. K., Blumenthal, R. S., Albert, M. A., Buroker, A. B., Goldberger, Z. D., Hahn, E. J., . . . Ziaeian, B. (2019a). 2019 ACC/AHA Guideline on the Primary Prevention of Cardiovascular Disease: A Report of the American College of Cardiology/American Heart Association Task Force on Clinical Practice Guidelines. *Circulation, 140*(11), e596-e646. doi:10.1161/CIR.0000000000000678

Arnett, D. K., Blumenthal, R. S., Albert, M. A., Buroker, A. B., Goldberger, Z. D., Hahn, E. J., . . . Ziaeian, B. (2019b). 2019 ACC/AHA Guideline on the Primary Prevention of Cardiovascular Disease: A Report of the American College of Cardiology/American Heart Association Task Force on Clinical Practice Guidelines. *J Am Coll Cardiol, 74*(10), e177-e232. doi:10.1016/j.jacc.2019.03.010

Aubrey, K. R., Rossi, F. M., Ruivo, R., Alboni, S., Bellenchi, G. C., Le Goff, A., . . . Supplisson, S. (2007). The transporters GlyT2 and VIAAT cooperate to determine the vesicular glycinergic phenotype. *J Neurosci, 27*(23), 6273-6281. doi:10.1523/JNEUROSCI.1024-07.2007

Aubrey, K. R., & Vandenberg, R. J. (2001). N[3-(4'-fluorophenyl)-3-(4'-phenylphenoxy)propyl]sarcosine (NFPS) is a selective persistent inhibitor of glycine transport. *Br J Pharmacol, 134*(7), 1429-1436. doi:10.1038/sj.bjp.0704381

Balkaya, M., Krober, J., Gertz, K., Peruzzaro, S., & Endres, M. (2013). Characterization of long-term functional outcome in a murine model of mild brain ischemia. *J Neurosci Methods, 213*(2), 179-187. doi:10.1016/j.jneumeth.2012.12.021

Bannerman, D. M., Good, M. A., Butcher, S. P., Ramsay, M., & Morris, R. G. (1995). Distinct components of spatial learning revealed by prior training and NMDA receptor blockade. *Nature, 378*(6553), 182-186. doi:10.1038/378182a0

Basu, A. C., Tsai, G. E., Ma, C. L., Ehmsen, J. T., Mustafa, A. K., Han, L., . . . Coyle, J. T. (2009). Targeted disruption of serine racemase affects glutamatergic neurotransmission and behavior. *Mol Psychiatry, 14*(7), 719-727. doi:10.1038/mp.2008.130

Benedek, A., Moricz, K., Juranyi, Z., Gigler, G., Levay, G., Harsing, L. G., Jr., . . . Albert, M. (2006). Use of TTC staining for the evaluation of tissue injury in the early phases of reperfusion after focal cerebral ischemia in rats. *Brain Res, 1116*(1), 159-165. doi:10.1016/j.brainres.2006.07.123

Benmerah, A., & Lamaze, C. (2007). Clathrin-coated pits: vive la difference? *Traffic, 8*(8), 970-982. doi:10.1111/j.1600-0854.2007.00585.x

Bergeron, R., Meyer, T. M., Coyle, J. T., & Greene, R. W. (1998). Modulation of N-methyl-D-aspartate receptor function by glycine transport. *Proc Natl Acad Sci U S A, 95*(26), 15730-15734. doi:10.1073/pnas.95.26.15730

Betz, H., Gomeza, J., Armsen, W., Scholze, P., & Eulenburg, V. (2006). Glycine transporters: essential regulators of synaptic transmission. *Biochem Soc Trans, 34*(Pt 1), 55-58. doi:10.1042/BST0340055

Biswas, S., & Barma, S. (2020). A large-scale optical microscopy image dataset of potato tuber for deep learning based plant cell assessment. *Sci Data, 7*(1), 371. doi:10.1038/s41597-020-00706-9

Borowsky, B., Mezey, E., & Hoffman, B. J. (1993). Two glycine transporter variants with distinct localization in the CNS and peripheral tissues are encoded by a common gene. *Neuron, 10*(5), 851-863. doi:10.1016/0896-6273(93)90201-2

Bouet, V., Boulouard, M., Toutain, J., Divoux, D., Bernaudin, M., Schumann-Bard, P., & Freret, T. (2009). The adhesive removal test: a sensitive method to assess sensorimotor deficits in mice. *Nat Protoc, 4*(10), 1560-1564. doi:10.1038/nprot.2009.125

Bowery, N. G., & Smart, T. G. (2006). GABA and glycine as neurotransmitters: a brief history. *Br J Pharmacol, 147 Suppl 1*, S109-119. doi:10.1038/sj.bjp.0706443

Can, A., Dao, D. T., Arad, M., Terrillion, C. E., Piantadosi, S. C., & Gould, T. D. (2012). The mouse forced swim test. *J Vis Exp*(59), e3638. doi:10.3791/3638

Carroll, R. C., & Zukin, R. S. (2002). NMDA-receptor trafficking and targeting: implications for synaptic transmission and plasticity. *Trends Neurosci, 25*(11), 571-577. doi:10.1016/s0166-2236(02)02272-5

Casals, J. B., Pieri, N. C., Feitosa, M. L., Ercolin, A. C., Roballo, K. C., Barreto, R. S., . . . Ambrosio, C. E. (2011). The use of animal models for stroke research: a review. *Comp Med, 61*(4), 305-313. Retrieved from https://www.ncbi.nlm.nih.gov/pubmed/22330245

Chen, J., Hu, R., Liao, H., Zhang, Y., Lei, R., Zhang, Z., . . . Wan, Q. (2017). A non-ionotropic activity of NMDA receptors contributes to glycine-induced neuroprotection in cerebral ischemia-reperfusion injury. *Sci Rep, 7*(1), 3575. doi:10.1038/s41598-017-03909-0

Chen, Z., Hu, B., Wang, F., Du, L., Huang, B., Li, L., . . . Wang, X. (2015). Glycine bidirectionally regulates ischemic tolerance via different mechanisms including NR2A-dependent CREB phosphorylation. *J Neurochem, 133*(3), 397-408. doi:10.1111/jnc.12994

Chen, Z., Wang, X., Liao, H., Sheng, T., Chen, P., Zhou, H., . . . Yao, H. (2020). Glycine attenuates cerebrovascular remodeling via glycine receptor alpha 2 and vascular endothelial growth factor receptor 2 after stroke. *Am J Transl Res, 12*(10), 6895-6907. Retrieved from https://www.ncbi.nlm.nih.gov/pubmed/33194080

Christmas, D., Diaper, A., Wilson, S., Rich, A., Phillips, S., Udo de Haes, J., . . . Nutt, D. (2014). A randomised trial of the effect of the glycine reuptake inhibitor Org 25935 on cognitive performance in healthy male volunteers. *Hum Psychopharmacol, 29*(2), 163-171. doi:10.1002/hup.2384

Cioffi, C. L. (2018). Glycine transporter-1 inhibitors: a patent review (2011-2016). *Expert Opin Ther Pat, 28*(3), 197-210. doi:10.1080/13543776.2018.1429408

Clark, W. M., Wissman, S., Albers, G. W., Jhamandas, J. H., Madden, K. P., & Hamilton, S. (1999). Recombinant tissue-type plasminogen activator (Alteplase) for ischemic stroke 3 to 5 hours after symptom onset. The ATLANTIS Study: a randomized controlled trial. Alteplase Thrombolysis for Acute Noninterventional Therapy in Ischemic Stroke. *JAMA, 282*(21), 2019-2026. doi:10.1001/jama.282.21.2019

Collaborators, G. B. D. M. M. (2016). Global, regional, and national levels of maternal mortality, 1990-2015: a systematic analysis for the Global Burden of Disease Study 2015. *Lancet, 388*(10053), 1775-1812. doi:10.1016/S0140-6736(16)31470-2

Collen, D., & Lijnen, H. R. (2009). The tissue-type plasminogen activator story. *Arterioscler Thromb Vasc Biol, 29*(8), 1151-1155. doi:10.1161/ATVBAHA.108.179655

Collingridge, G. L., Isaac, J. T., & Wang, Y. T. (2004). Receptor trafficking and synaptic plasticity. *Nat Rev Neurosci, 5*(12), 952-962. doi:10.1038/nrn1556

Cook, D. J., Teves, L., & Tymianski, M. (2012). Treatment of stroke with a PSD-95 inhibitor in the gyrencephalic primate brain. *Nature, 483*(7388), 213-217. doi:10.1038/nature10841

Coyle, J. T., & Tsai, G. (2004). The NMDA receptor glycine modulatory site: a therapeutic target for improving cognition and reducing negative symptoms in schizophrenia. *Psychopharmacology (Berl), 174*(1), 32-38. doi:10.1007/s00213-003-1709-2

Curtis, D. R., Hosli, L., & Johnston, G. A. (1967). Inhibition of spinal neurons by glycine. *Nature, 215*(5109), 1502-1503. doi:10.1038/2151502a0

Danysz, W., & Parsons, C. G. (1998). Glycine and N-methyl-D-aspartate receptors: physiological significance and possible therapeutic applications. *Pharmacol Rev, 50*(4), 597-664. Retrieved from https://www.ncbi.nlm.nih.gov/pubmed/9860805

Dingledine, R., Borges, K., Bowie, D., & Traynelis, S. F. (1999). The glutamate receptor ion channels. *Pharmacol Rev, 51*(1), 7-61. Retrieved from https://www.ncbi.nlm.nih.gov/pubmed/10049997

Dirnagl, U., Iadecola, C., & Moskowitz, M. A. (1999). Pathobiology of ischaemic stroke: an integrated view. *Trends Neurosci, 22*(9), 391-397. doi:10.1016/s0166-2236(99)01401-0

Dojo Soeandy, C., Salmasi, F., Latif, M., Elia, A. J., Suo, N. J., & Henderson, J. T. (2019). Endothelin-1-mediated cerebral ischemia in mice: early cellular events and the role of caspase-3. *Apoptosis, 24*(7-8), 578-595. doi:10.1007/s10495-019-01541-z

Doyle, S., Hansen, D. B., Vella, J., Bond, P., Harper, G., Zammit, C., . . . Fern, R. (2018). Vesicular glutamate release from central axons contributes to myelin damage. *Nat Commun, 9*(1), 1032. doi:10.1038/s41467-018-03427-1

Ehara, A., & Ueda, S. (2009). Application of Fluoro-Jade C in acute and chronic neurodegeneration models: utilities and staining differences. *Acta Histochem Cytochem, 42*(6), 171-179. doi:10.1267/ahc.09018

Emberson, J., Lees, K. R., Lyden, P., Blackwell, L., Albers, G., Bluhmki, E., . . . Stroke Thrombolysis Trialists' Collaborative, G. (2014). Effect of treatment delay, age, and stroke severity on the effects of intravenous thrombolysis with alteplase for acute ischaemic stroke: a meta-analysis of individual patient data from randomised trials. *Lancet, 384*(9958), 1929-1935. doi:10.1016/S0140-6736(14)60584-5

Eulenburg, V., & Gomeza, J. (2010). Neurotransmitter transporters expressed in glial cells as regulators of synapse function. *Brain Res Rev, 63*(1-2), 103-112. doi:10.1016/j.brainresrev.2010.01.003

Farr, T. D., Liu, L., Colwell, K. L., Whishaw, I. Q., & Metz, G. A. (2006). Bilateral alteration in stepping pattern after unilateral motor cortex injury: a new test strategy for analysis of skilled limb movements in neurological mouse models. *J Neurosci Methods, 153*(1), 104-113. doi:10.1016/j.jneumeth.2005.10.011

Ferguson, S. M., & De Camilli, P. (2012). Dynamin, a membrane-remodelling GTPase. *Nat Rev Mol Cell Biol, 13*(2), 75-88. doi:10.1038/nrm3266

Ge, Y., Chen, W., Axerio-Cilies, P., & Wang, Y. T. (2020). NMDARs in Cell Survival and Death: Implications in Stroke Pathogenesis and Treatment. *Trends Mol Med, 26*(6), 533-551. doi:10.1016/j.molmed.2020.03.001

Goldstein, L. B., & Hankey, G. J. (2006). Advances in primary stroke prevention. *Stroke, 37*(2), 317-319. doi:10.1161/01.STR.0000200456.43415.11

Gomeza, J., Ohno, K., Hulsmann, S., Armsen, W., Eulenburg, V., Richter, D. W., . . . Betz, H. (2003). Deletion of the mouse glycine transporter 2 results in a hyperekplexia phenotype and postnatal lethality. *Neuron, 40*(4), 797-806. doi:10.1016/s0896-6273(03)00673-1

Guastella, J., Brecha, N., Weigmann, C., Lester, H. A., & Davidson, N. (1992). Cloning, expression, and localization of a rat brain high-affinity glycine transporter. *Proc Natl Acad Sci U S A, 89*(15), 7189-7193. doi:10.1073/pnas.89.15.7189

Guo, D., Murdoch, C. E., Xu, H., Shi, H., Duan, D. D., Ahmed, A., & Gu, Y. (2017). Vascular endothelial growth factor signaling requires glycine to promote angiogenesis. *Sci Rep, 7*(1), 14749. doi:10.1038/s41598-017-15246-3

Hacke, W., Kaste, M., Bluhmki, E., Brozman, M., Davalos, A., Guidetti, D., . . . Investigators, E. (2008). Thrombolysis with alteplase 3 to 4.5 hours after acute ischemic stroke. *N Engl J Med, 359*(13), 1317-1329. doi:10.1056/NEJMoa0804656

Hacke, W., Kaste, M., Fieschi, C., Toni, D., Lesaffre, E., von Kummer, R., . . . et al. (1995). Intravenous thrombolysis with recombinant tissue plasminogen activator for acute hemispheric stroke. The European Cooperative Acute Stroke Study (ECASS). *JAMA, 274*(13), 1017-1025. Retrieved from https://www.ncbi.nlm.nih.gov/pubmed/7563451

Hama, H., Kurokawa, H., Kawano, H., Ando, R., Shimogori, T., Noda, H., . . . Miyawaki, A. (2011). Scale: a chemical approach for fluorescence imaging and reconstruction of transparent mouse brain. *Nat Neurosci, 14*(11), 1481-1488. doi:10.1038/nn.2928

Han, L., Campanucci, V. A., Cooke, J., & Salter, M. W. (2013). Identification of a single amino acid in GluN1 that is critical for glycine-primed internalization of NMDA receptors. *Mol Brain, 6*, 36. doi:10.1186/1756-6606-6-36

Harvey, R. J., & Yee, B. K. (2013). Glycine transporters as novel therapeutic targets in schizophrenia, alcohol dependence and pain. *Nat Rev Drug Discov, 12*(11), 866-885. doi:10.1038/nrd3893

Hatfield, R. H., Mendelow, A. D., Perry, R. H., Alvarez, L. M., & Modha, P. (1991). Triphenyltetrazolium chloride (TTC) as a marker for ischaemic changes in rat brain following permanent middle cerebral artery occlusion. *Neuropathol Appl Neurobiol, 17*(1), 61-67. doi:10.1111/j.1365-2990.1991.tb00694.x

Hernandes, M. S., & Troncone, L. R. (2009). Glycine as a neurotransmitter in the forebrain: a short review. *J Neural Transm (Vienna), 116*(12), 1551-1560. doi:10.1007/s00702-009-0326-6

Hill, M. D., Goyal, M., Menon, B. K., Nogueira, R. G., McTaggart, R. A., Demchuk, A. M., . . . Investigators, E.-N. (2020). Efficacy and safety of nerinetide for the treatment of acute ischaemic stroke (ESCAPE-NA1): a multicentre, double-blind, randomised controlled trial. *Lancet, 395*(10227), 878-887. doi:10.1016/S0140-6736(20)30258-0

Hill, M. D., Martin, R. H., Mikulis, D., Wong, J. H., Silver, F. L., Terbrugge, K. G., . . . investigators, E. t. (2012). Safety and efficacy of NA-1 in patients with iatrogenic stroke after endovascular aneurysm repair (ENACT): a phase 2, randomised, double-blind, placebo-controlled trial. *Lancet Neurol, 11*(11), 942-950. doi:10.1016/S1474-4422(12)70225-9

Hirst, J., & Robinson, M. S. (1998). Clathrin and adaptors. *Biochim Biophys Acta*, *1404*(1-2), 173-193. doi:10.1016/s0167-4889(98)00056-1

Hoeller, D., Volarevic, S., & Dikic, I. (2005). Compartmentalization of growth factor receptor signalling. *Curr Opin Cell Biol*, *17*(2), 107-111. doi:10.1016/j.ceb.2005.01.001

Hollmann, M., Boulter, J., Maron, C., & Heinemann, S. (1994). Molecular biology of glutamate receptors. Potentiation of N-methyl-D-aspartate receptor splice variants by zinc. *Ren Physiol Biochem*, *17*(3-4), 182-183. Retrieved from https://www.ncbi.nlm.nih.gov/pubmed/7518953

Hollmann, M., & Heinemann, S. (1994). Cloned glutamate receptors. *Annu Rev Neurosci*, *17*, 31-108. doi:10.1146/annurev.ne.17.030194.000335

Hopkin, J. M., & Neal, M. J. (1970). Thr release of 14C-glycine from electrically stimulated rat spinal cord slices. *Br J Pharmacol*, *40*(1), 136P-138P. Retrieved from https://www.ncbi.nlm.nih.gov/pubmed/4321078

Hu, R., Chen, J., Lujan, B., Lei, R., Zhang, M., Wang, Z., . . . Wan, Q. (2016). Glycine triggers a non-ionotropic activity of GluN2A-containing NMDA receptors to confer neuroprotection. *Sci Rep*, *6*, 34459. doi:10.1038/srep34459

Huang, B., Xie, Q., Lu, X., Qian, T., Li, S., Zhu, R., . . . Li, L. (2016). GlyT1 Inhibitor NFPS Exerts Neuroprotection via GlyR Alpha1 Subunit in the Rat Model of Transient Focal Cerebral Ischaemia and Reperfusion. *Cell Physiol Biochem*, *38*(5), 1952-1962. doi:10.1159/000445556

Huang, H., Barakat, L., Wang, D., & Bordey, A. (2004). Bergmann glial GlyT1 mediates glycine uptake and release in mouse cerebellar slices. *J Physiol*, *560*(Pt 3), 721-736. doi:10.1113/jphysiol.2004.067801

Ikonomidou, C., Stefovska, V., & Turski, L. (2000). Neuronal death enhanced by N-methyl-D-aspartate antagonists. *Proc Natl Acad Sci U S A*, *97*(23), 12885-12890. doi:10.1073/pnas.220412197

Ikonomidou, C., & Turski, L. (2002). Why did NMDA receptor antagonists fail clinical trials for stroke and traumatic brain injury? *Lancet Neurol*, *1*(6), 383-386. doi:10.1016/s1474-4422(02)00164-3

Jing, D., Zhang, S., Luo, W., Gao, X., Men, Y., Ma, C., . . . Zhao, H. (2018). Tissue clearing of both hard and soft tissue organs with the PEGASOS method. *Cell Res*, *28*(8), 803-818. doi:10.1038/s41422-018-0049-z

Jiwa, N. S., Garrard, P., & Hainsworth, A. H. (2010). Experimental models of vascular dementia and vascular cognitive impairment: a systematic review. *J Neurochem*, *115*(4), 814-828. doi:10.1111/j.1471-4159.2010.06958.x

Johnson, J. W., & Ascher, P. (1987). Glycine potentiates the NMDA response in cultured mouse brain neurons. *Nature*, *325*(6104), 529-531. doi:10.1038/325529a0

Ke, M. T., Fujimoto, S., & Imai, T. (2013). SeeDB: a simple and morphology-preserving optical clearing agent for neuronal circuit reconstruction. *Nat Neurosci*, *16*(8), 1154-1161. doi:10.1038/nn.3447

Ke, M. T., & Imai, T. (2014). Optical clearing of fixed brain samples using SeeDB. *Curr Protoc Neurosci*, *66*, Unit 2 22. doi:10.1002/0471142301.ns0222s66

Kermany, D. S., Goldbaum, M., Cai, W., Valentim, C. C. S., Liang, H., Baxter, S. L., . . . Zhang, K. (2018). Identifying Medical Diagnoses and Treatable Diseases by Image-Based Deep Learning. *Cell*, *172*(5), 1122-1131 e1129. doi:10.1016/j.cell.2018.02.010

Khoshnam, S. E., Winlow, W., Farzaneh, M., Farbood, Y., & Moghaddam, H. F. (2017). Pathogenic mechanisms following ischemic stroke. *Neurol Sci, 38*(7), 1167-1186. doi:10.1007/s10072-017-2938-1

Kleckner, N. W., & Dingledine, R. (1988). Requirement for glycine in activation of NMDA-receptors expressed in Xenopus oocytes. *Science, 241*(4867), 835-837. doi:10.1126/science.2841759

Kopec, K., Flood, D. G., Gasior, M., McKenna, B. A., Zuvich, E., Schreiber, J., . . . Marino, M. J. (2010). Glycine transporter (GlyT1) inhibitors with reduced residence time increase prepulse inhibition without inducing hyperlocomotion in DBA/2 mice. *Biochem Pharmacol, 80*(9), 1407-1417. doi:10.1016/j.bcp.2010.07.004

Lai, T. W., Shyu, W. C., & Wang, Y. T. (2011). Stroke intervention pathways: NMDA receptors and beyond. *Trends Mol Med, 17*(5), 266-275. doi:10.1016/j.molmed.2010.12.008

Lane, H. Y., Liu, Y. C., Huang, C. L., Chang, Y. C., Liau, C. H., Perng, C. H., & Tsai, G. E. (2008). Sarcosine (N-methylglycine) treatment for acute schizophrenia: a randomized, double-blind study. *Biol Psychiatry, 63*(1), 9-12. doi:10.1016/j.biopsych.2007.04.038

Lau, C. G., & Zukin, R. S. (2007). NMDA receptor trafficking in synaptic plasticity and neuropsychiatric disorders. *Nat Rev Neurosci, 8*(6), 413-426. doi:10.1038/nrn2153

Lee, C. J., Mannaioni, G., Yuan, H., Woo, D. H., Gingrich, M. B., & Traynelis, S. F. (2007). Astrocytic control of synaptic NMDA receptors. *J Physiol, 581*(Pt 3), 1057-1081. doi:10.1113/jphysiol.2007.130377

Lee, J. K., Park, M. S., Kim, Y. S., Moon, K. S., Joo, S. P., Kim, T. S., . . . Kim, S. H. (2007). Photochemically induced cerebral ischemia in a mouse model. *Surg Neurol, 67*(6), 620-625; discussion 625. doi:10.1016/j.surneu.2006.08.077

Leger, M., Quiedeville, A., Bouet, V., Haelewyn, B., Boulouard, M., Schumann-Bard, P., & Freret, T. (2013). Object recognition test in mice. *Nat Protoc, 8*(12), 2531-2537. doi:10.1038/nprot.2013.155

Lipton, S. A. (2004). Failures and successes of NMDA receptor antagonists: molecular basis for the use of open-channel blockers like memantine in the treatment of acute and chronic neurologic insults. *NeuroRx, 1*(1), 101-110. doi:10.1602/neurorx.1.1.101

Liu, L., Wong, T. P., Pozza, M. F., Lingenhoehl, K., Wang, Y., Sheng, M., . . . Wang, Y. T. (2004). Role of NMDA receptor subtypes in governing the direction of hippocampal synaptic plasticity. *Science, 304*(5673), 1021-1024. doi:10.1126/science.1096615

Liu, R., Liao, X. Y., Pan, M. X., Tang, J. C., Chen, S. F., Zhang, Y., . . . Wan, Q. (2019). Glycine Exhibits Neuroprotective Effects in Ischemic Stroke in Rats through the Inhibition of M1 Microglial Polarization via the NF-kappaB p65/Hif-1alpha Signaling Pathway. *J Immunol, 202*(6), 1704-1714. doi:10.4049/jimmunol.1801166

Liu, Y., Wong, T. P., Aarts, M., Rooyakkers, A., Liu, L., Lai, T. W., . . . Wang, Y. T. (2007). NMDA receptor subunits have differential roles in mediating excitotoxic neuronal death both in vitro and in vivo. *J Neurosci, 27*(11), 2846-2857. doi:10.1523/JNEUROSCI.0116-07.2007

Mallorga, P. J., Williams, J. B., Jacobson, M., Marques, R., Chaudhary, A., Conn, P. J., . . . Sur, C. (2003). Pharmacology and expression analysis of glycine transporter GlyT1 with [3H]-(N-[3-(4'-fluorophenyl)-3-(4'phenylphenoxy)propyl])sarcosine. *Neuropharmacology, 45*(5), 585-593. doi:10.1016/s0028-3908(03)00227-2

Mangin, J. M., Baloul, M., Prado De Carvalho, L., Rogister, B., Rigo, J. M., & Legendre, P. (2003). Kinetic properties of the alpha2 homo-oligomeric glycine receptor impairs a

proper synaptic functioning. *J Physiol*, *553*(Pt 2), 369-386. doi:10.1113/jphysiol.2003.052142

Marques, B. L., Oliveira-Lima, O. C., Carvalho, G. A., de Almeida Chiarelli, R., Ribeiro, R. I., Parreira, R. C., . . . Pinto, M. C. X. (2020). Neurobiology of glycine transporters: From molecules to behavior. *Neurosci Biobehav Rev*, *118*, 97-110. doi:10.1016/j.neubiorev.2020.07.025

Martina, M., Gorfinkel, Y., Halman, S., Lowe, J. A., Periyalwar, P., Schmidt, C. J., & Bergeron, R. (2004). Glycine transporter type 1 blockade changes NMDA receptor-mediated responses and LTP in hippocampal CA1 pyramidal cells by altering extracellular glycine levels. *J Physiol*, *557*(Pt 2), 489-500. doi:10.1113/jphysiol.2004.063321

Matsumoto, K., Mitani, T. T., Horiguchi, S. A., Kaneshiro, J., Murakami, T. C., Mano, T., . . . Ueda, H. R. (2019). Advanced CUBIC tissue clearing for whole-organ cell profiling. *Nat Protoc*, *14*(12), 3506-3537. doi:10.1038/s41596-019-0240-9

Mayer, M. L., MacDermott, A. B., Westbrook, G. L., Smith, S. J., & Barker, J. L. (1987). Agonist- and voltage-gated calcium entry in cultured mouse spinal cord neurons under voltage clamp measured using arsenazo III. *J Neurosci*, *7*(10), 3230-3244. Retrieved from https://www.ncbi.nlm.nih.gov/pubmed/2444678

Metz, G. A., & Whishaw, I. Q. (2009). The ladder rung walking task: a scoring system and its practical application. *J Vis Exp*(28). doi:10.3791/1204

Micu, I., Jiang, Q., Coderre, E., Ridsdale, A., Zhang, L., Woulfe, J., . . . Stys, P. K. (2006). NMDA receptors mediate calcium accumulation in myelin during chemical ischaemia. *Nature*, *439*(7079), 988-992. doi:10.1038/nature04474

Mittmann, N., Seung, S. J., Hill, M. D., Phillips, S. J., Hachinski, V., Cote, R., . . . Sharma, M. (2012). Impact of disability status on ischemic stroke costs in Canada in the first year. *Can J Neurol Sci*, *39*(6), 793-800. doi:10.1017/s0317167100015638

Morris, R. (1984). Developments of a water-maze procedure for studying spatial learning in the rat. *J Neurosci Methods*, *11*(1), 47-60. doi:10.1016/0165-0270(84)90007-4

National Institute of Neurological, D., & Stroke rt, P. A. S. S. G. (1995). Tissue plasminogen activator for acute ischemic stroke. *N Engl J Med*, *333*(24), 1581-1587. doi:10.1056/NEJM199512143332401

Nong, Y., Huang, Y. Q., Ju, W., Kalia, L. V., Ahmadian, G., Wang, Y. T., & Salter, M. W. (2003). Glycine binding primes NMDA receptor internalization. *Nature*, *422*(6929), 302-307. doi:10.1038/nature01497

Nong, Y., Huang, Y. Q., & Salter, M. W. (2004). NMDA receptors are movin' in. *Curr Opin Neurobiol*, *14*(3), 353-361. doi:10.1016/j.conb.2004.05.001

O'Brien, R. J., Kamboj, S., Ehlers, M. D., Rosen, K. R., Fischbach, G. D., & Huganir, R. L. (1998). Activity-dependent modulation of synaptic AMPA receptor accumulation. *Neuron*, *21*(5), 1067-1078. doi:10.1016/s0896-6273(00)80624-8

Ochoa, G. C., Slepnev, V. I., Neff, L., Ringstad, N., Takei, K., Daniell, L., . . . De Camilli, P. (2000). A functional link between dynamin and the actin cytoskeleton at podosomes. *J Cell Biol*, *150*(2), 377-389. doi:10.1083/jcb.150.2.377

Owen, D. J., Vallis, Y., Pearse, B. M., McMahon, H. T., & Evans, P. R. (2000). The structure and function of the beta 2-adaptin appendage domain. *EMBO J*, *19*(16), 4216-4227. doi:10.1093/emboj/19.16.4216

Paoletti, P., & Neyton, J. (2007). NMDA receptor subunits: function and pharmacology. *Curr Opin Pharmacol*, *7*(1), 39-47. doi:10.1016/j.coph.2006.08.011

Passafaro, M., Piech, V., & Sheng, M. (2001). Subunit-specific temporal and spatial patterns of AMPA receptor exocytosis in hippocampal neurons. *Nat Neurosci, 4*(9), 917-926. doi:10.1038/nn0901-917

Pontarelli, F., Ofengeim, D., Zukin, R. S., & Jonas, E. A. (2012). Mouse Transient Global Ischemia Two-Vessel Occlusion Model. *Bio Protoc, 2*(18). doi:10.21769/bioprotoc.262

Qin, X., Akter, F., Qin, L., Xie, Q., Liao, X., Liu, R., . . . Wu, S. (2019). MicroRNA-26b/PTEN Signaling Pathway Mediates Glycine-Induced Neuroprotection in SAH Injury. *Neurochem Res, 44*(11), 2658-2669. doi:10.1007/s11064-019-02886-2

Rapoport, I., Miyazaki, M., Boll, W., Duckworth, B., Cantley, L. C., Shoelson, S., & Kirchhausen, T. (1997). Regulatory interactions in the recognition of endocytic sorting signals by AP-2 complexes. *EMBO J, 16*(9), 2240-2250. doi:10.1093/emboj/16.9.2240

Renier, N., Wu, Z., Simon, D. J., Yang, J., Ariel, P., & Tessier-Lavigne, M. (2014). iDISCO: a simple, rapid method to immunolabel large tissue samples for volume imaging. *Cell, 159*(4), 896-910. doi:10.1016/j.cell.2014.10.010

Roche, K. W., Standley, S., McCallum, J., Dune Ly, C., Ehlers, M. D., & Wenthold, R. J. (2001). Molecular determinants of NMDA receptor internalization. *Nat Neurosci, 4*(8), 794-802. doi:10.1038/90498

Rossi, D. J., Oshima, T., & Attwell, D. (2000). Glutamate release in severe brain ischaemia is mainly by reversed uptake. *Nature, 403*(6767), 316-321. doi:10.1038/35002090

Saransaari, P., & Oja, S. S. (2009). Mechanisms of glycine release in mouse brain stem slices. *Neurochem Res, 34*(2), 286-294. doi:10.1007/s11064-008-9774-x

Saver, J. L. (2006). Time is brain--quantified. *Stroke, 37*(1), 263-266. doi:10.1161/01.STR.0000196957.55928.ab

Scain, A. L., Le Corronc, H., Allain, A. E., Muller, E., Rigo, J. M., Meyrand, P., . . . Legendre, P. (2010). Glycine release from radial cells modulates the spontaneous activity and its propagation during early spinal cord development. *J Neurosci, 30*(1), 390-403. doi:10.1523/JNEUROSCI.2115-09.2010

Schallert, T., Fleming, S. M., Leasure, J. L., Tillerson, J. L., & Bland, S. T. (2000). CNS plasticity and assessment of forelimb sensorimotor outcome in unilateral rat models of stroke, cortical ablation, parkinsonism and spinal cord injury. *Neuropharmacology, 39*(5), 777-787. doi:10.1016/s0028-3908(00)00005-8

Schubert, K. O., Focking, M., Prehn, J. H., & Cotter, D. R. (2012). Hypothesis review: are clathrin-mediated endocytosis and clathrin-dependent membrane and protein trafficking core pathophysiological processes in schizophrenia and bipolar disorder? *Mol Psychiatry, 17*(7), 669-681. doi:10.1038/mp.2011.123

Seibenhener, M. L., & Wooten, M. C. (2015). Use of the Open Field Maze to measure locomotor and anxiety-like behavior in mice. *J Vis Exp*(96), e52434. doi:10.3791/52434

Shank, R. P., & Aprison, M. H. (1970). The metabolism in vivo of glycine and serine in eight areas of the rat central nervous system. *J Neurochem, 17*(10), 1461-1475. doi:10.1111/j.1471-4159.1970.tb00513.x

Simon, R. P., Swan, J. H., Griffiths, T., & Meldrum, B. S. (1984). Blockade of N-methyl-D-aspartate receptors may protect against ischemic damage in the brain. *Science, 226*(4676), 850-852. doi:10.1126/science.6093256

Smith, K. E., Borden, L. A., Hartig, P. R., Branchek, T., & Weinshank, R. L. (1992). Cloning and expression of a glycine transporter reveal colocalization with NMDA receptors. *Neuron, 8*(5), 927-935. doi:10.1016/0896-6273(92)90207-t

Snyder, E. M., Philpot, B. D., Huber, K. M., Dong, X., Fallon, J. R., & Bear, M. F. (2001). Internalization of ionotropic glutamate receptors in response to mGluR activation. *Nat Neurosci, 4*(11), 1079-1085. doi:10.1038/nn746

Stroebel, D., Casado, M., & Paoletti, P. (2018). Triheteromeric NMDA receptors: from structure to synaptic physiology. *Curr Opin Physiol, 2*, 1-12. doi:10.1016/j.cophys.2017.12.004

Susaki, E. A., Tainaka, K., Perrin, D., Yukinaga, H., Kuno, A., & Ueda, H. R. (2015). Advanced CUBIC protocols for whole-brain and whole-body clearing and imaging. *Nat Protoc, 10*(11), 1709-1727. doi:10.1038/nprot.2015.085

Toussay, X., Tiberi, M., & Lacoste, B. (2019). Laser Doppler Flowmetry to Study the Regulation of Cerebral Blood Flow by G Protein-Coupled Receptors in Rodents. *Methods Mol Biol, 1947*, 377-387. doi:10.1007/978-1-4939-9121-1_22

Tsai, G., Ralph-Williams, R. J., Martina, M., Bergeron, R., Berger-Sweeney, J., Dunham, K. S., . . . Coyle, J. T. (2004). Gene knockout of glycine transporter 1: characterization of the behavioral phenotype. *Proc Natl Acad Sci U S A, 101*(22), 8485-8490. doi:10.1073/pnas.0402662101

Tsai, P. S., Kaufhold, J. P., Blinder, P., Friedman, B., Drew, P. J., Karten, H. J., . . . Kleinfeld, D. (2009). Correlations of neuronal and microvascular densities in murine cortex revealed by direct counting and colocalization of nuclei and vessels. *J Neurosci, 29*(46), 14553-14570. doi:10.1523/JNEUROSCI.3287-09.2009

Vahid-Ansari, F., Lagace, D. C., & Albert, P. R. (2016). Persistent post-stroke depression in mice following unilateral medial prefrontal cortical stroke. *Transl Psychiatry, 6*(8), e863. doi:10.1038/tp.2016.124

Vissel, B., Krupp, J. J., Heinemann, S. F., & Westbrook, G. L. (2001). A use-dependent tyrosine dephosphorylation of NMDA receptors is independent of ion flux. *Nat Neurosci, 4*(6), 587-596. doi:10.1038/88404

Wang, Y., Jin, K., & Greenberg, D. A. (2007). Neurogenesis associated with endothelin-induced cortical infarction in the mouse. *Brain Res, 1167*, 118-122. doi:10.1016/j.brainres.2007.06.065

Warach, S. J., Dula, A. N., & Milling, T. J., Jr. (2020). Tenecteplase Thrombolysis for Acute Ischemic Stroke. *Stroke, 51*(11), 3440-3451. doi:10.1161/STROKEAHA.120.029749

Warlow, C., Sudlow, C., Dennis, M., Wardlaw, J., & Sandercock, P. (2003). Stroke. *Lancet, 362*(9391), 1211-1224. doi:10.1016/S0140-6736(03)14544-8

Watson, B. D., Dietrich, W. D., Busto, R., Wachtel, M. S., & Ginsberg, M. D. (1985). Induction of reproducible brain infarction by photochemically initiated thrombosis. *Ann Neurol, 17*(5), 497-504. doi:10.1002/ana.410170513

Wilson, V. J., & Talbot, W. H. (1963). Integration at an Inhibitory Interneurone: Inhibition of Renshaw Cells. *Nature, 200*, 1325-1327. doi:10.1038/2001325b0

Yang, Y., Kimura-Ohba, S., Thompson, J., & Rosenberg, G. A. (2016). Rodent Models of Vascular Cognitive Impairment. *Transl Stroke Res, 7*(5), 407-414. doi:10.1007/s12975-016-0486-2

Yao, W., Ji, F., Chen, Z., Zhang, N., Ren, S. Q., Zhang, X. Y., . . . Lu, W. (2012). Glycine exerts dual roles in ischemic injury through distinct mechanisms. *Stroke, 43*(8), 2212-2220. doi:10.1161/STROKEAHA.111.645994

Yu, Z., Tan, E. L., Ni, D., Qin, J., Chen, S., Li, S., . . . Wang, T. (2018). A Deep Convolutional Neural Network-Based Framework for Automatic Fetal Facial Standard Plane

Recognition. *IEEE J Biomed Health Inform, 22*(3), 874-885. doi:10.1109/JBHI.2017.2705031

Zafra, F., Aragon, C., Olivares, L., Danbolt, N. C., Gimenez, C., & Storm-Mathisen, J. (1995). Glycine transporters are differentially expressed among CNS cells. *J Neurosci, 15*(5 Pt 2), 3952-3969. Retrieved from https://www.ncbi.nlm.nih.gov/pubmed/7751957

Zafra, F., Gomeza, J., Olivares, L., Aragon, C., & Gimenez, C. (1995). Regional distribution and developmental variation of the glycine transporters GLYT1 and GLYT2 in the rat CNS. *Eur J Neurosci, 7*(6), 1342-1352. doi:10.1111/j.1460-9568.1995.tb01125.x

Zhao, D., Chen, J., Zhang, Y., Liao, H. B., Zhang, Z. F., Zhuang, Y., . . . Wan, Q. (2018). Glycine confers neuroprotection through PTEN/AKT signal pathway in experimental intracerebral hemorrhage. *Biochem Biophys Res Commun, 501*(1), 85-91. doi:10.1016/j.bbrc.2018.04.171